# Electronic properties of functionalized carbon nanotubes

vorgelegt von
Diplom-Physiker
Matthias Müller
aus Herne

Von der Fakultät II - Mathematik und Naturwissenschaften
der Technischen Universität Berlin
zur Erlangung des akademischen Grades
Doktor der Naturwissenschaften
Dr.rer.nat.

genehmigte Dissertation

Promotionsausschuss:
Vorsitzender: Prof. Dr. Michael Lehmann
Berichter: Prof. Dr. Christian Thomsen
Berichter: Prof. Dr. Andreas Hirsch

Tag der wissenschaftlichen Aussprache: 8. Dezember 2010

Berlin 2011

D 83

## List of Publications

Parts of this thesis have already been published:

Electronic Properties of Propylamine-Functionalized Single-Walled Carbon Nanotubes.
M. Müller,R. Meinke, J. Maultzsch, Z. Syrgiannis, F. Hauke, A. Pekker, K. Kamaras, A. Hirsch, and C. Thomsen.
*ChemPhysChem* **11**, 2444 (2009).

Raman spectroscopy of pentyl-functionalized carbon nanotubes.
M. Müller, J. Maultzsch, D. Wunderlich, A. Hirsch, and C. Thomsen.
*phys. stat. sol. (RRL)* **1**, 144 (2007).

Raman Spectroscopy on Chemically functionalized Carbon Nanotubes.
M. Müller, J. Maultzsch, D. Wunderlich, A. Hirsch, and C. Thomsen.
*phys. stat. sol. (b)* **244**, 4056 (2007).

Diameter dependence of addition reactions to carbon nanotubes.
M. Müller, J. Maultzsch, D. Wunderlich, A. Hirsch, and C. Thomsen.
*phys. stat. sol. (b)* **245**, 1957 (2008).

Raman spectroscopy of single wall carbon nanotubes functionalized with terpyridine-ruthenium complexes.
M. Müller, J. Maultzsch, K. Papagelis, A. A. Stefopoulos, E. K. Pefkianakis, A. K. Andreopoulou, J. K. Kallitsis, and C. Thomsen.
*phys. stat. sol. (b)* **246**, 2721 (2009).

Observation of Breathing-like Modes in an Individual Multiwalled Carbon Nanotube.
C. Spudat, M. Müller, L. Houben, J. Maultzsch, K. Goss, C. Thomsen, C. M. Schneider and C. Meyer.
*Nano Lett.* ,(2010).

Resonant Raman scattering on carbon nanotubes covalently functionalized with lithium decyne.
M. Müller, R. Meinke, J. Maultzsch, B. Gebhardt, F. Hauke, A. Hirsch, and C. Thomsen.
*phys. stat. sol. (b)* , DOI:10.1002/pssb.201000349.

Selective Carboxylation of Semiconducting Single-walled Carbon Nanotubes.
B. Gebhardt, M. Müller, T. Plocke, J. Maultzsch, F. Hof, C. Backes, F. Hauke, A. Hirsch, and C. Thomsen.
In preparation.

Semiconducting polymer functionalized carbon nanotubes.
A. A. Stefopoulos, M. Müller, T. Plocke, J. Maultzsch, K. Papagelis, Souzana N. Kourkouli, Elina Siokou, A. K. Andreopoulou, J. K. Kallitsis, and C. Thomsen.
In preparation.

## Abstract

Carbon nanotubes are tiny cylinders which can be imagined as rolled up graphene monolayers. Their fundamental architecture is the honeycomb lattice with $sp^2$-hybridized carbon as known from natural graphite.

Functionalization means a chemical treatment, which adds molecules to the nanotubes by covalent or non-covalent bonding. Functionalized carbon nanotubes have many potential applications in the fields of nanoelectronics and chemistry. The functionalities allow to design tubes for special needs in specific environments and drastically increase the processability of nanotubes, e.g., by increasing the solubility in certain media.

Chemical functionalization highly influences the carbon lattice. The addition leads to local strain relaxation, which is revealed in the diameter dependence of the tube reactivity. Due to the different curvature of the tubes, small diameter tubes are more affected than larger ones. Depending on the applied reaction conditions also a preferred reaction to either metallic or semiconducting tubes can be achieved.

The charge transfer between the tube and the addend causes changes in the electronic structure of the tubes, depending on the moiety. This is probed via resonant Raman spectroscopy of the tubes, which reveals changes in the optical transitions.

Due to their extraordinary mechanical properties, nanotubes are also desirable for composite materials, e.g., the integration into polymers. The electronic properties of such composites after polymerization are studied. It is shown that electronic effects can be separated from pure structural effects after covalent sidewall additions.

The investigation of functionalized material is typically performed on nanotube ensembles, i.e., solutions or bulk material. Isolated tubes or small bundles on a grid allow polarization dependent measurements in addition to the experimental benefit to combine the spectroscopical analysis with the structural characterization by the transmission electron microscopy measurements.

## Zusammenfassung

Kohlenstoffnanotubes sind winzige Zylinder, die man sich wie aufgerollte Graphenmonolagen vorstellen kann. Sie besitzen die gleiche sechseckige Wabenstruktur, wie sie auch in Graphit vorkommt. Unter Funktionalisierung versteht man die chemische Veränderung der Tubes, dabei werden Moleküle an die Seitenwand der Nanotubes gebunden. Man unterscheidet kovalente und nicht-kovalente Funktionalisierungen. Funktionalisierte Nanotubes sind in vielen Bereichen der Nanotechnik und der Chemie einsetzbar; die Funktionalisierung erlaubt das Anpassen der Röhren an bestimmte Umgebungen, z.B. durch Verändern ihrer Löslichkeit.

Kovalente Bindungen beinflussen die atomare Sturuktur der Seitenwände, u.a. führt die Bindung lokal zu einer Entspannung des Gitters. Dieser Effekt wird in der Durchmesserabhängigkeit der Reaktivität verschiedener Tubes sichtbar, Röhren kleiner Durchmesser werden bevorzugt funktionalisiert. Durch geeignete Reaktionsbedingungen kann auch die Reaktivität halbleitender oder metallischer Nanotubes bevorzugt sein.

Je nach Art der funktionellen Gruppen wird die elektronische Struktur der Nanotubes unterschiedlich stark beeinflusst. Die resonante Ramanspektroskopie erlaubt eine detaillierte Untersuchung dieser Einflüsse. Die Veränderungen der optischen Übergänge lassen sich anhand der Resonanzprofile der sog. Atmungsmode der Tubes untersuchen. Dabei können elektronische Effekte durch Ladungstransfer von Einflüssen durch strukturelle Veränderungen, hervorgerufen durch die kovalenten Bindungen, unterschieden werden. Die außergewöhnlichen mechanischen Eigenschaften der Nanotubes machen diese auch interessant für Verbundmaterialien, insbesondere in Verbindungen mit Polymeren. Die elektronischen Eigenschaften der Röhren nach der Polymerisation werden untersucht.

Üblicherweise werden funktionalisierte Nanotubes anhand von Ensembles untersucht. Einzelne Tubes, auf einem Gitter gewachsen, ermöglichen auch polarisationsabhängige Ramanmessugen. Darüber hinaus ergeben sich interessante experimentelle Möglichkeiten durch die Kombination von Ramanmessungen mit hochauflösender Elektronenmikroskopie.

# Contents


**1 Introduction** **1**

**2 Basic Concepts** **5**

2.1 Carbon Nanotubes . . . . . 5

2.2 Raman Scattering . . . . . 9

2.2.1 Raman Scattering in Carbon Nanotubes . . . . . 11

2.2.2 Resonance Profiles . . . . . 13

2.2.3 Experimental Setup . . . . . 14

2.3 Additional characterization . . . . . 15

**3 Functionalized Carbon Nanotubes** **19**

3.1 Covalent Sidewall Functionalization . . . . . 21

3.1.1 Evidence for the addition reaction by Raman spectroscopy . . . . . 22

3.1.2 Radial breathing mode and resonance profiles . . . . 24

3.1.3 Influence on RBM frequencies . . . . . 25

3.1.4 Attenuation of Raman features due to functionalization 28

3.2 Reactivity of Carbon Nanotubes . . . . . 29

3.2.1 Selectivity on Tube Species . . . . . 30

3.2.2 Selectivity on Tube Diameter . . . . . 35

3.3 Endohedral Functionalization and Isotopic Engineering . . . . 39

**4 Functionalization and electronic structure** **41**

4.1 RBM and optical transitions . . . . . 42

4.1.1 HEM and $D$ mode features . . . . . 47

4.2 Functionalization with decyne . . . . . 50

4.3 The D* mode and functionalization . . . . . 54

**5 Composite materials, nanotubes and polymers** **57**

5.1 Influence on RBM and optical transitions . . . . . 58

5.2 Semiconducting polymer-functionalized nanotubes . . . . . 62

**6 Individual carbon nanotubes** **67**
6.1 Breathing-like modes in multi-walled carbon nanotubes . . . 68
6.2 Small bundles, special configurations . . . . . 72

**7 Summary and Outlook** **75**

**Appendix** **79**

**A Sample preparation** **79**
A.1 Propylamin-tubes . . . . . 79
A.2 Decyne-tubes . . . . . 80
A.3 Pentyl-tubes . . . . . 80
A.4 tpy-Ru(II)-tpy tubes . . . . . 80
A.5 Quinoline-tubes . . . . . 81

**Bibliography** **83**

*There is Plenty of Room at the Bottom.*

Richard P. Feynman

# 1 Introduction

Feynman's classic talk "There is Plenty of Room at the Bottom" was given in 1959 at the annual meeting of the American Physical Society and it was subtitled "An Invitation to Enter a New Field of Physics". It is often stated to be the beginning of nanotechnology, and amazingly it is addressing some major issues of science still under investigation half a century later. And it's not only about computing and miniaturization, Feynman also gives a hint at science itself; different sciences will come closer to each other driven by nanotechnology. This is exactly what we observe today: biology, chemistry and physics all make a great impact on nano-science. Carbon nanotubes are a prime example of successful interdisciplinary work, with researchers in the field moving together from different scientific backgrounds being enamored of their unique properties. Ballistic transport which is maintained over large distances, tensile strength up to some hundred Gigapascal, excitons to be observable at room temperature, the electronic bandstructure changing from metallic to semiconducting due to small changes in the framework structure, just to name a few.

Nanotubes are among those fancy objects that science sometimes seems to create by accident: Iijima reported the self-assembled growth of multi-walled carbon nanotubes as a byproduct of fullerene production in an arc discharge process [1]. Only two years later the next breakthrough was made, the first single-walled tubes were discovered and the report by Bethune *et al.* in $Nature$ also sounds a little accidentally: "the initial aim of our experiments was to produce metallofullerenes and graphite-encapsulated nanocrystals..." [2]. However, there has been an enormous development, carbon nanotubes have been investigated intensively since then, and very fast they became a promising new material in two main respects: fundamental research on low-dimensional systems accompanied by a lot of theoretical

work and research to prospect for various applications. Those may again be divided into nanoelectronics [3] like electron emitters or semiconductor devices and chemistry. Especially the idea that the whole organic chemistry could - in general - be adaptable to carbon nanotubes may have constituted a definite undertaking to future applications in the beginning of nanotube chemistry.

Selectivity has been an issue ever since their discovery, because none of the growth processes allows to produce only one tube species or diameter, let alone one particular chirality. Therefore, separation has been addressed by various techniques including dielectrophoresis [4], chromatography [5, 6] and chemical functionalization [7]. Addition reactions to the sidewalls yield nanotube derivatives exhibiting a considerably increased solubility in organic solvents. As soluble nanotubes with defined electronic properties are the basic requirement especially for electronic applications, tailored reaction sequences yielding appropriate samples in a large amount are of major interest. In order to open access routes to this kind of architectures, the understanding of the basic reaction mechanism and the influence of the attached functional moieties is a major prerequisite [8]. There are different ways to charge a tube, probably the strongest effect is due to intercalation followed by electrochemical doping. Both have been studied in detail from the early days of nanotube research on, either by UV-Vis [9], X-Ray diffraction [10] or Raman spectroscopy [11]. Another opportunity of doping a tube is due to addition reactions to its sidewall. The influence of chemical functionalization and charge transfer on the optical transitions is the main topic of the presented work. The influence of various moieties and composites is discussed.

Chapter 2 gives a very brief introduction to pristine carbon nanotubes, their optical and electronic properties. They have been reviewed many times and therefore I focus on the absolute basics necessary to follow the presented work. Also the experimental methods used for analysis are briefly described. Chemical functionalization highly influences the carbon framework and may cause changes in the electronic bandstructure of the tubes, thus all Raman features are more or less influenced by functionalization. Chapter 3 gives a detailed view of the possible influences and how they pronounce in the Raman spectra. Chapter 4 focuses on the electronic bandstructure under covalent sidewall additions. Charge transfer between the addend and the nanotubes is reflected especially in the optical transitions. The strength and stiffness make nanotubes desirable for composite materials, e.g., the integration into polymers. Chapter 5 gives an introduction

to this issue, focusing on the electronic properties of such composites after polymerization. The investigation of functionalized material is typically established on nanotube ensembles, i.e., solutions or bulk material. In contrast, chapter 6 introduces measurements on individual nanotubes. The advantage of isolated tubes or small bundles on a TEM grid is the additional feature of polarization dependent measurements in addition with the experimental benefit to combine the spectroscopical analysis with TEM measurements. This part reveals that it is possible to record resonance profiles of the radial breathing mode on as-prepared samples in order to come full circle to the main idea of future analysis of functionalized materials.

There *still* is plenty of room at the bottom...

*Was du ererbt von Deinen Vätern hast,*
*erwirb es, um es zu besitzen.*

Goethe, Faust

# 2

# Basic Concepts

Raman spectroscopy is among the most common characterization methods for carbon nanotubes [12, 13]. While the defect-induced $D$ mode allows to observe changes in the atomic structure of the tubes, which is of vital interest while studying covalent functionalization, the radial breathing mode offers information about tube diameter and makes it possible to measure the transition energies. Thus, the exact atomic structure can be assigned to each breathing mode and the tube species, metallic or semiconducting, can be determined by a single spectrum. This chapter gives an introduction to pristine, i.e., non-functionalized carbon nanotubes, followed by an overview on Raman spectroscopy in general and on carbon nanotubes in particular. The chapter closes with a brief description of additional characterization methods helpful especially for investigating functionalized material.

## 2.1 Carbon Nanotubes

Carbon nanotubes are tiny cylinders which can be imagined as seamlessly rolled up graphene sheets, i.e., a monolayer of the same poly-aromatic honeycomb lattice with $sp^2$-hybridized carbon as natural graphite is made of. During the growth process tubes of various diameters and structures originate, differing also in electronic properties. Wang $et\ al.$ reported the preparation of 4 Å diameter tubes, prepared in channels of porous zeolithe crystals [14]. However, the typical diameter of the tubes is about one nanometer. The length can be up to some millimeters or even higher; the controlled growth of ultra long single-walled carbon nanotube arrays was reported using an improved chemical vapor deposition strategy that leads to nanotubes over 18.5 cm long [15]. One can distinguish between single and multi-

walled tubes, which consist of an array of nanotubes located concentrically into one another. Carbon nanotubes show some extraordinary mechanical and electronic properties. The $sp^2$ carbon-carbon bond is among the strongest known bonds and so nanotubes were expected to be extremely strong structures. The first direct measurement of the mechanical properties was reported by Wong *et al.* in 1997 [16]. Atomic force microscopy (AFM) was used to measure the tensile modulus of multi-walled tubes fixed at one end. They report an E modulus of 1.28 TPa. Nanotubes also show a very high thermal conductivity which is a magnitude higher compared to copper. This holds for room temperature, but also for up to some hundred degree centigrade [17, 18]. These high values are associated with the long phonon free paths in carbon nanotubes, the $1/T^2$ behavior is attributed to a second-order three-phonon processes with a scattering time proportional to $1/T^2$ [18].

Concerning electronic properties carbon nanotubes show both metallic or semiconducting behavior depending on their atomic structure. The most decisive structural parameter concerning the electronic properties of a nanotube is the way it is rolled up, the so-called chiral index. There are infinite ways to construct a seamless nanotube from a graphene sheet, resulting in unit cells containing from very few to some hundred carbon atoms. A precise description of each nanotube is possible by the use of the chiral vector, which is a multiple $(n, m)$ of the basis vectors $\vec{a_1}$ and $\vec{a_2}$ of graphene (see Fig. 2.1): $\vec{C} = n\vec{a_1} + m\vec{a_2}$.

The electronic properties can be derived from the bandstructure of graphene using the so-called zone-folding procedure. The zone-folding approximation takes into account the carrier confinement and hence the limitation of available states because of the one-dimensional structure of the tubes [12]. The graphene bandstructure reveals the valence and conduction band to touch only in the six high-symmetry points $K$ and $K'$ at the edges of the Brillouin zone, making graphene a semimetal. In nanotubes, waves along the circumference additionally have to fulfill the boundary condition

$$\vec{C_h} \cdot \vec{k} = 2\pi m \, (m \in N). \tag{2.1}$$

This introduces lines of allowed states in k-space, their distance and length depends on the tube diameter and the length of the unit cell of the tube, respectively (see Fig 2.2). This reveals the basic phenomena of tubes being either metallic or semiconducting, depending if the $K$ point of the graphene bandstructure is among the allowed states, i.e., the allowed $\vec{k}$, or not. If $(n - m) mod 3 = 0$, the tube is metallic, otherwise it is semiconducting.

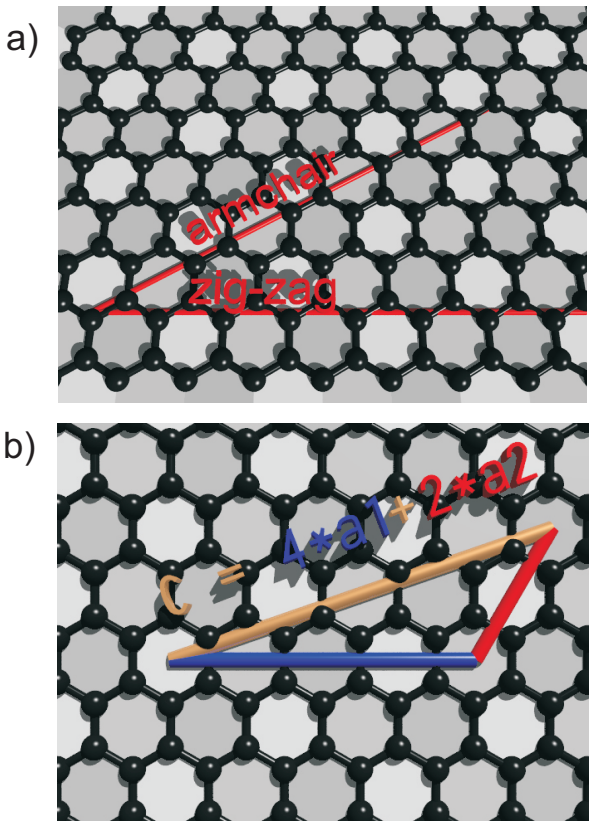


Figure 2.1: Sketch of a carbon lattice showing (a) directions of armchair and zig-zag roll-up vectors,
(b) nomenclature of nanotubes according to circumference vector, which is an $(n, m)$ multiple of the basis vectors of the honeycomb graphene lattice (shown here: (4,2) tube).

Hence, 1/3 of all carbon nanotubes should be metallic and 2/3 should be semiconducting. This is correct except for tubes of very small diameters. In this case the zone folding approximation reaches its limits, because it neglects the curvature of the tube walls, which forces a bending of the the originally flat $sp^2$ bonds. This was addressed in a symmetry-adapted non-orthogonal tight-binding model reported by Popov [19].

In low-dimensional systems, the electronic density of states (DOS) undergoes some essential modifications compared to a parabolic dispersion relation, such as applies to free electrons in a Fermi gas [20]. In one-dimensional systems, the DOS forms peaks as shown in Fig. 2.3, commonly referred to as van Hove singularities. It also reveals the difference between semiconducting and metallic tube species with vanishing or non-vanishing DOS close to the Fermi level, respectively [21]. This is important discussing the different reactivities of either tube species (see section 3.2). Corresponding to the density of states, the bandstructure of nanotubes consists of many sub-bands. However, incident light only leads to transitions $E_{ii}$ between

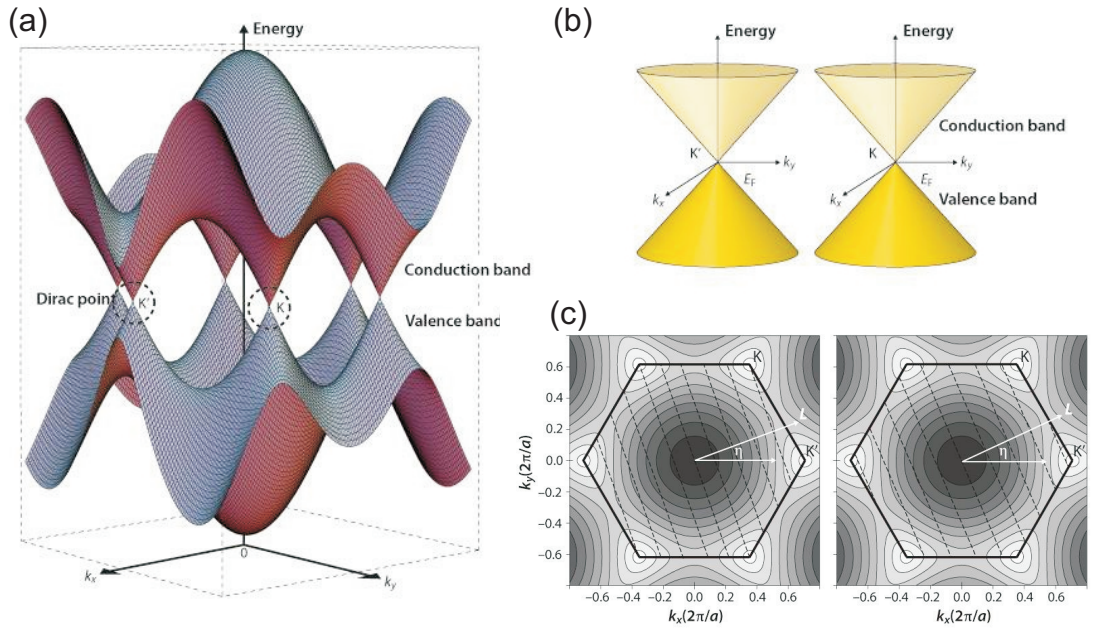


Figure 2.2: (a) Energy bands in graphene. The bands cross at points K and K'. (b) Conic energy bands close to the K and K' points. Lines of same energy on the valence band in reciprocal space. The hexagon denotes the first Brillouin zone, L is the chiral vector and $\eta$ is the chiral angle. Dashed lines denote allowed wave vectors when graphene is rolled into a cylinder to form a carbon nanotube, and show the orientation perpendicular to L. The K and K' points lie on the dashed lines in metallic carbon nanotubes (c, left), and lie away from the dashed lines in semiconducting nanotubes (c,right). From Ref [22].

corresponding bands. This is because only light polarized perpendicular to the tube axis can change the band index, but only parallel polarized light interacts with the tube [13].

A very useful tool for identification of a particular tube chirality by observing the RBM spectra is the so-called Kataura plot. It is a representation of the transition energies $E_{ii}$ as a function of tube diameter and/or Raman shift as shown in Fig. 2.4. Each data point in the Kataura plot represents a transition energy of a particular nanotube $(n, m)$. The data points form a typical pattern of branches which allows a unique assignment of certain tube chiralities. This is often referred to as index assignment [23]. The most

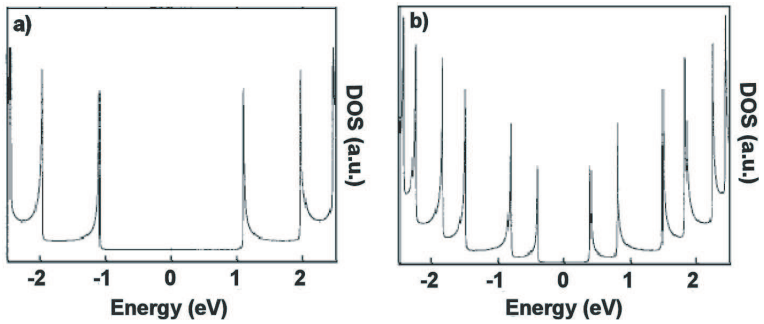


Figure 2.3: The electronic density of states (DOS) for a (a) metallic and (b) semiconducting carbon nanotube. The essential difference is the vanishing or non-vanishing DOS close to the Fermi level (0 eV). From Ref. [21].

obvious characteristic in the pattern is the overall 1/d dependence given by the optical transitions $E_{ii}$.

## 2.2 Raman Scattering

Observing - not necessarily monochromatic - light being scattered by molecules or crystal lattices one can distinguish between elastic (Rayleigh-scattering) or inelastic scattering. The inelastic process is called Raman scattering [25]. The Raman effect is named after Sir Chandrasekhara Venkata Raman, recognized for his work on the scattering of light by molecular vibrations and awarded the Nobel price in 1930.

In the electro-magnetic wave picture the process of inelastic scattering on a crystal lattice can be understood as follows [26]: a wave with frequency $\omega_i$ and wave vector $k_i$ travels trough the medium inducing a polarization $P_i$, which causes periodic displacements in the lattice. If the displacement $Q(r,t)$ changes the polarizability $\chi$ of the medium $(d\chi/dQ)|_0 \neq 0)$, the polarization $P_i(r,t)$ induced by the light will be modulated by the vibrations of the atoms. These vibrations and their amplitudes are usually small compared to the typical spacing between the atoms in a crystal lattice and therefore, $\chi$ can be expanded as a Taylor series in the displacement:

$Q(r,t)$:$\chi(k_i,\omega_i,Q) = \chi_0 + (d\chi/dQ)_0 Q(r,t) + ...$

whith $\chi_0$ the electric susceptibility without any atomic vibrations.

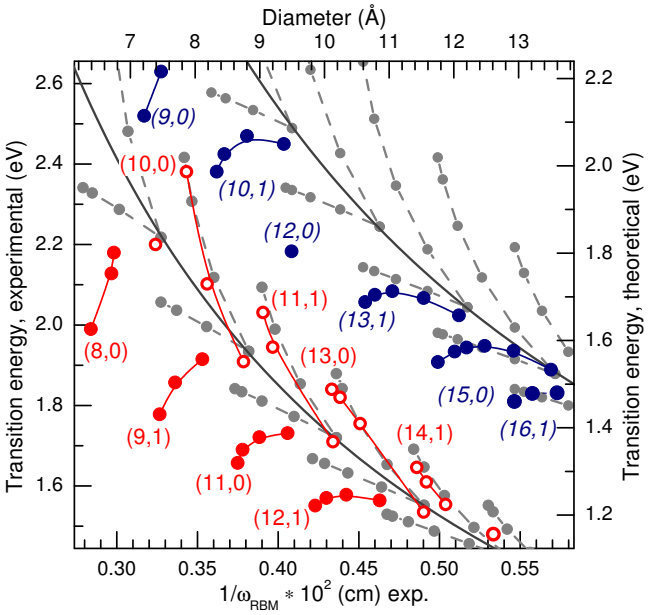


Figure 2.4: Kataura plot from Ref. [24]. Shown here are the are transitions $E_{22}^S$ (red) and $E_{11}^M$ (blue) of semiconducting and metallic tubes, respectively.

The modulated wave $P(r,t)$ can be described in terms of $P_i(r,t)$, the polarization wave moving in phase with the incident light and a polarization wave $P_{ind}$ induced by a vibration:

$$\begin{aligned} P(r,t) &= P_i(k_i,\omega_i)cos(k_i \cdot r - \omega t) \\ &\quad + P_{ind}(k_i,\omega_i,Q)cos[(k_i+q)\cdot r - (\omega_i+\omega_0)t] \\ &\quad + P_{ind}(k_i,\omega_i,Q)cos[(k_i-q)\cdot r - (\omega_i-\omega_0)t] \end{aligned} \tag{2.2}$$

So $P_{ind}$ consists of two parts with frequencies and wave vectors increased (anti-Stokes) or decreased (Stokes) by the frequency and wave vector of the atomic vibration. These changes compared to the incident light are called Raman shifts. The ratio between the intensities of Stokes and anti-Stokes signals depends on temperature, because it reflects the relative numbers of molecules in states of different energy, and this is given by the Boltzmann distribution.

It is well-known that the normal modes of atomic vibrations can be quantized in terms of phonons like the electromagnetic field is quantized into photons. From this point of view the Raman process can be described in three steps:

1. The incident light excites an electron
2. The electron interacts with the molecule/lattice creating or destroying a phonon $\omega_\nu$, which means the electron looses/gains energy.
3. The electron relaxes emitting a photon $\omega_S = \omega_L \pm \omega_{ph}$, "-": Stokes scattering "+": anti-Stokes scattering.

Of course, during the scattering process energy and momentum have to be conserved. Therefore the momentum of the phonon cannot exceed twice the photon wavevector (backscattering). In Raman experiments in the visible light range the momentum of the light is much smaller compared to the Brillouin zone. Hence a one phonon scattering process (first-order process) only probes phonons close to the center of the Brillouin zone ($\Gamma$-point). For two (or even multiple) phonon processes these restriction is expanded, because only the sum of momentums has to be close to zero. This allows overtones to probe the whole Brillouin zone and makes them a measure of the density of states inside the zone.

The intensity of the scattered light depends on its polarization, $e_s$, as $|P_{ind} \cdot e_s|^2$. With $e_i$ and $e_s$ the polarization of incident and scattered light respectively, the scattered intensity is $I_s \propto |e_i \cdot \Re \cdot e_s|$ with $\Re$ the Raman tensor. This tensor is given by the displacement and the derivative of the susceptibility with respect to the displacement: $(d\chi/dQ)_0 \cdot Q(\omega_0))$. With Raman spectroscopy one may get information on both frequency and symmetry of a Raman-active phonon [26].

### 2.2.1 Raman Scattering in Carbon Nanotubes

Figure 2.5 shows Raman spectra typical for SWCNTs. The Raman spectrum of carbon nanotubes consists mainly of three first-order Raman active modes, as there are:

– the radial breathing mode (RBM), which belongs to a concentral in-phase vibration. It offers information about the diameter of the tube and its electronic structure. Depending on the diameter of the tube the RBM frequencies vary in the range of about 150 cm$^{-1}$ to 350 cm$^{-1}$. The RBM is a highly resonant feature and very sensitive to electronic or structural changes and environmental effects [24, 27, 28]. Therefore, the recording of resonance profiles provides a very powerful analysis tool dealing with carbon nanotubes. From the resonance profiles it is

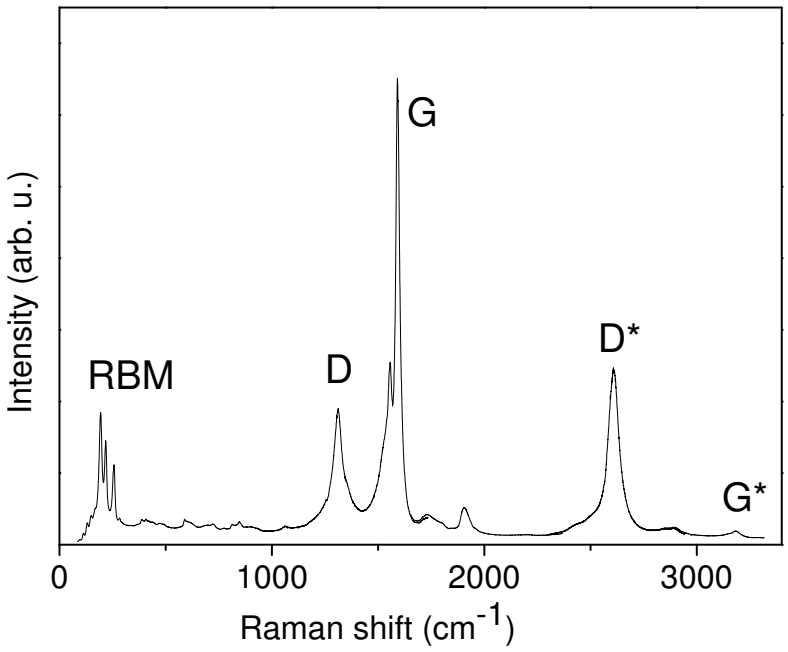


Figure 2.5: Typical Raman spectrum of a carbon nanotube ensemble: various radial-breathing modes (RBM), the defect-induced $D$ mode and the high energy mode (G mode) and the overtones (labeled with*)

possible to assign the RBM signal to the different tube chiralities via Kataura plots [23, 24].

- the defect induced $D$ mode at about 1320 cm$^{-1}$ arises from a double-resonant scattering process which reveals structural changes in the tube framework [29, 30]. The intensity of this mode increases with the concentration of defects in a nanotube. The successful sidewall addition similarly breaks the translational symmetry and changes the Raman selection rules resulting in an increased $D$ mode intensity [31, 32]. From another point of view the covalent bonds change the hybridization of the attacked carbon atoms from $sp^2$ to $sp^3$ and therefore make a contribution to the $D$ mode intensity.
- the G mode at about 1600 cm$^{-1}$, referring to the $E_{2g}$ mode in graphene. It belongs to an in-plane vibration of the hexagon structure and is often called high energy mode (HEM). In individual tubes the lineshape offers information about the tube species [33]. Shifts or changes in the lineshape are also important concerning temperature effects or the

doping level of a tube[11].

– Additionally, the spectra contains overtones, especially G* and D*. In general, all combinations of different phonons are allowed in a two-phonon process. If the phonons belong to the same mode, they are called overtones. The lineshape of the D* mode is offering information about defects and the doping level [34].

### 2.2.2 Resonance Profiles

Raman spectroscopy is a very helpful tool for the characterization of carbon nanotubes since resonant scattering processes are highly influenced by the vibrational properties and electronic states/optical transitions of a system. As mentioned above the RBM is a resonant Raman feature. The Raman intensity is enhanced by some orders of magnitude, if the energy of the incident or scattered light matches the energy of an electronic transition. These resonance conditions are called incoming and outgoing resonance, respectively (see Fig.: 2.6). A resonance profile is rendered by recording the Raman intensity as a function of excitation energy. This leads to an M-shaped resonance profile with a slight dent between the local maxima. The Raman susceptibility close to the resonance can be described as follows [13, 33, 35]: To derive a mathematical expression for resonant Raman scattering in carbon nanotubes one assumes an individual intermediate excitonic state and the initial and final electronic states to be the same. Then the susceptibility is:

$$|\chi_R|^2 = \frac{2\omega_{ph}V}{\omega_i^2}K \tag{2.3}$$

$$K = \frac{M_R^2}{((\hbar\omega_i - E_{ii})^2 + (\gamma/2)^2)((\hbar\omega_i - \hbar\omega_{ph} - E_{ii})^2 + (\gamma/2)^2)} \tag{2.4}$$

where $E_{ii}$ is the energy of the optical transition and $M_R$ the Raman matrix element. $\gamma$ refers to the lifetime and therefore the natural linewidth of the optical transition. In many cases the optical transitions are additionally

broadened by impurities or functionalization. This causes longer lifetimes and thus larger values for $\gamma$. Therefore $\gamma$ is also referred to as the broadening parameter. K describes the convolution of two Lorentzian curves of width $\gamma$ and phonon frequency $\omega_{ph}$.

However, at first glance the recorded profiles look like Lorentzian-shaped profiles with only one maximum. This is because the distance between the maxima is the phonon energy and for RBMs it is usually in the range of 20 to 40 meV which is too small to appear as two distinct maximums, especially measuring bulk samples where the accuracy of the intensities is less than in solutions or on isolated tubes because of surface roughness, inhomogeneities or other environmental effects. The recording of resonance profiles makes use of a relatively narrow resonance window of the radial breathing mode in carbon nanotubes. This allows to observe an RBM intensity rising and vanishing again within a range of about 100 meV, which can be displayed with common tunable lasers.

### 2.2.3 Experimental Setup

The Raman measurements were carried out using a micro-Raman setup in backscattering geometry. The typical setup is shown in figure 2.7. For excitation different lasers were used offering a range of energies from about 1.5 eV to 2.6 eV (blue to near IR). In order to record resonance profiles, tunable lasers are necessary. Dye lasers with various dyes and a Ti:Sapphire laser, pumped by a Nd:YAG laser were used and enabled to record profiles between yellow/light red and near IR. In a Raman setup the elastically scattered light (Rayleigh peak) of the exciting laser has to be suppressed. Recording the resonance profiles, the signal was analyzed by a triple monochromator (dilor XY), in some cases a different setup with notch filters was used. While notch filters, even of high quality, cut quite a broad range and make it difficult to observe Raman modes closer than about 200 $cm^{-1}$ to the excitation wavelength, a triple monochromator offers the chance to come very close to the laser peak, signal below 50 $cm^{-1}$ can be recorded with such a setup (with excitation wavelength in the visible range) [37]. In the triple monochromator setup the first two monochromators (premonochromators) are coupled in a subtractive configuration: they act as a bandpass filter, highly efficient suppressing the rest of the spectrum. The final analysis is done by the third monochromator (spectrometer). The signal is detected by charge-coupled devices(CCDs). Depending on the wavelength, different

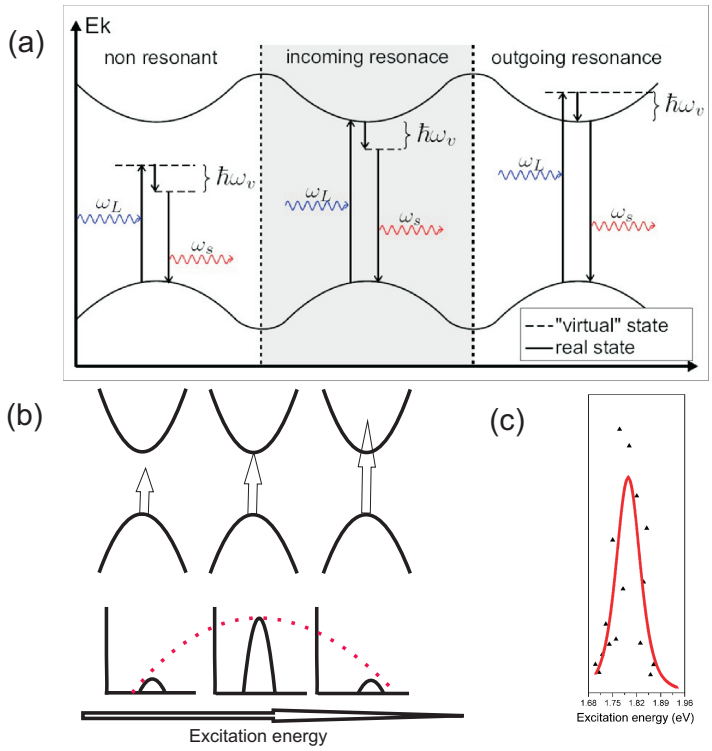


Figure 2.6: (a) In a non-resonant Raman scattering process, virtual states are taking part. If the incident or outgoing light matches a real state, resonance occurs, from Ref. [33]. (b) Recording a resonance profile means tuning the excitation energy in small steps from below to above the resonance condition (c) Resonance profile fitted with function according to Eq. 2.4. Due to the low phonon energy the local minimum in between in-/outgoing resonance cannot be observed.

CCDs were used with optimized sensitivities for either red/IR or visible light. The CCDs were cooled by a Peltier device or liquid nitrogen respectively for better signal-to-noise ratio. To avoid heating of the nanotube bulk material, laser power had to be reduced to about 0.4 mW on the sample, the spot size on the sample was about 1 $\mu$m. All measurements were realized at room temperature.

## 2.3 Additional characterization

Raman spectroscopy is a very powerful method to study carbon nanotubes and their chemical functionalization, however there are more characteriza-

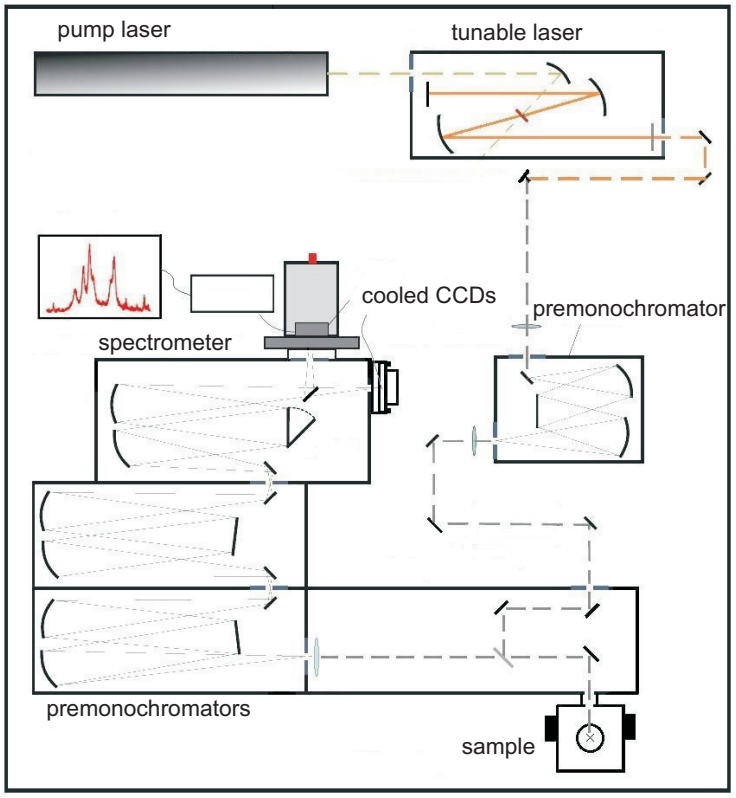


Figure 2.7: Raman spectroscopy set-up: The premonochromator absorbs plasma or dye lines. The samples are illuminated through far-distance object lenses, the scattered light is analyzed by a triple monochromator and detected with CCD cameras (liquid nitrogen or Peltier-cooled). Figure adapted from [36].

tion methods needed. Since these measures were usually carried out by Coworkers, only a brief description is provided here.

### Thermogravimetric analysis

Thermogravimetric analysis (TGA) is performed usually with functionalized material to study the degree of functionalization. This works due to determine the weight loss of a sample as a function of temperature. The analyzer usually consists of a high-precision balance where the sample can be placed on. The analysis is carried out in an electrically heated oven which

can be purged with inert gas to prevent oxidation. During the analysis the sample is heated with a constant heating rate, controlled by a thermocouple. The weight loss of the material is plotted, usually in percentage, as a function of temperature. A sufficient heating range for functionalized nanotube samples is usually between 100 °C and 700 °C where the attached addends are split of. Pronounced steps in the weight loss function in particular temperature regions indicate the nature of the attachment, e.g., in the temperature region between 300 °C and 500 °C the covalent attached addends are split of. For more precise analysis the measurements are accompanied by online-monitoring of the volatile products via mass spectrometry. Herein, the different fragments with various m/z ratio originating from the attached addends are detected. Over the whole heating range the sample exhibits a total mass loss which is corrected to the the mass loss of the starting material (pristine nanotubes) in the corresponding temperature region, yielding a corrected value for the mass loss. From the corrected mass loss the degree of functionalization for the functionalized derivatives of the tubes can be calculated. The TGA measurements presented have been performed in the groups of Prof. A. Hirsch, university of Erlangen, Germany and Prof. I. Kallitsis, university of Patras, Greece.

#### Transmission spectroscopy

Optical spectroscopy is among the most often used methods for characterization of carbon nanotubes. Usually the recorded transmission $T$ is converted to optical density by taking $-log\, T$. The nanotube spectra show distinct peaks in the visible and near infrared range corresponding to transitions between Van Hove singularities in the density of states [38]. Transmission spectroscopy provides information about the electronic structure of the nanotubes. The absence of resonance conditions makes this method suitable for measuring all nanotube species in the sample, but lacks the possibility to assign these features to specific tubes. By investigating the spectra of functionalized material, one may observe shifts in the transition energies or a frequency dependent decrease of transition intensities. As a functional group can highly influence the solubility of tubes in certain (organic) media, the intensity decrease is sometimes gilded by improved solubility [27]. The transmission spectroscopy data presented here was recorded in the group of Prof. K. Kamaras, university of Budapest, Hungary.

### High resolution transmission electron microscopy (HRTEM)

Electron microscopy is the analogue to common light microscopes with an electron beam instead of light. It uses magnetic lenses and benefits from (de Broglie) wavelengths of electrons being magnitudes shorter compared to visible light. In Transmission electron Microscopy (TEM) a beam of electrons is transmitted through an ultra thin sample, interacting as it passes through. The image formed by the interaction is magnified and then detected by a sensor, e.g., a charge coupled device. The first TEM was built by Ernst Ruska in 1931 [39], who was awarded the Nobel prize in 1986. At acceleration voltages below 100 keV, nanotubes are supposed to be undamaged by the irradiation of the electron beam [40]. At this voltage, the theoretical resolution for electrons is about 4 pm, compared to about 0.2 $\mu$m for visible light. The HRTEM pictures were made by the group of Dr. Carola Meyer in collaboration with AG Urban at the Forschungszentrum Jülich, Germany

*These nanotubes are so beautiful that they must be useful for something.*

Richard Errett Smalley

# 3

# Functionalized Carbon Nanotubes

Functionalization is - generally spoken - the chance for a well-defined reaction of the tube to a special environment. For example, this could be the solubility in certain media [41]. Naturally it fired the chemist's imagination to apply all the powerful procedures of organic chemistry developed for decades to the new carbon allotrope. But it turned out to be challenging to handle nanotubes, because they are difficult to dissolve in water or common organic media. The variety of nanotube chemistry is still not as rich as compared to, e.g., fullerene chemistry. However, various types of reactions have been established, and the possible ways to functionalize carbon nanotubes can be divided in (see Fig. 3.1):

- non-covalent functionalization: it is mainly based on supramolecular complexation due to adsorption forces, namely van der Waals and $\pi$-stacking interactions
- functionalization of defects: defects in carbon nanotubes can be the open caps of a tube or holes in the sidewalls or so-called (7,5) defects, which means an irregularity in the hexagon framework of an tube.
- direct and covalent functionalization of the sidewalls accompanied by a change of hybridization from $sp^2$ to $sp^3$. Addition reactions have been established with various moieties.[1] Covalent functionalization of the sidewall through addition reactions has become promising for targeted modifications of nanotubes, although there are still difficulties concern-

[1] The word "moiety" is often used synonymously to "functional group" in the present work, although, according to the IUPAC definition, a moiety is a part of a molecule that may include functional groups as substructures [42].

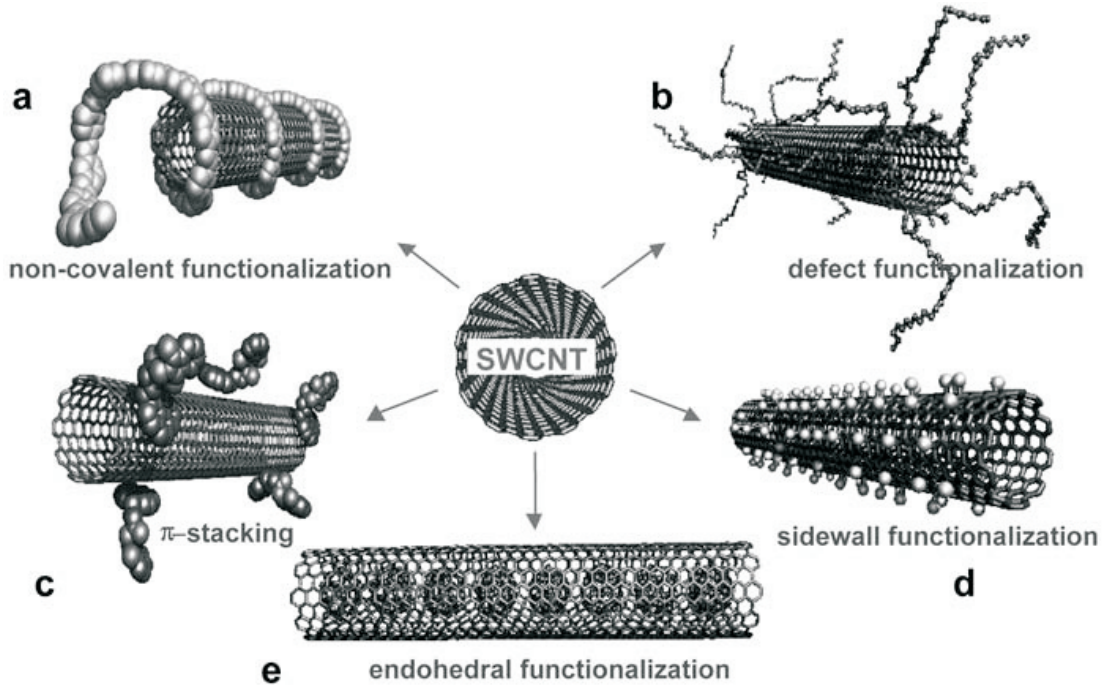


Figure 3.1: Different ways of functionalization, Fig. from Ref [45].

ing the regioselectivity, and it is still a challenge to find the exact localization of functional groups [43].

– endohedral functionalization, one might object it does not fit in this list, because it is not exactly an organic chemistry topic. Endohedral functionalization means filling the tubes with small atoms or molecules, e.g., with fullerenes. This filling leads to the so-called “peapods”, playing a major role in the production of double-walled nanotubes and it also leads to the fancy field of “isotopic engineering” [44] (see Chapter 3.3).

This chapter focuses on covalent addition reactions to the sidewalls of nanotubes. It shows the power of Raman experiments constituting conclusive evidence for successful reactions and giving the opportunity to study the different reactivity of various nanotubes driven by their different electronic bandstructure or diameter dependent curvature effects. The chapter introduces the recording of resonance profiles from the radial breathing mode to study the effects of functionalization. Also the impact of addition reactions on the other Raman features is discussed.

## 3.1 Covalent Sidewall Functionalization

Covalent sidewall functionalization of carbon nanotubes has become a key issue for a variety of nanotube applications and therefore the chemical reactions have been reviewed in many related articles [46, 47]. To attack the tubes framework one has to overcome the problem of low inherent reactivity of the tube. However, various addition reactions have successfully been applied, they all have in common fairly harsh reaction conditions to attack the tubes' sidewall [48], so-called "hot addends" like halogenes, carbenes etc. have been used to form chemical bonds [45]. One method is the nucleophilic addition of organometallic reagents such as alkyl lithium [49] lithium amides [50] and lithium acetylides [51]. A major task of synthesis and characterization is the improvement of the solubility of carbon nanotubes in certain media.

In the beginning most of the work on functionalized tubes focused on whether or not a reaction took place and on characterization of the new material. Graupner *et al.* [32] reported a new reaction sequence for the sidewall functionalization of single-walled carbon nanotubes (SWNT), treated with $t$-butyllithium and a reoxidation of a $t$-Bu$_n$SWNT$^{n-}$ intermediate state to an uncharged $t$-Bu$_n$SWNT. In their Raman studies they report on the defect mode ($D$ mode) and the high energy mode (HEM): an increase of the $D$ mode and a different, less shouldered line shape in the HEM is observed. After an annealing process the $D$ mode is reduced again and the original lineshape of the HEM is restored. For this reason one can rule out selective destruction or removal of tubes due to the addition reaction. Concerning the radial breathing mode (RBM), most of the literature focuses on a small number of laser lines used for excitation, usually measurements at 532 nm and 633 nm excitation wavelength are made [7, 52]. These energies display the resonance windows of both semiconducting and metallic tubes.

The first measurements in the present work were established on nanotubes functionalized with alkanes of various chain length. More or less accidentally this offered the possibility for a quasi "evolutionary" study of functionalization, with alkyl groups not being "functional" in a narrower sense [42]. For the first measurements pentyl-SWCNT were used functionalized by reductive alkylation with sodium and 1-bromopentane in liquid ammonia. The bulk-like samples contain 1.7 % alkylated C atoms, as determined by thermogravimetric analysis. Additionally, a reference sample from the same raw material as the functionalized one was used for comparison. Both samples were HiPCO-grown and HCl-purified.

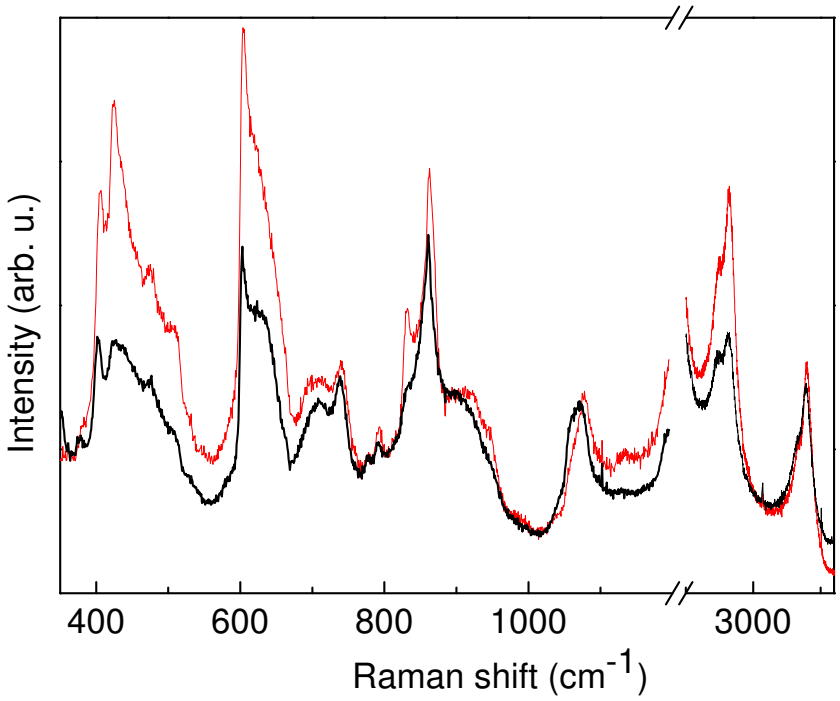


Figure 3.2: Raman spectra of pentyl-functionalized carbon nanotubes and an unfunctionalized reference (black) in the region of the intermediate-frequency region of carbon nanotubes. The shaded areas show the enhancement due to functionalization. At frequencies $\geq$ 2600 $cm^{-1}$ the C-H-stretch vibration and the second order of the HEM ($\approx$ 3200 $cm^{-1}$) are seen.

### 3.1.1 Evidence for the addition reaction by Raman spectroscopy

At a first glance three pieces of Raman-spectroscopic evidence for the functionalization seem promising: a) Additional lines in the spectra due to the alkyl group, b) strong C-H stretching vibrational modes and c) an increase of the $D$ mode and other defect-related modes of the carbon nanotube. The most common way to show by Raman spectroscopy whether a reaction to the sidewalls of carbon nanotubes has occured is to analyze the lineshape of the high energy mode and the intensity of the $D$ mode [53]. This is natural, because for most commercially traded Raman systems these features are observable with “one shot”, as the Raman shift between the modes is

only about 300 cm$^{-1}$, which is small compared to common gratings in the visible range of light. For more direct evidence, one has to search for vibrational modes of the added groups (here: pentane) in the tube spectra. Fig.3.2 shows two lines around $420$ and $830$ cm$^{-1}$. These two additional lines are in good agreement with the lines to be observed for pure pentane [54]. The strongest lines of pentane occur at $(2800 - 3000)$ cm$^{-1}$, the region of the carbon-hydrogen stretch vibration. As can be seen in Fig. 3.2, there is a strong signal enhancement in this region in the pentyl-SWNT compared to the signal in the reference sample. We also expect to observe lines around $(1200-1500)$ cm$^{-1}$, but the strong $D$ mode in that region makes them difficult to detect. We thus have direct spectroscopic evidence that the functionalization with pentyl groups was successful. However, this is only possible for samples of higher degrees of functionalization and one has to be lucky that the lines are not varnished by stronger lines coming from the nanotubes. The measurements in the so-called fingerprint region of many functional groups are in the range of the intermediate frequency modes of the nanotubes, which is very rich of features and makes the whole procedure difficult and time-consuming.

As mentioned before, an independent and powerful piece of evidence for the functionalization is given by the $D$ mode in the Raman spectrum at $1330$ cm$^{-1}$ in Fig. 3.3. The intensity of this mode, which is seen in the Raman spectra through a double-resonance process [55], is proportional to the defect concentration in a nanotube. A successful sidewall functionalization breaks the translational symmetry, relaxes the Raman selection rules, and shows up in the spectra as an increased $D$ mode. Another way of looking at this is that $sp^3$-hybridized C-atoms in the place of $sp^2$-bonded carbon in the nanotube contribute to the intensity of the mode at $1330$ cm$^{-1}$. In Fig. 3.3 one can see that the intensity of the $D$ mode increases by a factor of 1.8, normalized to the second-order mode D* [13]. The $D$ mode confirms the addition reaction of pentane to the sidewall of the carbon nanotubes. A similar increase in intensity is noted for the signal near 450 and 650 cm$^{-1}$ (shaded areas in Fig. 3.2) for modes already present in the reference material. These so-called intermediate frequency modes are partly defect induced as well [56], and thus are increased for similar reasons and by a similar amount as the $D$ mode.

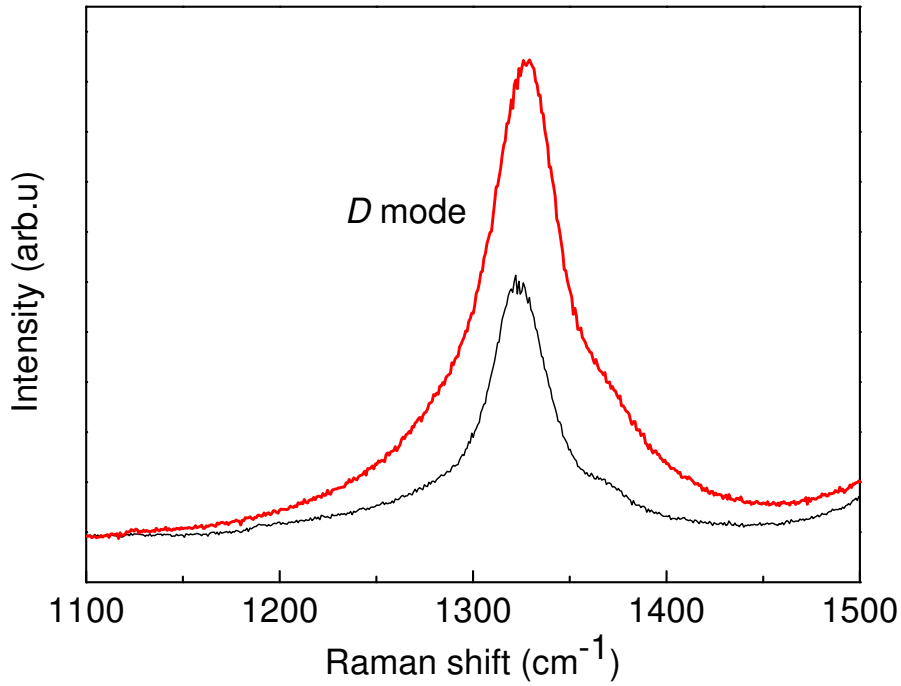


Figure 3.3: The $D$ mode intensity of pentyl-functionlized carbon nanotubes almost doubles compared to the reference sample . The D mode is much stronger than the intermediate-frequency modes in Fig. 3.2. The excitation energy was E=1.96 eV.

### 3.1.2 Radial breathing mode and resonance profiles

From the resonance profiles it is possible to obtain the transition energies $E_{ii}$ and assign the chiral index $(n, m)$. Recording resonance profiles in the case of functionalized material only makes sense comparing both reference and functionalized nanotubes, because the absolute values of the optical transitions are often changed during preparation even without the addend due to changes of the environment. For example, compared to the isolated nanotubes in solution used in Ref. [23, 24] the observed transition energies are shifted about 60-70 meV to lower energies due to the bundling in the samples [28].

Comparing the transition energies of alkane-functionalized and reference nanotubes it is obvious that they are very similar, possibly slightly red-shifted (a few meV) compared to non-functionalized data. The width of the profiles

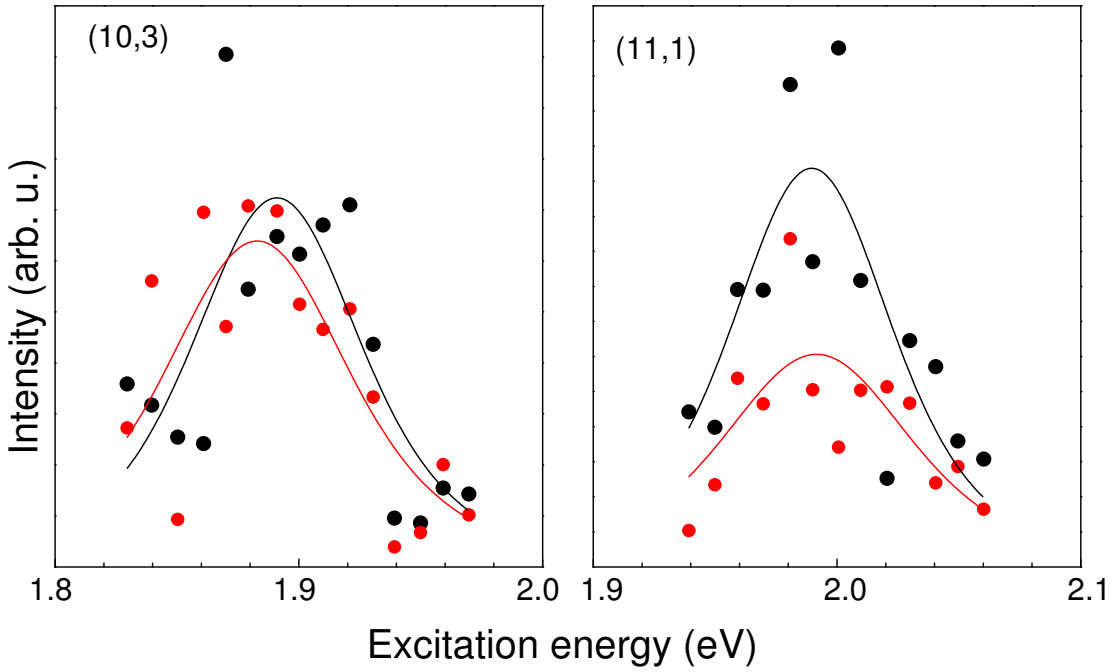


Figure 3.4: Resonance profiles taken from a pentyl-functioanlized sample (red) and the pristine nanotubes (black). The alkane functionalization only causes negligible shifts of the transion energies.

is about 70 meV. The small influence on the transition energies reveals the non-functionality of the added alkanes, and it shows up what will become even more important discussing the influence of different moieties to the electronic structure: the combined investigation of all Raman features allows to separate effects into structural or defect-related effects on the one hand and direct impact on charge transfer or doping effects on the other hand. Only observing one feature may lay a false trail.

### 3.1.3 Influence on RBM frequencies

So far the RBM features have been discussed in terms of resonance profiles, but somehow this is like walking before one can crawl. It is worth stepping back to the spectra itself, Raman shifts and intensities and how

Table 3.1: The assignment of the strongest Radial-breathing modes observed for the used excitation energy range, according to Ref [23]. Various-chirality nanotubes of the reference material and after functionalization with $n$-pentane, the typical experimental accuracy is about 1 $cm^{-1}$.

| $(n,m)$ | $RBM_{ref}$ | $RBM_{funct}$ |
|---|---|---|
| (13,4) | 196.1 | 196.2 |
| (11,1) | 255.3 | 255.7 |
| (10,3) | 250.5 | 251.3 |
| (7,5) | 281.7 | 282.7 |
| (8,3) | 295.2 | 296.7 |
| (12,2) | 223.9 | 224.6 |
| (9,9) | 191.8 | 192.5 |
| (10,7) | 203.2 | 204.6 |
| (11,5) | 211.3 | 212.2 |
| (12,3) | 216.6 | 216.7 |

they are influenced by added groups. Table 3.1 shows data for a pentyltube sample with 1.7% degree of functionalization. The radial-breathing mode frequencies tend to shift to slightly higher energies. For most peaks the shift is within the experimental accuracy of about 1 $cm^{-1}$, but it holds for all measured tube chiralities.

For a more detailed study of the upshift of the RBM a pair of samples functionalized with amines to different degrees (2% and 6%) has been investigated (see Fig. 3.5). Predominant at a first glances is the data divides into tubes with only slight and tubes with more pronounced shifts, respectively. This could be understood either in terms of a different reactivity of certain tubes, changes of the environment (like debundling etc.) or in another effect of added groups towards shifts of different nanotubes itself. To answer this it is helpful to adapt an analytical approximation by Dobardžić *et al.*, they studied the radial breathing mode of double-walled carbon nanotubes in an analytical approximation using coupled oscillators [57].

Their results can be qualitatively transferred to exohedral functionalization: though the coverage of the tube is less for a functionalization, the force constant of each bond is much higher for a covalent bonding than in case of the Van-der-Waals interaction between an inner and outer tube. The shifts can be understood as the moiety is sticking to the tubes' sidewall with a certain spring constant. In any case the model predicts an upshift of the Raman frequency that fits perfect to the observed findings. For small diameter tubes the approximation for the upshift is:

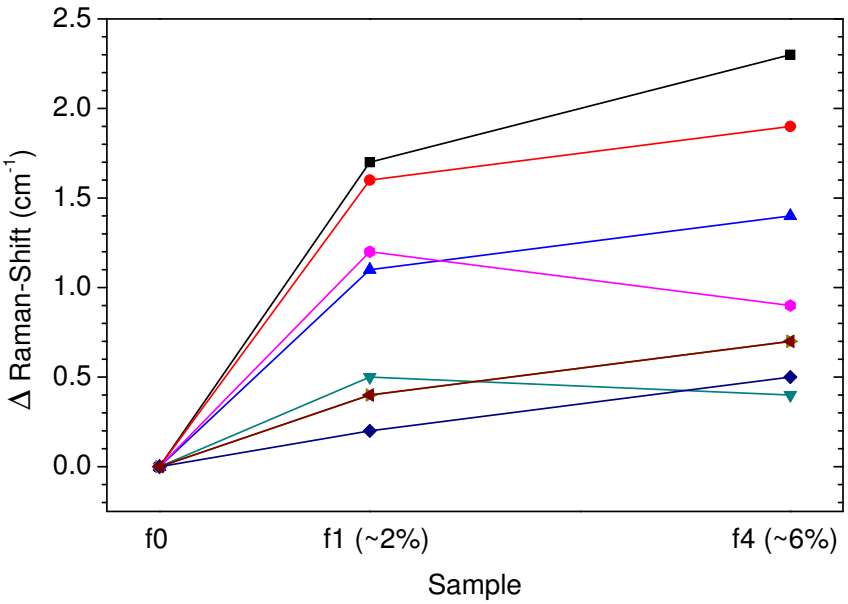


Figure 3.5: Up-shift of RBM frequencies due to functionalization: pristine material and two functionalized samples with different degrees of functionalization (2% and 6%).

$$\Delta\omega \approx \frac{k}{2m\omega_{RBM}}$$

Fig. 3.6 shows the RBM shifts for all observed tubes as a function of tube diameter: the inverse behavior to RBM frequency is a strong evidence to show the model works properly, because it is countered by the diameter dependence of the reaction itself which is discussed in section 3.2. Hence a real system is not as homogeneous concerning the reactivity, the moieties will be preferably added to small diameter tubes, i.e., larger $\omega_{RBM}$. This would lead to an opposite effect on the shifts as observed, so it can be ruled out to be the reason for the observed upshifts. It shows up that the shifts are less pronounced between the 2% and 6% samples than between the pristine and 2% sample which also stresses that the different reactivity is not of great impact for the RBM frequencies. Another point that can be ruled out is the different environment or debundling effects. In contrast to the transition energy the frequencies are not affected by bundling as shown by O'Connell [28]. In conclusion the simple mechanical model allows to refer the RBM shifts directly to the sidewall functionalization.

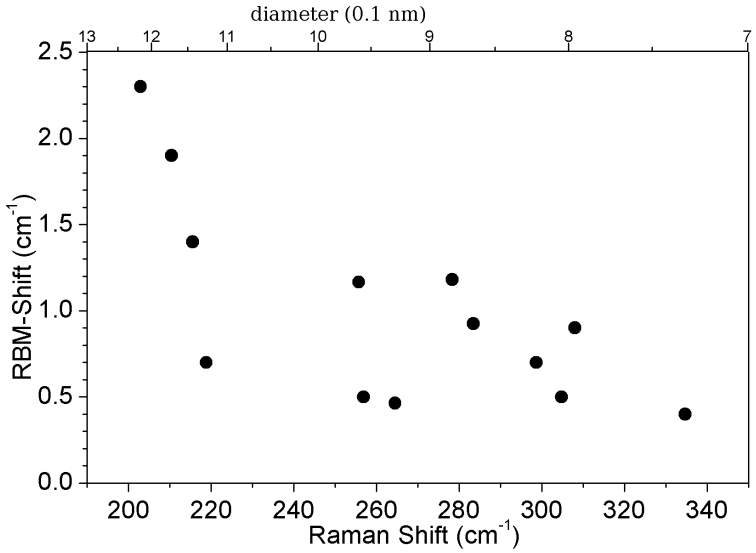


Figure 3.6: RBM shifts as a function of diameter, shifts tend to be higher for larger diameter.

### 3.1.4 Attenuation of Raman features due to functionalization

Sidewall additions especially lead to an attenuation of the radial breathing mode. The decrease due to functionalization can be described as a disruption of the electronic structure, i.e., a disruption of the extended $\pi$-conjugation of nanotubes causing a loss of free electrons in the periodic potential responsible for the formation of van Hove singularities [58, 59].

The decrease of RBM, combined with an increase of the $D$ mode, is the most common analysis to study selectivities of chemical reactions (see section 3.2). At times the decrease is suchlike pronounced that a recording of resonance profiles becomes impossible due to a low signal to noise ratio or even the signal for certain tube chiralities completely vanishes sometimes. Not only the radial, but also the tangential mode peaks in the Raman spectra can be drastically influenced. This can be impressively observed on tubes functionalized with perfluorocarbons. Due to their heavy weight the influence on the Raman intensities is much higher than those of the comparable hydrocarbon samples. Fig. 3.7 shows Raman spectra recorded from perfluorhexane-functionalized nanotubes and the starting material for comparison. Most of the RBM features are vanished (3.7(a)) and the high energy mode has been reduced to a small $G^+$ peak, the $G^-$ peak almost

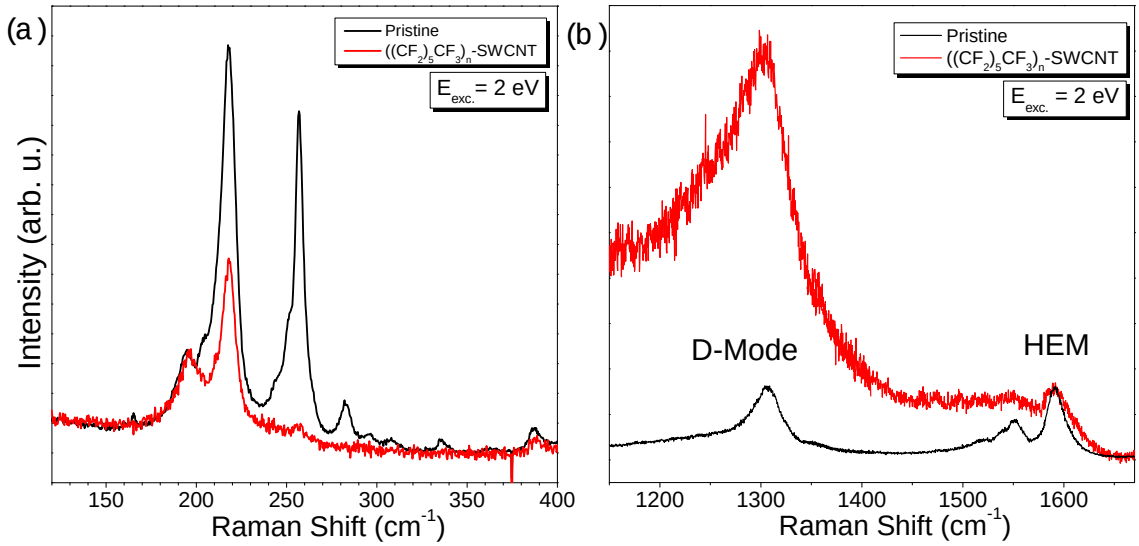


Figure 3.7: (a) Radial-breathing mode for highly functionalized material (red, black: reference), showing strong attenuation. The intensity is normalized to the very left peak in the spectrum. (b) The high-energy mode almost vanished, accompanied by an enormous increase of the defect mode.

got lost in the noise. The substantial decrease of most Raman features accompanied by an enormous increase in the $D$ mode indicates disruption of the $\pi$-bonded structure of the sidewalls, suggesting both a high degree of functionalization and possible changes on the framework itself.

## 3.2 Reactivity of Carbon Nanotubes

A nanotube is a quasi 1-dimensional cylindrical aromatic system, and therefore it is expected to be fairly chemically inert. However a growing number of reactions is reported, leading from flourination [53] to nanotube composites [60]. Selectivity of a chemical reaction to carbon nanotubes has been a hot topic right from the start, because it allows exactly the selection which is not offered during the common growth processes. The driving force of carbon nanotube chemistry is the local strain relaxation, whereas strain is a result of either $\pi$-orbital misalignment - which is the main source of strain in carbon nanotubes - and curvature - induced pyramidalization. Both effects scale inversely with diameter, hence a diameter dependence in reactivity of nanotubes is expected. Higher reactivity of either tube species, especially

metallic tubes has been observed with various moieties [32, 61], and well-established theoretical concepts do explain this [7, 62]. Additionally steric demands of the addends for the reactivity have been reported [63]. Reaction conditions, sort of addend and degree of functionalization probably play a decisive role which demands are becoming more or less predominant. However, the major effects of selectivity are tube species and diameter.

### 3.2.1 Selectivity on Tube Species

Discussing the reactivity of any kind of molecules, the well-established chemistry concepts are aromaticity, HOMO-LUMO structure and orbital symmetry, which are discussed in real space (e.g. Woodward-Hoffmann rules [64] or frontier orbital theory [65]). The different reactivity of semiconducting and metallic carbon nanotubes has been explained by various chemistry concepts by Joselevich, stating the metallic species as less aromatic and having a smaller HOMO-LUMO gap [62]. On the other hand the more solid state physics-like language, using the bandstructure in reciprocal space, density of states etc. is successful in the prediction of the selectivity of addition reactions driven by the metallic or semiconducting characteristics of a tube. The interlink between the two pictures is the Hückel molecular orbital method, using a linear combination of atomic orbitals (molecular orbitals) for the calculation of energies of molecular orbitals of $\pi$-electrons in conjugated hydrocarbon systems. It is somehow analogous to the tight-binding method, which is more familiar in solid state physics. In the bandstructure picture, the higher reactivity of metallic tubes is explained by their non-vanishing density of states at the Fermi level. The density of states (DOS) near the Fermi level shows a more or less constant value for metallic tubes in a range of about 1 eV around the Fermi level and a vanishing DOS for the semiconducting in a range, which is also about 1 eV around the Fermi level [66]. The allowed states at the Fermi level lead to the stabilization of transition states during the covalent attachment of an electron rich functional group to a nanotube [67]. A preferred reaction to metallic tubes has been reported for different molecules, e.g., diazonium salts [67] or metallorganic molecules like tert-butyllithium [32].

A selectivity towards semiconducting tubes has been observed by Miyata *et al.*, reporting on $H_2O_2$-oxidized nanotubes [68]. They suggest that semiconducting SWCNTs are more reactive than metallic SWCNTs because of hole-doping by $H_2O_2$, resulting in faster oxidation.

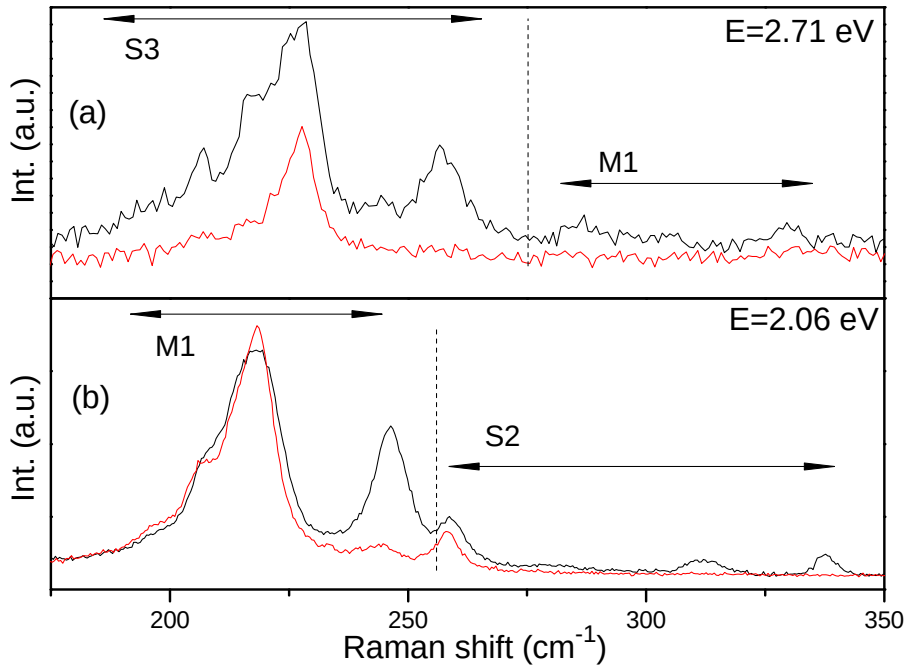


Figure 3.8: Raman spectra of carbon nanotubes functionalized under modified birch conditions (red) and reference sample (black). The intensities are normalized to the G mode.

To probe the selectivity of either nanotube species towards a certain reaction mechanism it is essential to separate this effect - as much as possible - from the diameter dependence, which is pronounced for both tube species. In most cases a change in a relevant Raman feature, especially an attenuated RMB intensity, is caused by an overlap of both effects. To overcome the diameter effect, one has to measure in two different ranges of excitation energies where in the first range large diameter metallic and small diameter semiconducting tubes are resonant and vice versa in the second range. However, one always observes a *preferred* tube species, not an *exclusive* reaction.

The preferred reaction to the semiconducting tubes in our samples has been achieved by a modified Birch reaction pathway (for more preparation details see A. In a first step the tubes are negatively charged and the $(SWCNT)^{n-}$ is then further functionalized by the electrophilic reagent.

The two excitation energies, 2.71 and 2.06 eV, used for measuring have also been used in [68] and can be separated to diameter and tube species according to Refs. [23, 69]. Fig. 3.8 (a) can be separated into optical transitions belonging to large diameter semiconducting ($E^S_{33}$) and small diameter

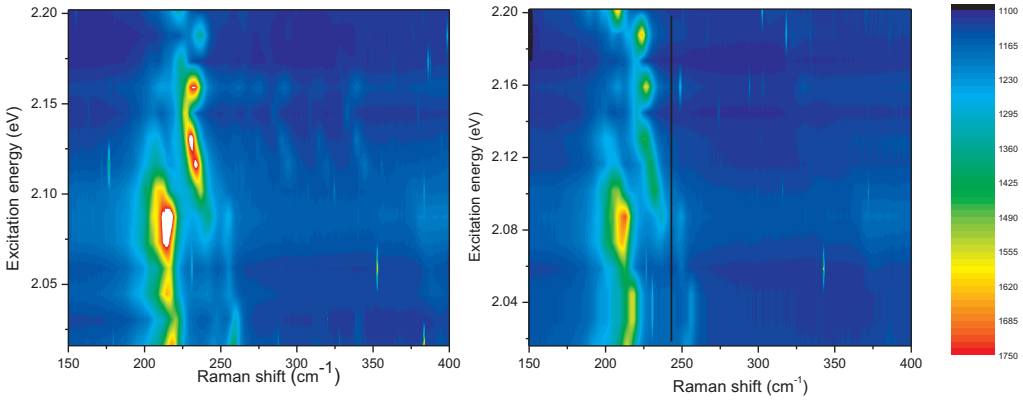


Figure 3.9: Raman 3D-plots of pristine (left) and functionalized (right) material. The functionalized groups obviously do not cause significant shifts of the optical transitions, which allows to compare single spectra for particular excitation energies.

metallic ($E_{11}^M$), whereas in (b) the RBMs can be assigned to larger metallic (again $E_{11}^M$) and smaller diameter semiconducting ($E_{22}^S$). So the two excitation energies $E_{Exc}$ = 2.7 eV and $E_{Exc}$ = 2.1 eV offer a complementary diameter distribution.

To check if the intensity changes are only "accidentally", driven by a shift of the resonance window, the samples had to undergo a more detailed study recording RBM data in a range between 564 nm and 613 nm. In this energy range various metallic and semiconducting tubes are resonant. The 3D plots in figure 3.9 show the data of fourteen single spectra. They prove that the optical transitions are only slightly redshifted by the carboxyl functionalities and therefore it is sufficient to compare the RBM data of the samples at one particular exciation energy. Additionally the plots confirm that the carboxylated material shows a pronounced signal for metallic tubes except for small diameter chiralities, whereas the semiconducting are almost vanished. Only the very intense signals survive, but are tremendously decreased. This ensures that the semiconducting tubes are more reactive for the applied procedure, but there is obviously an additional diameter effect. The preferred functionalization of the semiconducting species might be understood in terms of the Fermi level. Miyata *et al.* state their hole-doping procedure to shift the Fermi level into the first van Hove singularity. This would cause a drastic increase of allowed states next to the level even compared to the metallic tubes. This stabilizes intermediate states of the

reaction and therefore prefers the semiconducting species. This argument follows the same trace as usually given for the metallic tube reactivity. It is well-known from solid state physics, that the Fermi level in semiconductors is much more sensitive towards doping effects than this of a metal. In a metal the Fermi energy is equivalent to the work function, which is almost independent from adding charge to the metal. In contrast, little doping of a semiconductor introduces donator or acceptor states close to the edges of the band gap, and for higher doping levels the semiconductor degenerates, i.e., the Fermi energy shifts into either valence or conduction band. Transferring this to the different tube species reveals the observed behavior: the reactivity to metallic tubes should stay the same, because the DOS keeps constant during the doping process. Therefore, the metallic tubes - especially of small diameter - keep being reactive, but under special reaction conditions, they are less affected than the semiconducting. This is in excellent agreement with the observed data.

However, this picture seems incomplete. If the argument holds for all reactions using charged intermediates, *all* reactions should become selective to semiconducting tubes at a certain degree of functionalization, because the bandsturcture/DOS argument is fully symmetric. The DOS in semiconducting tubes will be dramatically increased in both cases, an up- or downshift of the Fermi level, i.e., both types of doping. Whenever the first van Hove singularity is reached, the samples should show the same behavior. The selectivity would only be driven by the *degree* of functionalization, and be independent from the functional group itself. The carboxylated material has also been analyzed by thermogravimetric analysis, revealing a degree of functionalization of about 3.1 %. This is not extraordinary high compared to many other reported reactions and the carboxyl group is not supposed to be of stronger impact on the electronic structure than most of the other functionalities. In fact, the analysis of their resonance profiles implies a shift of only about 20 meV, which is compaprable to other samples (see Chapter 4). Therefore the influence on the position of the Fermi level should not exceed those compared to most nanotube derivatives. This implies that a lot of groups working in the field should have observed a comparable effect, which is not the case.

In addition to bandsturcture/DOS arguments, it seems useful to discuss the effect of the modified Birch conditions on the tubes in the real space picture and what drives the reaction in this concept. The addition occurs due to the coulomb interaction between the negative charge, which was introduced to the tube by the birch conditions, and the addend. The charge in the

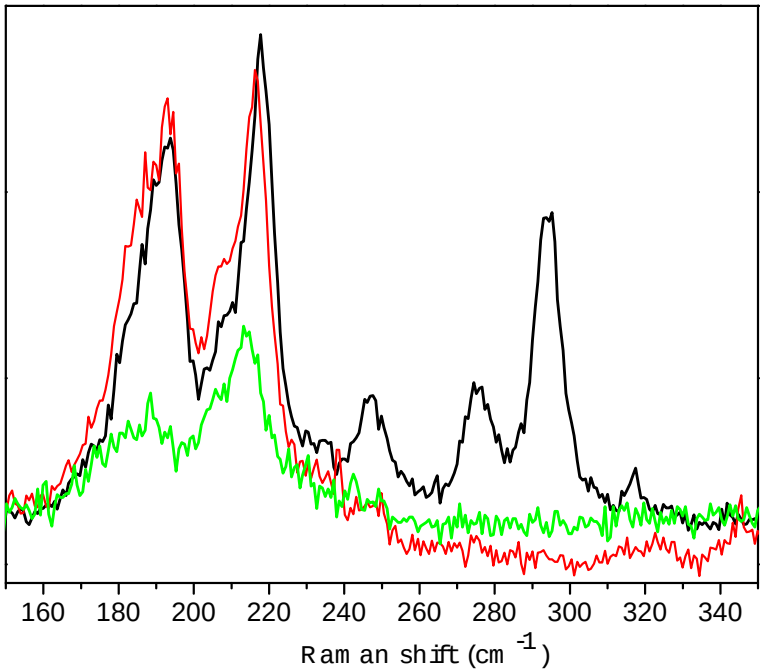


Figure 3.10: RBM signal of $CO_2$-tubes (red) and defunctionalized(green) material after thermal treatment in TGA. Obviously the RBM features are not fully restored by thermal treatment compared to the pristine material (black).

metallic tubes is completely delocalized, whereas in the semiconducting the transferred charge should be more localized. This seems beneficial for the addition of the functional group, because the electrophilic reagent needs the charge for the attack of the tube sidewall. Therefore the preferential reaction of semiconducting tubes is also very likely in this picture.

After thermal treatment in the TGA, the material was again analyzed with Raman spectroscopy. The heating process usually restores the Raman features of the pristine sample, due to annealing of defects and the reduction of amorphous carbon it is often observed that the TGA treated samples show an even smaller defect mode than the starting material (e.g., section 4.1.1). In case of the $CO_2$-derivatives the results are different: after annealing, the $D$ mode is decreased but still more than double of the starting material. Additionally, the RBM data of the tubes is not restored completely. In contrast to restoring, the signal of semiconducting tubes is still almost vanished, whereas the metallic tube signals are even more pronounced than in the functionalized or pristine material. This leads to the conclusion that the addition of carboxyl groups has led to a lower thermal stability of the functionalized tubes. As the semiconducting (and the small diameter metal-

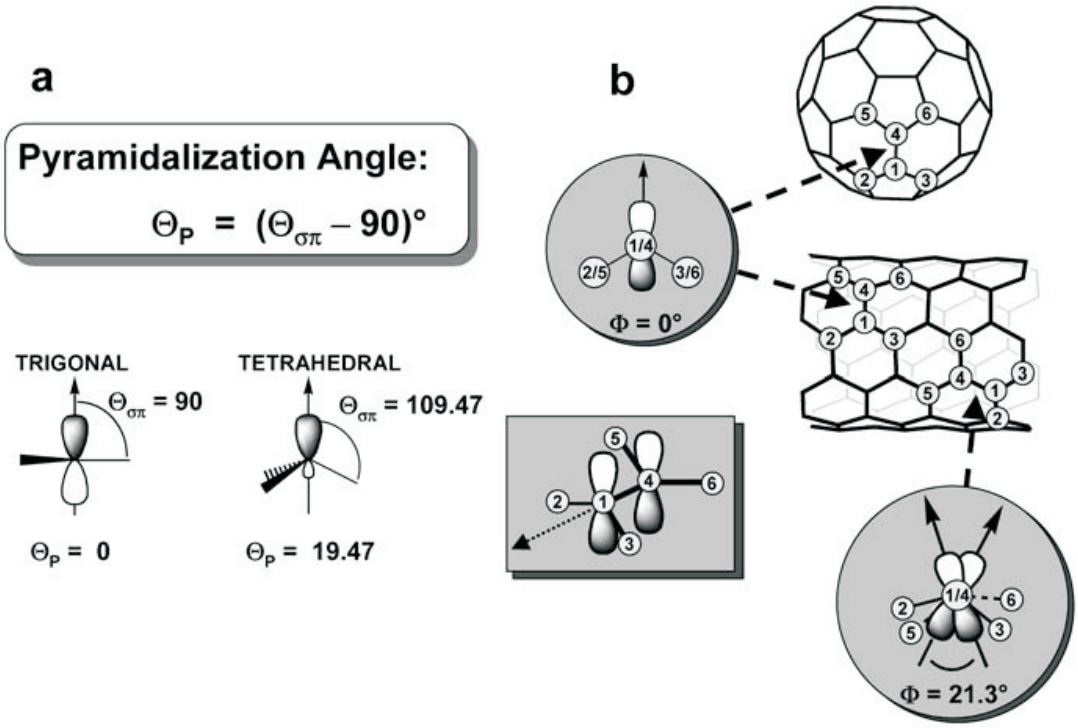


Figure 3.11: The pyramidalization angle describes the difference from a given structure to a trigonal planar structure. For fullerenes the angle is large due to their two-dimensional curvature, for nanotubes it is less, revealing the lower chemical reactivity. From Ref [45, 70].

lic) tubes are observed to react preferably, their signal is erased from the spectra, whereas most of the metallic tubes survived the heating and are now quasi enriched in the $df$-$CO_2$-derivatives. This shows up in their RBM signal.

### 3.2.2 Selectivity on Tube Diameter

As a further effect Niyogi *et al.* were the first to predict the reactivity being diameter dependent [70]. More precisely it depends on the pyramidalization angel of the carbon atom where the reaction takes place and $\pi$-orbital misalignment angles in different carbon nanotubes. the pyramidalization angel $\Theta$ is definded as the angle between the $\pi$-orbital and the close-by $\sigma$-

bonds, minus 90° (see Fig.: 3.11). This concept also reveals the different chemistry of fullerenes and nanotubes. Since the curvature of a buckyball is in two dimensions, the pyramidalization angle is larger for comparable structures, i.e., structures of same diameter. The strain energy is approximately proportional to $\Theta^2$, so fullerenes are driven by exceptionally higher strain than nanotubes. Generally speaking, an $sp^2$ bonded carbon prefers a planar structure ($\Theta = 0$) whereas an $sp^3$ is preferably tetrahedral ($\Theta = 19.5°$). The hybridization locally changes with attachment and therefore strain can be partially relaxed by sidewall addition [71].

Full resonance profiles for various tubes and samples have been recorded, here showing profiles of the sample with highest degree of functionalization as it can be observed from the increase of the $D$-mode. The transition energies of all samples are shifted about 60-70 meV to lower energies compared to isolated nanotubes due to the bundling of the measured nanotube bulk samples [28].

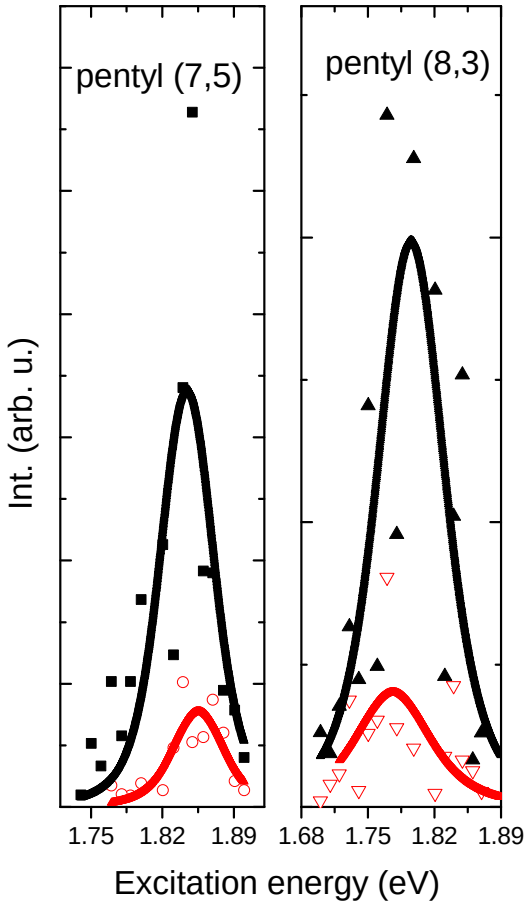


Figure 3.12: Resonance profiles of low-diameter (about 8 Å) RBMs: functionalized samples (red open symbols) and reference samples (black symbols). The profiles of the functionalized material indicate the strong attenuation of the RBM feature, the small shifts of the optical transition guarantee, that it is due to the addend, not because of leaving the resonance.

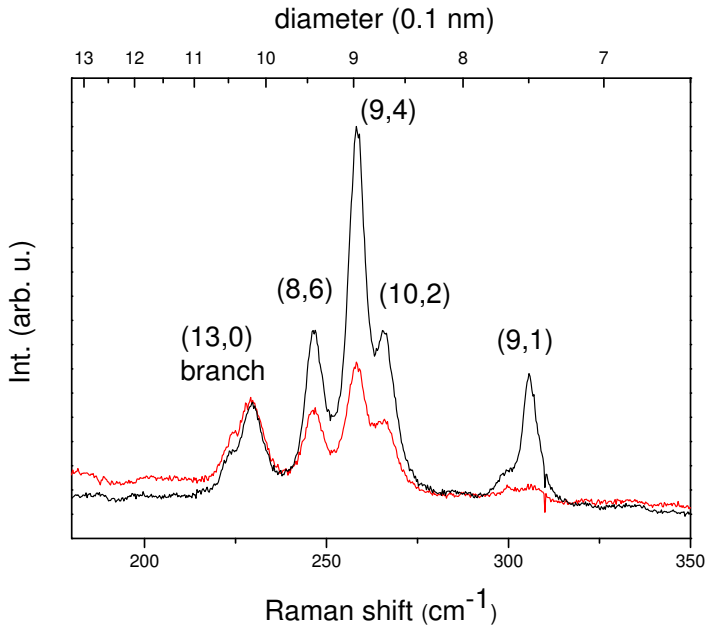


Figure 3.13: Raman spectra of pentyl-SWCNT (red) and non-functionalized reference sample (black) at 724 nm excitation, probing various semiconducting tubes.

Alkanes are very useful moieties for observing curvature effects, because a possible influence on the transition energies by functionalization is very small for non-polar bonds as between tubes and alkanes, especially compared to the full width at half maximum of the profiles itself (see Fig. 4.8). This is important to show the effects of addition reactions to the sidewall on the RBM intensity. The remarkable decrease of the intensity is not because the resonance window is left, but possibly due to effects on the electronic band structure, influencing the resonant Raman process by decreasing absorption strength [7].

Therefore the decrease of RBM intensity reveals a successful addition to a certain tube and is a viable feature to probe preferential functionalization of certain nanotubes. The samples show a pronounced selectivity to diameter. Figure 3.13 shows the general trend in the RBM intensities of the functionalized tubes that are decreasing with higher Raman frequencies, i.e., smaller diameter. The figure illustrates the inversely proportional relation between reactivity and diameter: in the bigger-diameter region around 230 $cm^{-1}$ the RBM signals of both functionalized and reference sample are of comparable intensity, the signals of the middle-diameter region ($\approx$ 250 $cm^{-1}$) are remarkably downsized and small-diameter signals around 300 $cm^{-1}$ are al-

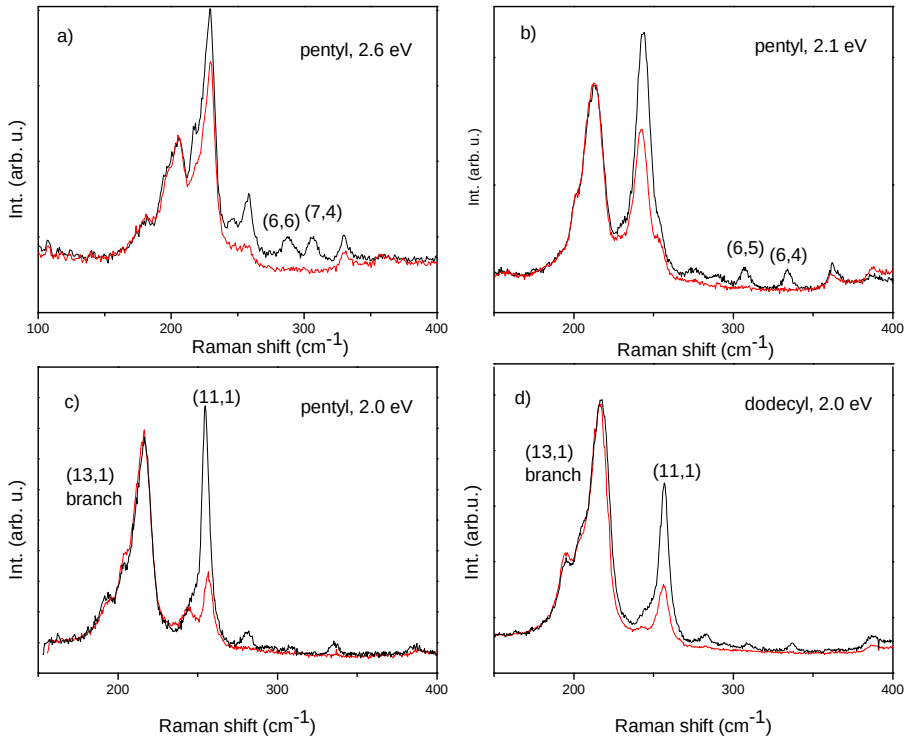


Figure 3.14: RBM of functionalized samples (red) and reference samples (black) at different excitation energies. The signal is decreasing or even vanishing with higher frequencies for both metallic and semiconducting tubes (top) and holds for different chain length (bottom). The intensities are normalized to the very left band in the spectra.

most vanishing. It is worth pointing out that Fig. 3.13 shows semiconducting tubes only so that the downsizing can be attributed exclusively to the diameter effect in this case.

Comparing the different tube species reveals that the effect is present for both metallic and semiconducting tubes. One can see that both species generally display the same diameter-dependent behavior, signal related to small-diameter tubes is almost vanishing with functionalization. It is obvious for small-diameter metallic tubes like (6,6) or (7,4), and also holds for small semiconducting tubes like (6,5) or (6,4) (see Fig. 3.14 a), b)).

For primary alkyl groups the chain length, as expected, does not significantly influence this behavior. As shown in Fig.3.14 c) and d), for different moieties the RBM intensities show the same effect, quantitatively differences referring to slightly different degrees of functionalization. This holds for the whole range of excitation energies (roughly 1.7 - 2.6 eV). That shows

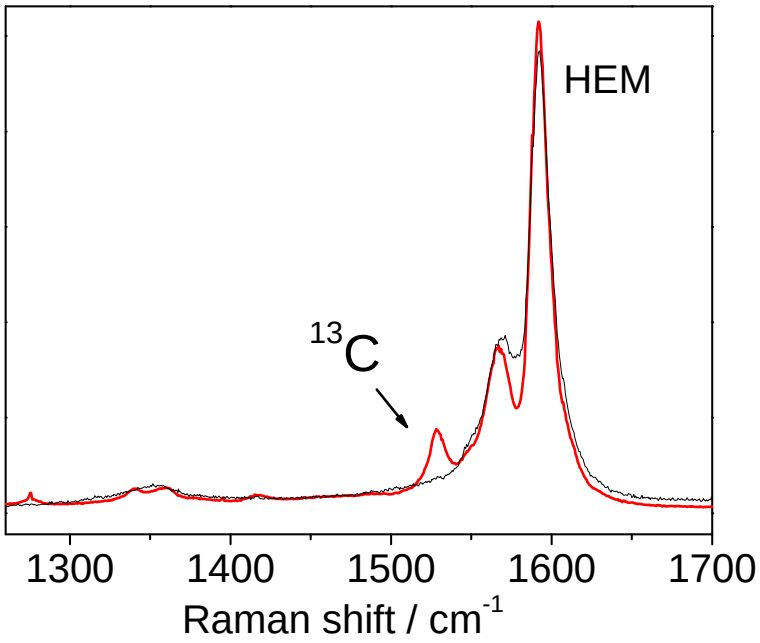


Figure 3.15: High Energy Mode of double-walled nanotubes, Black spectra: $^{13}C$ (outer tube), Red spectra: $^{13}C$ (inner tube)

the selective reactivity being inversely proportional to diameter is observable for both tube species.

## 3.3 Endohedral Functionalization and Isotopic Engineering

Double walled tubes have been prepared by fullerenes $C_{70}$ made of $^{13}C$ entering single-walled tubes due to high vapor pressure, so-called "peapods". At 1250 ℃ they transform into double-walled tubes with different types of isotopes: $^{12}C$ for the outer and $^{13}C$ for the inner tube [44]. The transformation can easily been checked with Raman spectroscopy, because new features emerge after a successful transformation. These new features appear at frequencies shifted by $\sqrt{12/13}$ (i.e. about 4%) because of the higher mass of the carbon isotopes the inner tube is made of. This is clearly shown in Fig. 3.15.

In this chapter the investigation of functionalized carbon nanotubes by Raman spectroscopy has been introduced. Chemical functionalization has a

great influence on all Raman features, especially the defect mode and the radial breathing mode are highly affected. Since Raman data allows an assignment to particular nanotube chiralities, it is a powerful tool to analyze the reactivity of a certain group of tubes in an ensemble. It has been shown that the reactivity of carbon nanotubes is mainly driven by curvature effects and additionally by the tube species. The next chapter elaborates on the impact of functional groups concerning the electronic structure of the nanotube derivatives.

*If you torture the data long enough, it will confess.*

Ronald Harry Coase

# 4

# Functionalization and electronic structure

The understanding of how a functional group influences the atomic structure of the tube and its electronic structure is an important topic in view of possible applications. Raman spectroscopy and transmission spectroscopy are powerful non-destructive techniques for the investigation of both structural changes in the tube lattice and changes of the electronic structure of nanotubes [12]. As discussed in section 3.2 the electronic structure and therefore the tube species are supposed to play a major role in the selectivity of the chemical reaction. This selectivity underscores the importance of the electronic structure in determining or may be designing a particular reactivity.

In this chapter the shifts of the transition energies and the broadening of the resonance profiles which can be observed are interpreted. The change of the tube environment leads to variations in the intensity of the radial breathing mode (RBM) showing the influence on the electronic structure. It is well-known that the optical transitions are highly sensitive to the tube environment, solvents, bundling, doping etc. [23, 28, 72]. Therefore, analyzing the influence of chemical modification one has always to take into account a possible overlap of these effects. Also structural changes such as defects in the nanotube also lead to changes in spectroscopic features [73]. Investigation of the defect-induced $D$ mode and high energy mode (HEM) after annealing indicates a highly efficient and well-controllable reaction that fulfills the requirement to preserve the intact tube structure, i.e., the sidegroups can be eliminated completely, leaving both the sigma- and pi-system intact. Therefore influences on the optical transitions due to structural effects can be ruled out making use of $all$ Raman features.

## 4.1 RBM and optical transitions

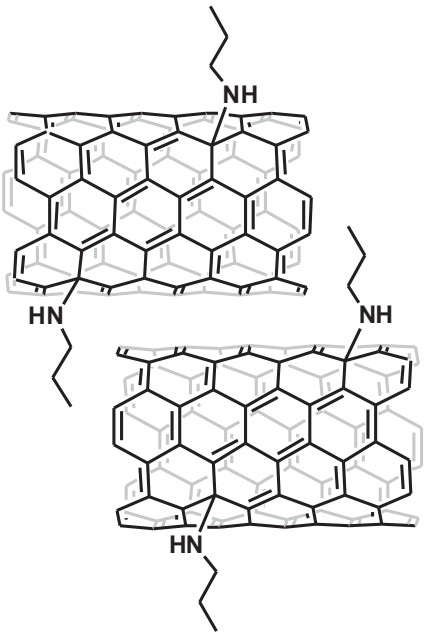


Figure 4.1: Sketch of a carbon nanotube structure functionalized with propylamine groups.

To study the effect on the optical transitions of single-walled carbon nanotubes samples with $n$-propylamine functionalization are very useful, because they provide a polar carbon-nitrogen bond on the tube surface. This is expected to influence the electronic structure much more than, e.g., an alkyl chain. The reaction used here is a two-step process: a direct nucleophilic addition followed by reoxidation in oxygen of a negatively charged $(n\text{PrNH})_n$-SWCNT$^{n-}$ intermediate that leads to covalently bound amine functionalities as shown in Fig. 4.1 [8, 50]. This reaction causes a drastic increase of the solubility of the SWCNT-derivative in organic solvents. Therefore a functionalization sequence based on amines provides a promising tool towards SWCNT derivatives with a rich variety of functional groups.

Full resonance profiles for the second transition of semiconducting tubes $E_{22}^S$ and the first transition of metallic tubes $E_{11}^M$ have been recorded, the chiral indices were assigned following the procedure of [23, 24]. Due to bundling the transition energy of all the samples including the starting material is redshifted in comparison to the data taken on dissolved nanotubes in the related articles. Fig. 4.8 (a) shows the resonance profiles of tubes belonging to the $E_{11}$-transition of the metallic (13,1) branch. Both functionalized samples show a pronounced redshift of the optical transition accompanied by a broadening of the resonance window compared to the refer-

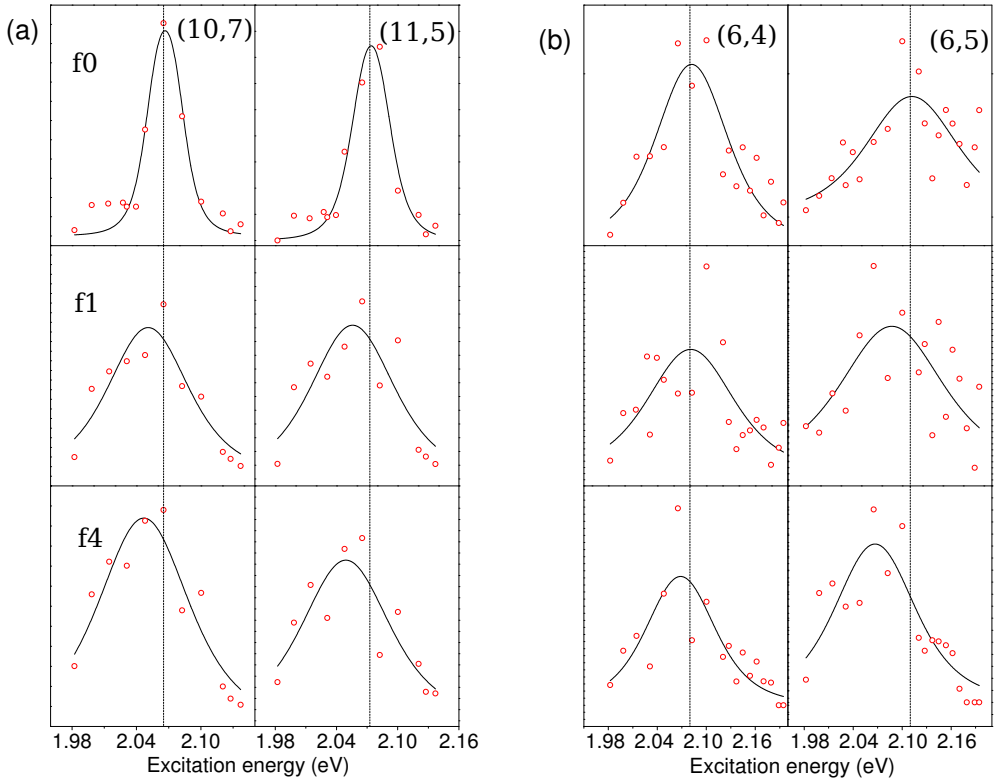


Figure 4.2: Resonance profiles: reference samples (on top), functionalized samples with 2%(middle, f1) and 6%(bottom, f4) degree of functionalization. (a) metallic tubes (b) semiconducting tubes. The profiles are fitted according to Ref. [23]

ence sample. Comparable effects are also observed for the $E_{22}$ of semiconducting tubes as shown in Fig. 4.8 (b). The average transition energy shift between the non-functionalized material and the functionalized samples is about 20 meV to lower energies for the lower degree of functionalization (f1) and about 25 meV for the higher one (f4) (see also Tab. 4.1). This is consistent with the findings concerning the tube reactivity: all data, including UV/Vis/NIR absorption show a redshift of the optical transition but do not indicate a selectivity between metallic and semiconducting nanotubes towards the direct nucleophilic addition [50].

The samples have also been characterized by transmission spectroscopy. Wide range transmission spectroscopy and Raman spectroscopy are complementary methods. By utilizing the benefits of both techniques one can make results more reliable. Changes in the electronic structure have direct influence on the features of the optical spectrum. Whereas the Raman

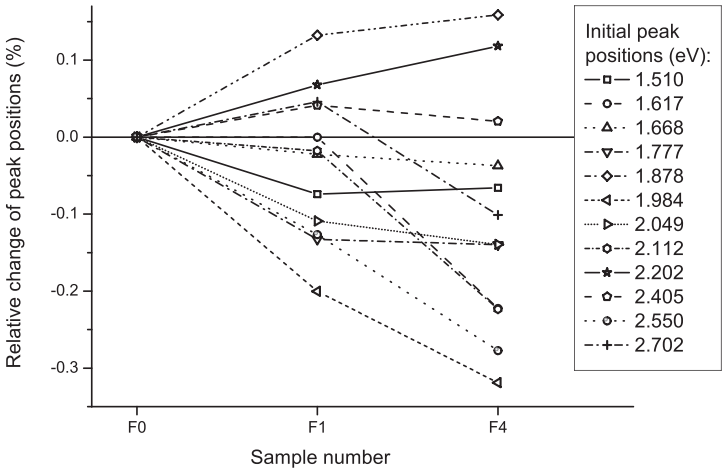


Figure 4.3: The evolution of the peak positions related to $E_{22}^S$ transitions from optical conductivity measurements. The plot shows the relative change in the position of the different $E_{22}^S$ peaks versus the sample type (from left to right: pristine tube (f0), lower/higher (f1,f4) functionalized sample).

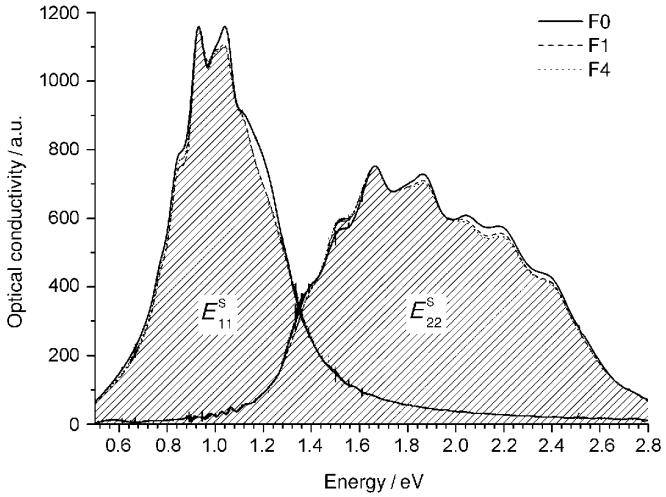


Figure 4.4: The effect of functionalization on the $E_{11}^S$ and $E_{22}^S$ transitions. The higher frequency part of the peaks decrease due to higher reactivity of the smaller diameter tubes. The area under the peaks related to the higher functionalized sample was striped to emphasize the change in the intensity.

| (n,m) | sample | $E_{ii}$ (eV) | $\gamma$ |
|---|---|---|---|
| (6,4) | f0 | 2.072 | 0.100 |
| | f1 | 2.046 | 0.167 |
| | f4 | 2.048 | 0.143 |
| (6,5) | f0 | 2.084 | 0.116 |
| | f1 | 2.063 | 0.151 |
| | f4 | 2.068 | 0.222 |
| (10,7) | f0 | 2.054 | 0.040 |
| | f1 | 2.038 | 0.133 |
| | f4 | 2.034 | 0.150 |
| (13,1) | f0 | 2.053 | 0.035 |
| | f1 | 2.022 | 0.118 |
| | f4 | 2.031 | 0.114 |
| (11,5) | f0 | 2.061 | 0.050 |
| | f1 | 2.043 | 0.146 |
| | f4 | 2.036 | 0.154 |
| (12,3) | f0 | 2.057 | 0.066 |
| | f1 | 2.024 | 0.155 |
| | f4 | 2.020 | 0.185 |

Table 4.1: Transition energies obtained from Raman resonance profiles for various metallic and semiconducting nanotubes, $\gamma$: fit parameter related to the width of the resonance window from Ref. [23]. f0: pristine tubes, f1/f4: lower/higher functionalized sample.

resonance profiles follow the absorption spectrum of a specific type of nanotube, transmission spectra on the other hand yield the overall spectrum of the nanotube ensemble. It should be noted that the absolute values for the transition energies obtained from the different spectroscopic methods cannot be compared, because the samples have been prepared either in solution or as bulk material. It is well-known that these different environments lead to shifts of the optical transitions [72]. Comparison of the peak positions of different samples results in most of the peaks being redshifted as a consequence of functionalization (Fig. 4.3). Although these shifts have the same trends as in the case of Raman measurements, the magnitudes are considerably smaller. The possible explanation is that without resonance condition we measure the contribution of all nanotubes at certain energies. These overlapping peaks, especially the ones related to the unaffected tubes, make the shifts less pronounced. To investigate the effect of functionalization on the whole nanotube mixture, the group of $E_{11}^S$ and $E_{22}^S$ peaks of different samples was compared. The evolution of the intensities

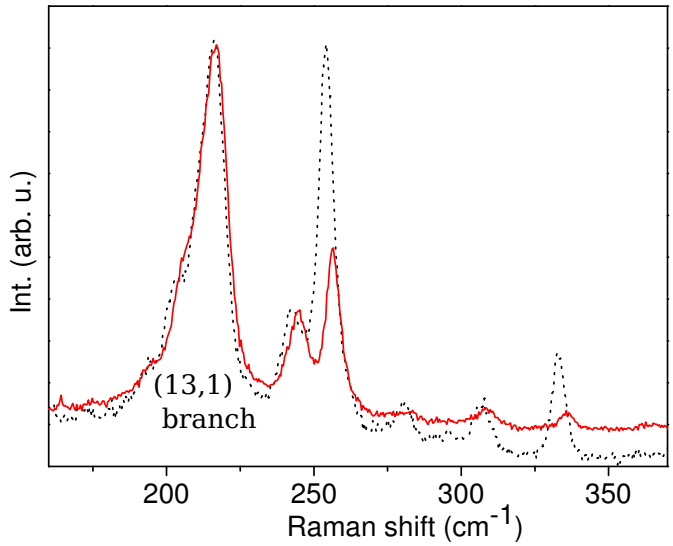


Figure 4.5: Raman spectra taken in resonance of the (13,1) tube of pristine (f0, excitation energy: 2.05 eV) and functionalized material (f4, 2.03 eV) respectively, probing various nanotubes. The intensities are normalized to the RBM of the (13,1) tube. Red: functionalized sample, black (dashed): starting material.

of the first and second semiconducting transitions indicates the diameter selectivity of the functionalization. The higher frequency part of the peaks is related to nanotubes with smaller diameter. In Fig. 4.4 the high frequency part of both the first and second transition peaks decrease in the case of functionalized samples. This proves the higher reactivity of smaller tubes.

The effect on the optical transition can be explained by a charge transfer between the tube and the functional group. The charge transfer arises from the attachment of a heteroatom (nitrogen) to the sidewall of the tube due to the difference in electronegativity. The polar bonding appears as a doping effect, introducing donor or acceptor levels within the gap of the $E_{ii}$ transition. This leads to a redshift, because the effective gap is decreased, and in a broadening of the resonance window, because it offers more real states to be possibly matched in an incoming or outgoing resonance of the Raman process. In this picture the shifts are completely independent of the reaction sequence itself. This is consistent with results on nanotubes functionalized with Ru(II)-terpyridine complexes which also show a redshift. They are discussed in Chapter 5. Additionally, in non-polar covalent bonding such as

alkyl chains, no comparable shifts of the transition energy have been observed [74]. For larger charge transfer the displacement of the Fermi level itself and its movement towards either valence or conduction band has to be taken into account, which leads to an increase in the difference of electronic states between conduction band and occupied valence band, inducing a blueshift. Therefore the amount of charge transfer due to functionalization is determined by the degree of functionalization as well as the polarity of the bond. Fantini $et\ al.$ have studied similar effects on SWCNTs functionalized with diazonium salts [58]. Their D/G ratio is larger than the one observed here [58] though the degrees of functionalization are smaller. This larger D/G ratio may indicate also structural changes in addition to the ”defects” introduced by the covalent bonds.

As discussed above, the decrease of the RBM intensities due to functionalization is commonly used to investigate the reactivity depending on either tube species or diameter. For this purpose it is of particular importance to analyze the influence of functionalization on the resonance condition. This ensures that the changes in intensity refer to the quenching due to loss of translational symmetry and are not merely due to leaving the resonance window. The predominant effect determining the chemical reactivity in the samples is the tube diameter as it has been reported for other reactions [74, 75]. This curvature effect, shown above for the optical transitions, can easily be seen from Fig. 4.5. The RBM intensity is attenuated on functionalization; this becomes more and more pronounced for small diameters, i.e., higher Raman shifts. We observe this by normalizing to certain tube chiralities. A comparison of the absolute values of the Raman intensities between different samples is not possible, because due to the preparation process the surface of the bulk material is changed. Therefore, very different absolute intensities for the functionalized samples are obtained. Concerning the Raman frequencies of the RBMs, slight shifts are observable. All RBMs show a clear trend to higher frequencies, discussed in 3.1.3. It should be noted that the width and lineshape of the RBMs seem unaffected.

### 4.1.1 HEM and $D$ mode features

As discussed above, the $D$ mode at about 1320 cm$^{-1}$ arises from a double-resonant scattering process which reveals structural changes in the tube framework [29, 30]. Fig. 4.6 shows a mapping of the D/G mode ratio of the functionalized sample f4, indicating a good homogeneity on the sample

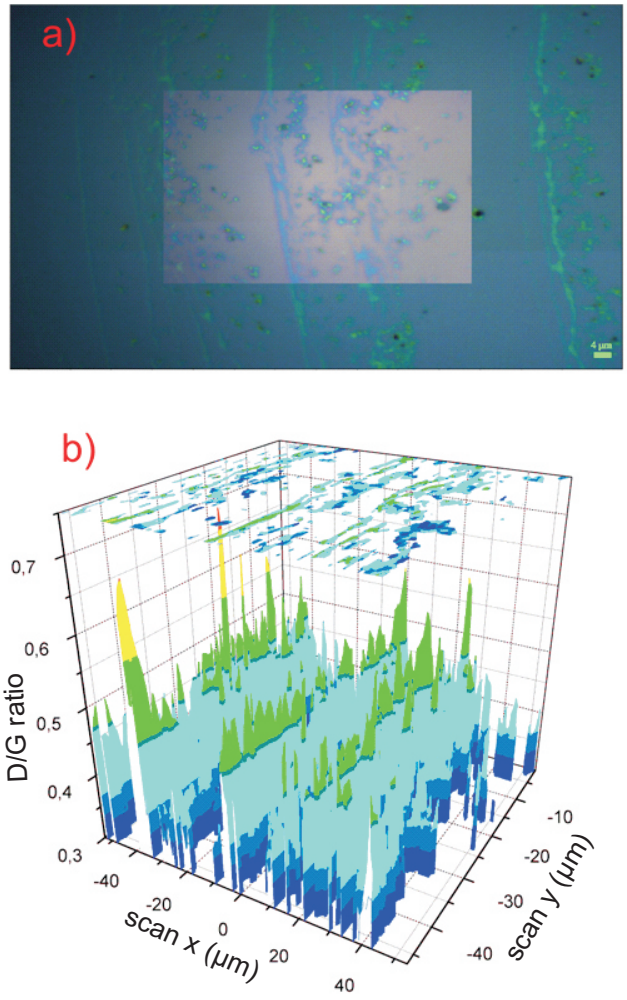


Figure 4.6: Line mapping of sample f4 dispersed in 2% SDC/H2O solution followed by spincoating deposition onto a silicon wafer. (a) optical image of sample area. (b) normalized D/G ratio of the mapped area.

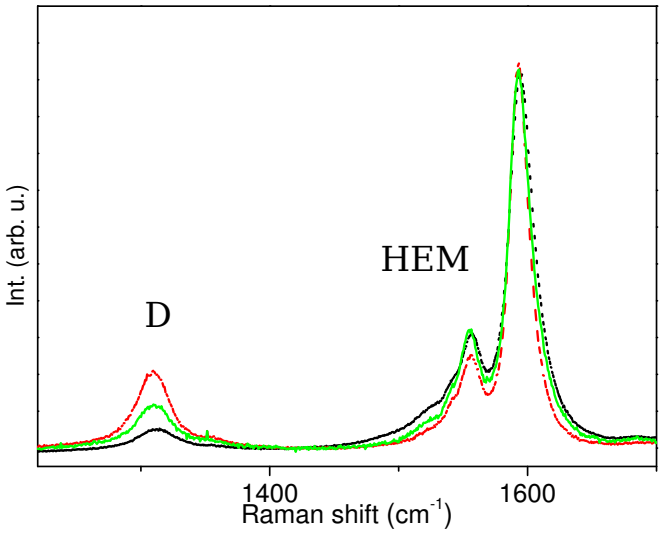


Figure 4.7: $D$ mode and HEM of functionalized sample f4 (red, dashed), annealed (black, dotted) and reference samples (green, solid) at 633 nm excitation wavelength.

surface. In the case of functionalized tubes the $D$ mode may reflect both a successful addition reaction or a possible damage of the tube during the reaction. The intensity of this mode increases with the concentration of defects in a nanotube [73]. The successful sidewall addition similarly breaks the translational symmetry and changes the Raman selection rules resulting in an increased $D$ mode intensity [31, 32]. From another point of view the covalent bonds change the hybridization of the attacked carbon atoms from $sp^2$ to $sp^3$ and therefore make a contribution to the $D$ mode intensity. Fig. 4.7 shows Raman spectra of the functionalized sample f4 before and after annealing together with the starting material. The $D$ mode intensity increases on functionalization. After annealing, the intensity is even weaker than in the pristine material. This clearly shows that the side groups can be eliminated leaving the sigma-bonds intact and the pi-system reconstructed. This is important to ensure that the observed changes in the transition energies are predominantly driven by charge transfer and less related to structural damage of the tube.

Concerning the high energy modes (HEM) of either functionalized and reference samples, no significant shifts with functionalization are observable; the lineshape is also unaffected. Only a slight decrease of the $G^-$ peak can be

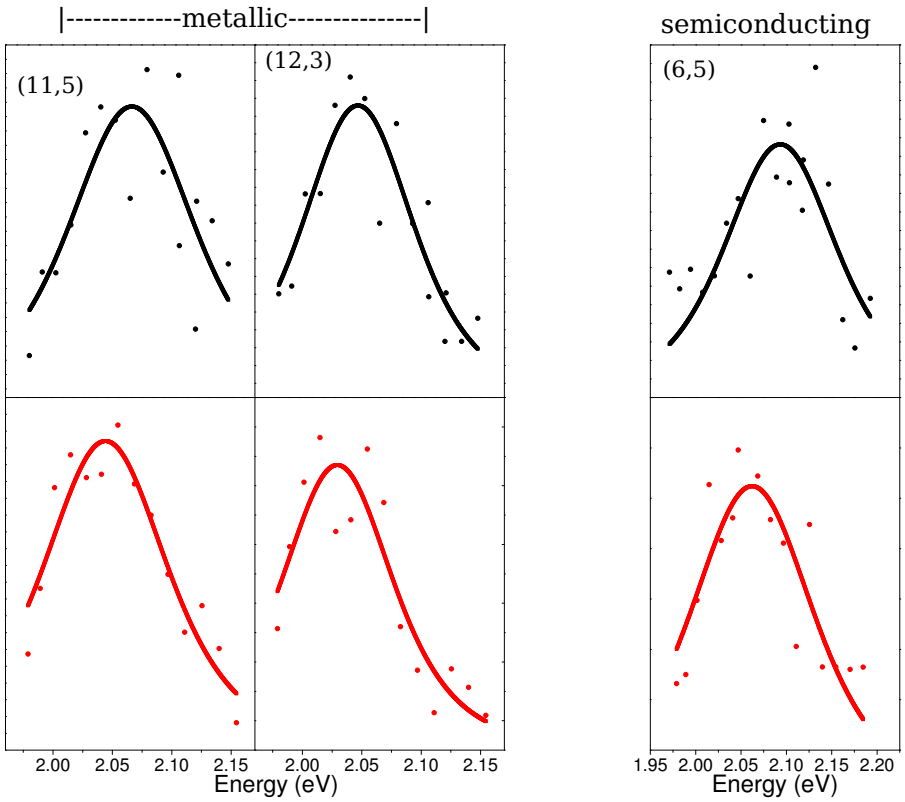


Figure 4.8: Resonance profiles of the radial breathing mode, recorded for various metallic and semiconducting tubes. top (black): non-functionalized sample, bottom (red): functionalized sample.

seen. After annealing, the intensity of the $G^-$ peak is restored. The absence of hardening or softening of the HEM indicates a quite low doping level as compared to, e.g., electrochemical doping [11]. This supports the findings concerning the redshift of the optical transitions as described above.

## 4.2 Functionalization with decyne

The triple bond close to the tube surface is among the weakest charging effects to be imagined, because it is a single C-C bond between tube and moiety with only the two $\pi$-electrons of the triple bond close to the tube surface. The influence of alkynylide functionalities on the optical transitions of the nanotubes has been investigated.

Resonance profiles of the RBMs have been recorded for several different tube chiralities and for both, the functionalized sample and the non-functionalized starting material for comparison. The functionalized material shows a redshift of the optical transition energies of about 15-20 meV as depicetd in figure 4.8. The resonance profiles are not significantly broadened, compared to other functional groups [75, 76]. Concerning the shift of the transition energy one has to take into account the other environmental effects like bundling etc. A partial debundling due to functionalization could also influence optical transitions. However, two facts allow us to rule out the redshifts being caused by debundling: It has been shown that bundling causes redshifts of the optical transitions [72], which is also very obvious in all our materials, compared to non-bundled tubes in solution. According to this a debundling should lead to blue-shifted transition energies, which is not the case in our samples. Furthermore, the comparison with measurements on as-prepared samples including various alkanes do not show a comparable behavior [74](see 3.1). The whole reaction mechanism dealing with metalorganic reactants and the preparation process of the thin films was analogous for all SWCNT derivatives. As shown above, alkanes do not show significant influences on the resonance window, neither on the transition energy nor on the width of the resonance. This is reasonable, because there is no polar-like bonding or other possiblity of a charge transfer for alkanes on tubes.

As mentioned before, charge transfer to nanotubes can be detected in the Raman spectra, observing shifts of the G mode. This will be used again in chapter 5. However, the recording of resonance profiles of the RBMs appears to be even more sensitive than G mode features. For very small doping levels the shifts of the G mode are negligible, but the electronic structure is affected so as to shift the optical transition energy. In the case of the decyne the $\pi$-electrons close to the surface of the nanotube are expected to be responsible for the charging. The presented derivative bears an alkyne moiety next to the SWCNT surface in contrast to the previous reported studies of nucleophilic addition adducts. The alkyne unit contains two occupied C-C ($\pi$)-bonds additionally to the s-C-C bond in every carbon framework. These additional electrons are supposed exhibiting an impact on the electronic bandstructure.

The sample shows a pronounced diameter dependence of reactivity, with small diameter tubes being highly affected by the reaction. The intensity of the RBM is decreased due to functionalization (see section 3.1.4), this becomes more and more distinct for small diameters, i.e., higher Raman

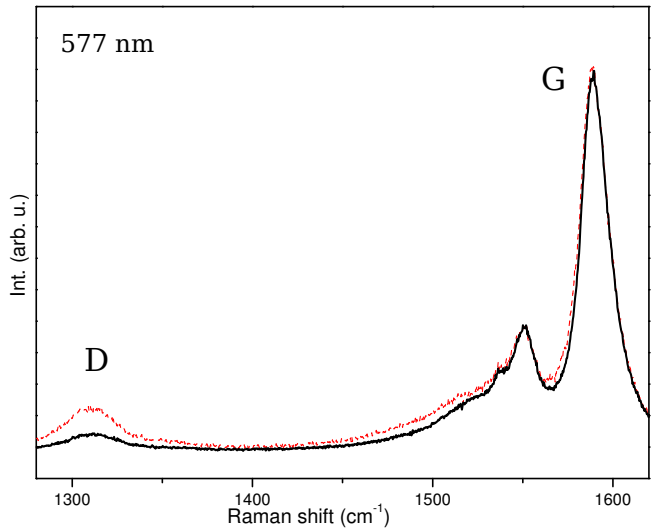


Figure 4.9: The defect induced D mode - increased with functionalization - and the G mode are shown. The G mode does not show observable shifts or differences in the lineshape. Red(dashed): functionalized sample, black: reference sample

shifts. The curvature effect can easily been shown by normalizing the intensities to a certain tube chirality as presented in figure 4.10 (normalized to the signal of the metallic branch on the very left of the spectra). The width and lineshape of the RBMs itself seem unaffected.

The nucleophilic addition step in this reaction is accompanied by the introduction of a negative charge to the SWCNT framework, yielding a charged intermediate species. The resulting Coulomb repulsion of the negatively charged SWCNTs leads to a debundling of the aggregated tube material as revealed by the formation of a homogeneous black dispersion. The subsequent reoxidation of the charged intermediates by oxygen yields neutral derivatives, which exhibit a pronounced dispersability in organic solvents. Due to these increased dispersability, such as N-Methyl-2-pyrrolidon (NMP) UV/Vis/nIR spectroscopic investigations of the derivatized material can be carried out in homogeneous solution as shown in Fig. 4.11. The spectrum of pristine SWCNT exhibits the characteristic absorption signals evolving from the excitonic transitions between the van Hove singularities in the density of states of metallic and semiconducting nanotubes. A covalent attachment of functionalities on the SWCNT sidewall and the concomitant variation of the $\pi$-system by the generation of $sp^3$ defects usually leads to a broadening and reduction of van Hove singularities and an unstructured absorption spectrum in comparison to the unfunctionalized SWCNT material. The ac-

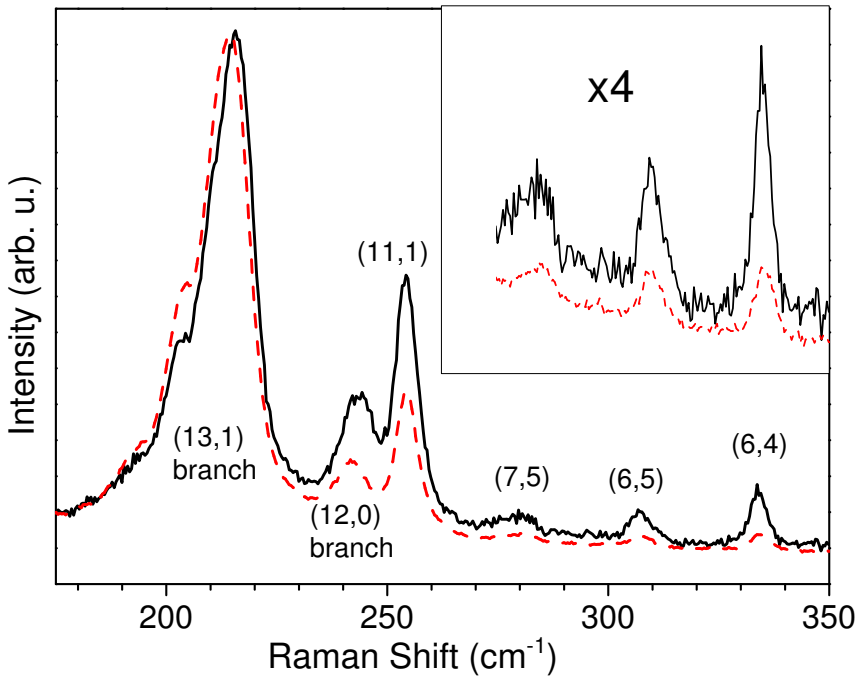


Figure 4.10: Excitation energy: 2.04 eV. red (dashed line): functionalized sample, black: reference sample

quired spectrum of decyne functionalized SWCNTs $(decyne)_n$-SWCNT in NMP more pronounced absorption signals wich is attributed to the relatively low degree of functionalization and the significant increase in the solubility of the functionalized material. This yields in an increased individualization of the SWCNTs, which is associated with more intense excitonic van Hove transitions [77]. This increase in the spectrum of the functionalized derivatives can be nicely detected in the metallic region (M11 - 300-800 nm).

The functionalized derivative $(decyne)_n$-SWCNT has also been characterized by thermogravimetric analysis (TGA) in combination with the online-monitoring of the volatile products by mass spectrometry (MS). Herein, the cationic decyne fragments (m/z = 15, 24, 29, 43, 57, 71, 85, 99, 113, 137) - originating from the covalently attached alkyne addend can easily be detected in the temperature range between 300 °C and 500 °C with a pronounced maximum at about 400 °C (see Fig. 4.12). Over the whole heating range (100 - 700 °C) the sample exhibit a total mass loss of 27.4 % (values

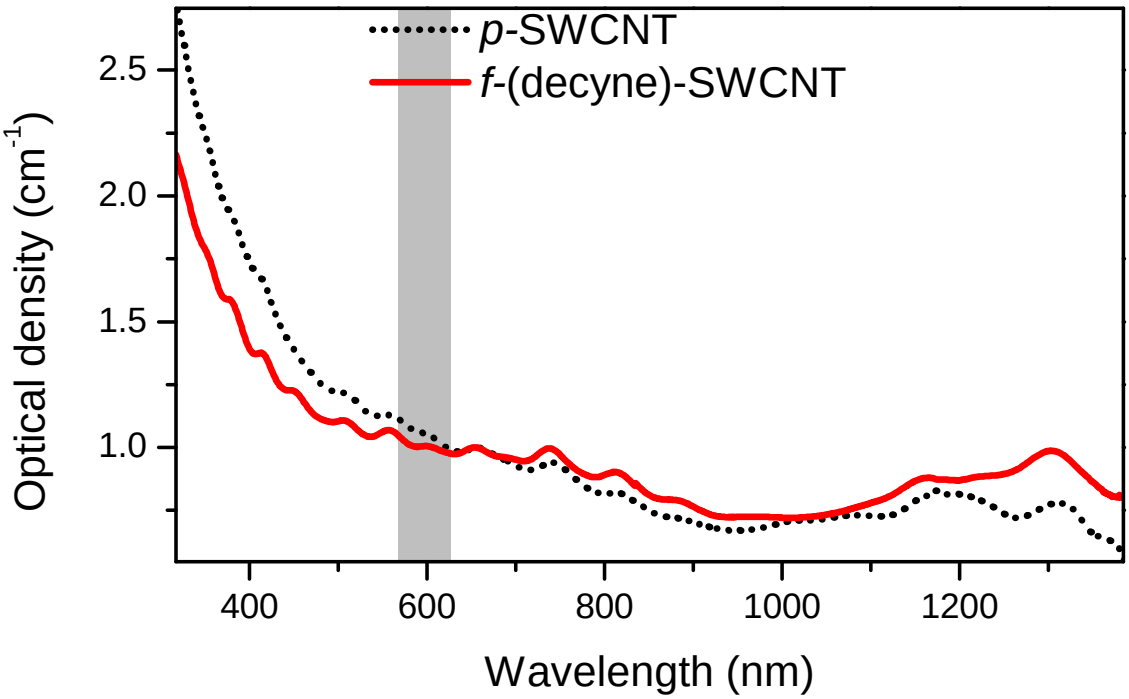


Figure 4.11: UV/VIS spectra, red (solid line): functionalized sample, black (dashed): reference sample, the gray area indicates the range of excitation wavelength for the Raman measurements

corrected to the starting material), respectively. Furthermore, the detected weight loss of the functionalized sample is 16 % in the temperature region (300 - 500 °C) where the covalent attached addends are splitted of. The mass loss of the starting material (p-SWCNT) in the corresponding temperature region is 3.9 % yielding a corrected value of 12.1 % mass loss. From the corrected mass loss a degree of functionalization for the functionalized derivatives $(decyne)_n$-SWCNT of 1.2 % can be calculated.

## 4.3 The D* mode and functionalization

D*, the overtone of the $D$ mode which is confusingly often referred to as G'in the literature, is another Raman feature sensitive towards the electronic structure of a nanotube. The D* is observable in any $sp^2$ carbons and shows doping and defect-related shifts and changes of the lineshape [34]. Graphene and undoped carbon nanotubes show a quite sharp single peak,

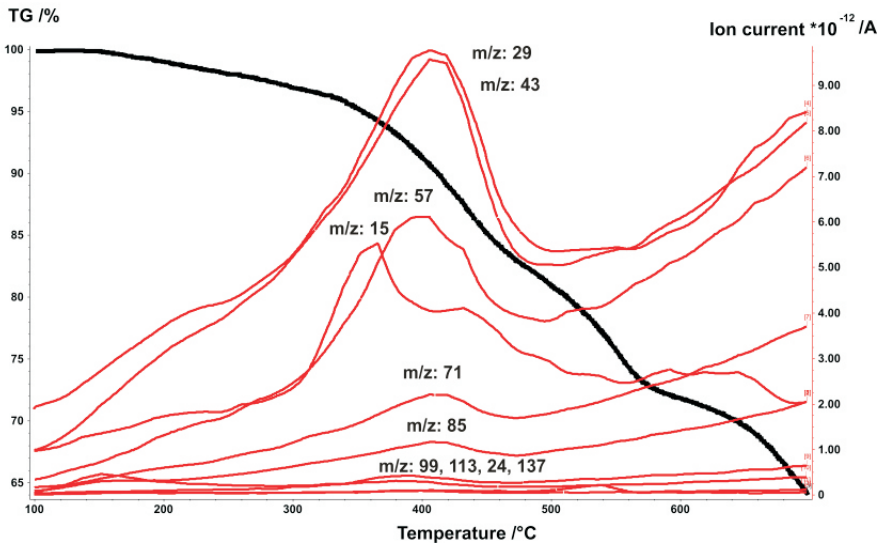


Figure 4.12: Thermogravimetric profile (weight loss) of (decyne)n-SWCNT - heating rate: 10K/min (black trace). Additionally the online-monitored mass fragments of the decyne functionality are depicted (red traces).

whereas for high defect densities or doping the lineshape broadens and shows up a double peak structure. As mentioned before, it is always difficult to judge an effect on tubes by only one Raman feature. The D* observation is a prime example for this: having a look on an amine-functionalized sample and the pristine starting material (Fig. 4.13) reveals a double peak structure for both of them. Following the analysis of Maciel *et al.*, the samples both show an n doping [34]. But especially the lineshape of the pristine material would also fit well to the defect-related asymmetric lineshape they report on an individual nanotube. Taking into account the considerable $D$ mode of the pristine nanotubes (see upper left spectrum in fig. 4.13, dotted) this seems to be the more likely reason. The functionalized material in comparison shows a versed relation of the two peaks which is - having in mind the energy shifts discussed above - likely to be due to charge transfer. However, the studies on doping by Maciel *et al.* were established with boron/nitrid doped material. The charge transfer onto the tubes is surely different from covalent sidewall functionalization, so the results can only be transfered in a qualitative manner.

To conclude this chapter it should be pointed out how susceptible the opti-

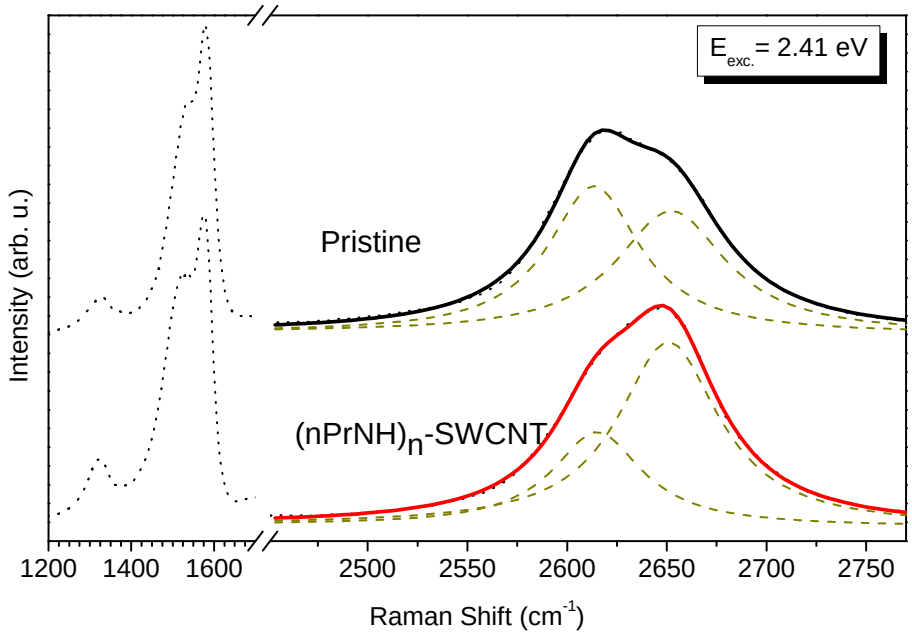


Figure 4.13: D* mode of pristine material(black) and 2% functionalized $(nPrNH)_n$-SWCNT (red), normalized to G mode. The double peak structure and a significant change of the lineshape with functionalization are observable.

cal transitions react to minor changes of the nanotube and how sensitive the Raman analysis is. Functional groups affect the electronic structure of the tubes due to charge transfer, which shows up in the Raman features, especially in the resonance windows of the radial breathing mode. This analysis is of great avail also for composite materials, as shown in the next chapter.

*The chemist does a mysterious thing when he wants to make a molecule. He sees that it has got that ring, so he mixes this and that, and he shakes it, and he fiddles around. And, at the end of a difficult process, he usually does succeed in synthesizing what he wants.[...]*

Richard P. Feynman

# 5 Composite materials, nanotubes and polymers

Bringing carbon-based composites to the level of a technologically relevant material depends upon a deep understanding not only of their synthesis and atomic structure, but also the associated electronic structures. Composite materials including carbon nanotubes are a hot spot of latest research offering a variety of different applications such as artificial muscles [78] or biochemical sensors [79]. Photo-induced mechanical actuation has been reported for polymernanotube composites under infrared radiation [80]. Recently, graphene has come to the fore with the Nobel prize being awarded for graphene preparation. Polymer-functionalized graphene is also under investigation especially for electronics [81].

As mentioned before, functionalization improves the handling of the tubes concerning their processability and one of the most interesting fields is the integration of nanotubes into polymers in compound materials [82]. This offers the chance to create a new class of composites that take advantage of the outstanding properties of the nanotubes, their mechanical, thermal and electronic properties which make them desirable additive for a wide range of materials. One issue is the use of nanotubes for the production of electrically or thermally conductive composites [83, 84]. Also promising is the use of carbon nanotubes as structural reinforcement, improving the mechanical strength of nanotube-polymer composites [60, 85]. The nanotube reinforcements increase the toughness of the composites by absorbing energy [85].

Another issue is about combinations of metal ions with polymers and nanotubes providing an interesting route towards supramolecular structures with well-defined catalytic, electrochemical or magnetic properties [86]. Metal-ligand coordination bonding with terpyridine has become a promising tool

towards such structures [87]. While the combination of well-established polymer chemistry and the versatile functionality of metal ions is, in general, a promising approach to novel material fabrication [88]. In this chapter the decoration of tubes with various polymers and Ruthenium complexes is discussed. In the first section the influence on the optical transitions is discussed and the hardening of the radial breathing due to wrapping effects. In a second approach tubes have been prepared with chinoline polymers with and without metal comlexes. The preparation pathway using initiator groups ensures the same degree of functionalization for all samples. Therefore this set of samples offers a detailed study of the charge transfer between the nanotubes and the functional group.

## 5.1 Influence on RBM and optical transitions

Nanotubes decorated with terpyridine-ruthenium complexes have been prepared, the surface modification of SWCNTs has been accomplished using either the grafting to or the grafting from approaches [89]. Through these approaches a combination of Ru(II) ions with CNTs using metal-ligand coordination bonding is achieved. Besides the novelty of these materials from the synthetic point of view, they provide a unique opportunity to understand how the tpy-Ru(II)-tpy complexes will affect the processability and most importantly the electronic properties of CNTs.

Metal mediated atom transfer radical generation/addition (ATRA) of a bromomethyl terminated tpy-Ru(II)-tpy complex BrCH2Ph-tpyRu(II)tpy-2x$C_{12}H_{25}$ was employed for the direct attachment of monomeric tpy-Ru(II)-tpy complexes onto the SWCNTs surface, using CuBr/PMDETA as the catalytic system. Based on the thermogravimetric analysis (TGA) results, the SWCNTtpyRu( II)tpy-2x$C_{12}H_{25}$ presented a 28.5 $\%$ weight loss corresponding to 1 functional group per 400 carbon atoms [89]. Using the grafting from approach, SWCNTs were decorated with polymeric side chain dendritic tpy-Ru(II)- tpy complexes.

For tubes of relatively larger diameter, i.e. Raman shifts less than 180 $cm^{-1}$, an assignment was not possible because of lack of data for comparison. Compared to the energies given for tubes in dispersion, the data - even for the pristine material - is redshifted due to bundling effects [72]. Comparing the pristine tubes with the tpy- and poly-tpy-decorated samples, an additional downshift of the transition energies is observed with functionalization,

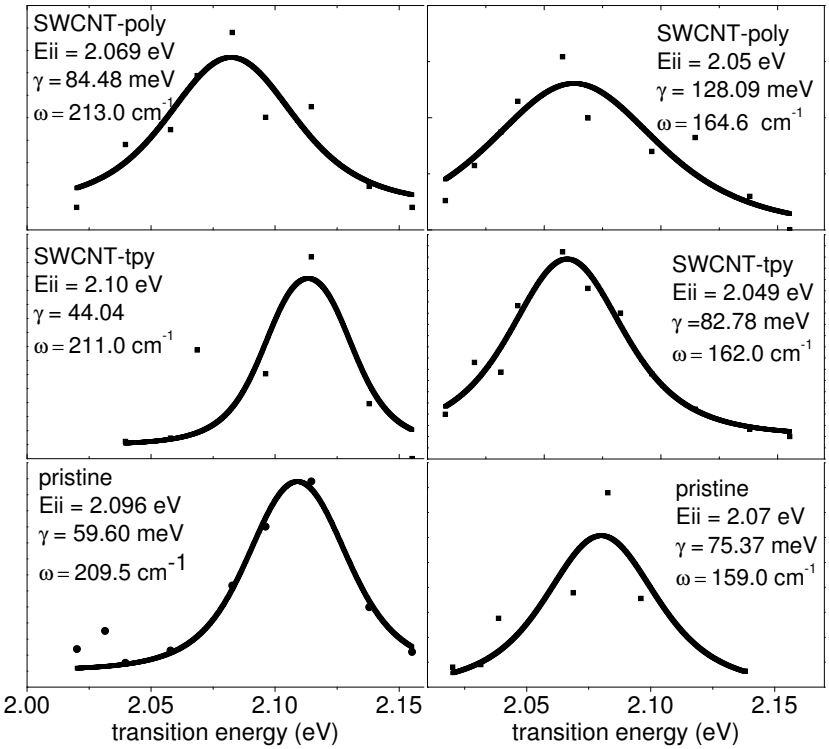


Figure 5.1: Resonance profiles of the decorated and non-decorated reference sample with $E_{ii}$: transition energy, $\gamma$: fit parameter related to width from Ref. [23], $\omega$: Raman shift of the observed RBM peak.

as it can be seen in Fig. 5.1. This trend holds for all the recorded profiles. Also a broadening of the resonance profile is obvious for the polymer-decorated tubes (see Fig. 5.1). The full width at half maximum is increased by approximately 50%. For the monomeric sample this effect is less pronounced.

Concerning the RBM frequencies a hardening with functionalization can be observed. Shifts of approximately 2 $cm^{-1}$ and 5 $cm^{-1}$ for monomeric or polymeric decoration are observed respectively (see Fig.5.2). The pronounced shift in the polymeric sample is most probably due to wrapping of the polymer chain around the tube as it has been observed for certain polymers [90]. The frequency shifts are accompanied by drastic effects on the intensity of the RBM signal. In general, the RBM intensity decreases with functionalization. For excitation energies below 1.8 eV, Raman signal from both monomeric and polymeric samples could hardly be recorded, because the

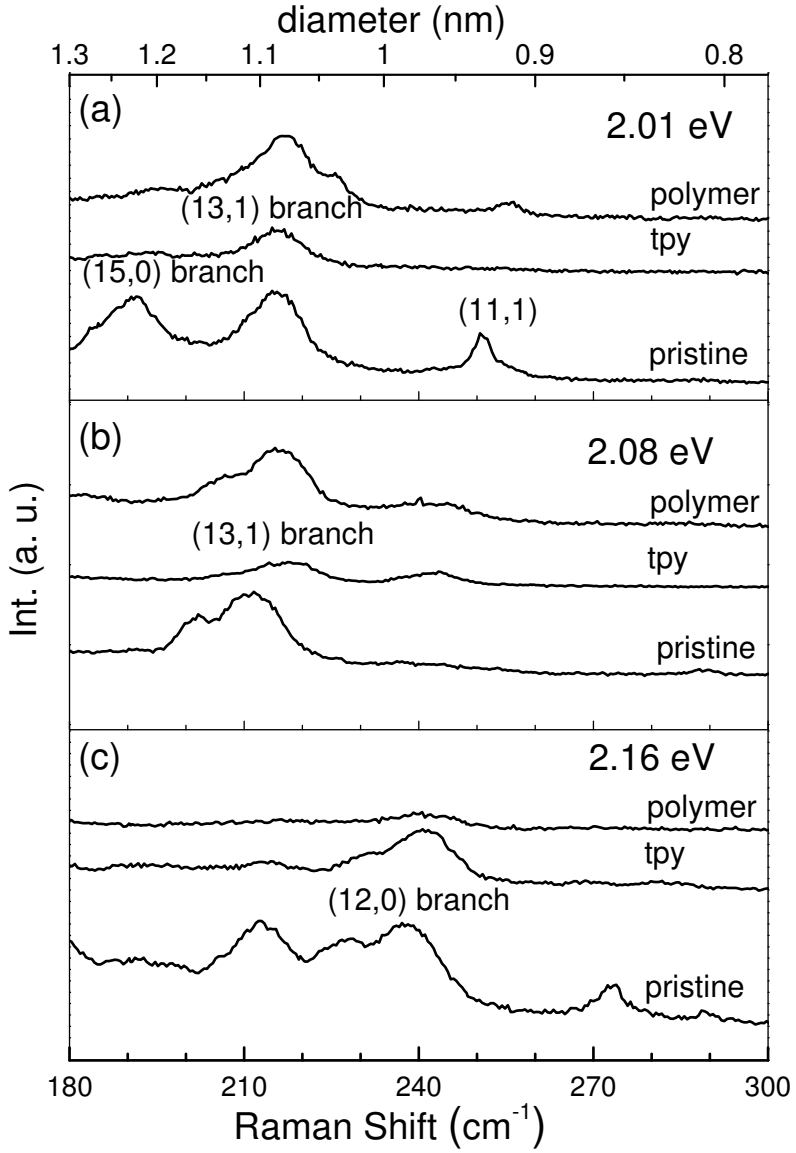


Figure 5.2: RBMs at various excitation energies. The RBM frequencies in the polymer samples are upshifted due to the wrapping effect. The functionalized materials show a strong decrease of the intensities.

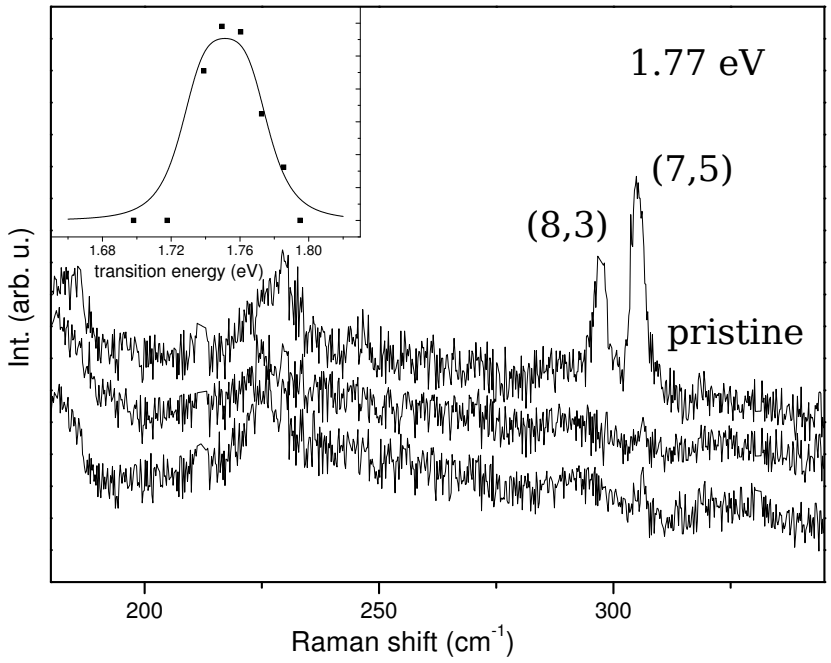


Figure 5.3: RBM signal in the long wavelength area with almost vanishing signal for the functionalized material. Inset: resonance profile for (8,3) tube in the pristine sample.

signal almost vanishes with functionalization (see Fig. 5.3). Interestingly, the decrease of the intensity and therefore the chemical reaction seems driven by two effects: small diameters are highly affected, as it can be observed, e.g. for the (11,1) tube, but also for tubes with relatively larger diameters like the entire (15,0) branch [Fig. 5.2 (a)]. This effect holds for different tube chiralities observed at different excitation energies [Fig. 5.2(b), (c)]. The preferred reaction of small diameter tubes is expected due to higher strain relaxation and has been discussed in Chapter 3.

The at first sight strange behavior of larger diameter tubes is confirmed by the fact that the same reaction sequence applied to multi-walled nanotubes leads to higher degrees of functionalization, as observed by TGA. As multi-walled tubes offer even larger diameters, this is consistent with the behavior in the single-walled samples. It may possibly be due to defect functionalization, because even if the defect density is the same in all starting materials, bigger tube diameters lead to a higher amount of defects in absolute num-

bers. Steric demands may also come into play, with less curved material offering more space for the reactants to attack the sidewall. However, a considerable functionalization is achieved for both grafting to and grafting from approaches of sidewall decoration. The chemical treatment affects both Raman shifts, especially due to wrapping, and transition energies. The changes of the electronic structure of the tubes are not too strong, so one is not completely leaving the resonance window with decoration. Therefore an intensity alteration is a valuable sign for successful functionalization.

## 5.2 Semiconducting polymer-functionalized nanotubes

In another approach nanotubes have been decorated with different polymeric quinoline using the ”grafting from” method. The focus of this synthesis is to develop new composite materials that combine the properties of the semiconducting polymers with those of the nanotubes. Again the investigation of their electronical/optical properties is part of the basic characterization of the material to improve processability and handling.

Three different samples have been prepared, with two of them only functionalized with quinoline chains and a third one with chinoline polymer containing a Ruthenium complex in addition (see Fig. 5.4). The synthesis of the polymer functionalized nanotubes was made via the atom transfer radical polymerization (ATRP) of the monomers on the nanotube surface. The nanotube surfaces have been prepared for polymerisation in two main steps: first, hydroxyl groups are introduced and afterwards the initiator molecules for the ATRP are added to the hydroxyl anchor molecules (for more preparation details see A). The final composite materials were characterized first with the thermogravimetric analysis and the results proved, in all cases, the attachment of the quinolines on the nanotubes surface (Fig.5.5. For the quinoline samples (CM1, CM2)one observes that almost the same amount of quinolines was immobilized on the CNT, the weight loss compared to the initiator functionalized tubes (C2) is about 10%. The Ruthenium sample (CM3), as expected due to the much higher molecular weight, shows more weight loss, almost 30% higher compared to the initiator.

Comparing the G mode positions of the tubes decorated with the Ruthenium complex with those of the other samples, it is obvious that the metal com-

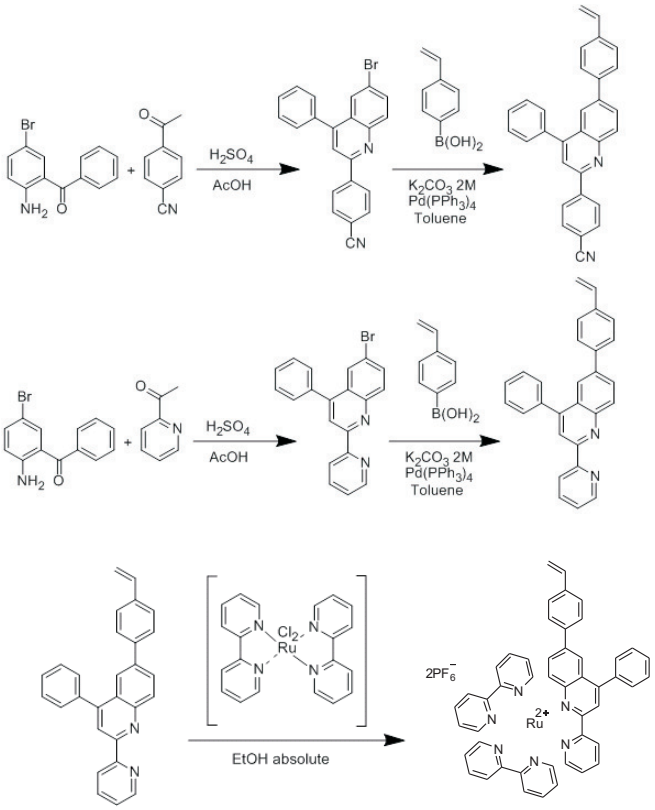


Figure 5.4: Reaction scheme for Quinoline-momomers: the synthesis of the quinoline monomer starts from the 2-amino-5-bromophenyl phenyl methanone, p-Cyanacetophenon (top) and acetyl pyridine (middle) are added, respectively. Two quinoline monomers are produced, the second one is additionally brought to reaction with cis-$(tpy)_2$-$RuCl_2$ (bottom). For more details see A.

plex leads to a G mode shift in the opposite direction than the other samples. Due to the preparation pathway the degree of functionalization of all samples is exactly the same, because all polymerizations have been started from the same properly modified nanotubes, prepared with the ATRP initiator groups. This ensures that the influence on the phonon energies of the high energy mode is not driven by structural changes. As a consequence, it is even more likely to consider a charge transfer between the nanotubes and the polymers to be responsible for the shifts. Obviously the charge transfer between the metal complex and the tubes is of opposite sign than the others. Surprisingly the $G^+$ peak is affected here, whereas typically the $G^-$ peak is supposed to be much more sensitive to any changes of the tube [92]: Kohn anomalies in doped nanotubes have been predicted by Caudal *et al.* [92], however they limit the phenomena to the $G^-$ peak. The G mode in carbon nanotubes is split into two peaks denoted $G^+$ and $G^-$,

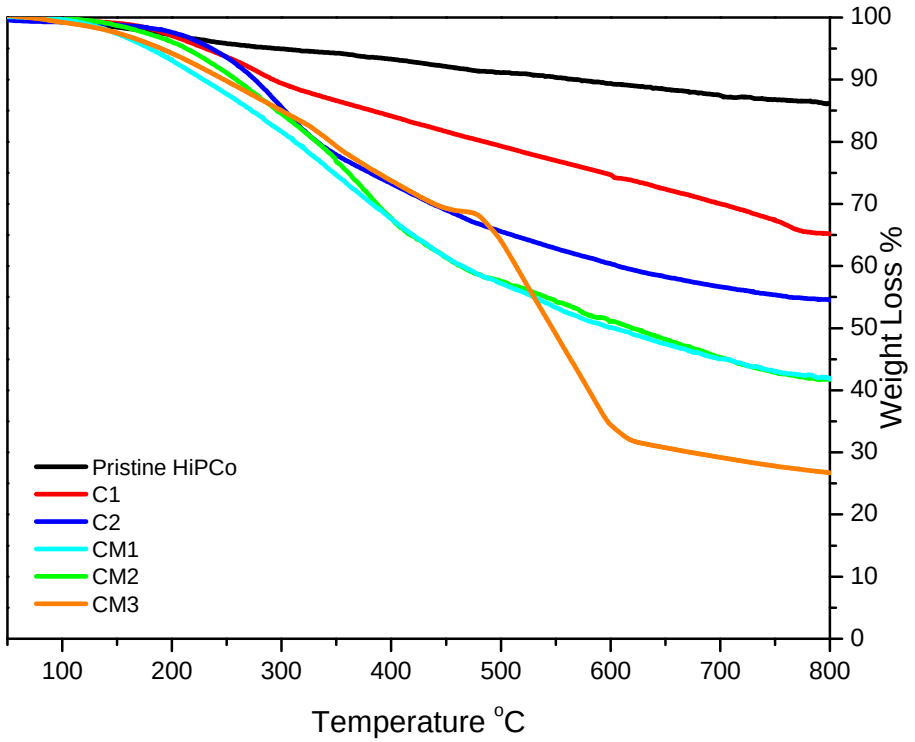


Figure 5.5: TGA data for pristine (black) and functionalized (colored) nanotubes: hydroxy functionalized tubes are prepared (C1) and ATPR initiator molecules are added to the hydroxy anchors (C2). Then the differently prepared quinoline chains without (CM1, CM2) and with (CM3) a metal complex polymerize to the tube.

respectively. Whereas in graphite the two related phonons are degenerate, in nanotubes the curvature leads to two peaks, with the $G^-$ peak frequency decreasing with decreasing tube diameter [93, 94]. Sasaki *et al.* [91] recently reported DFT calculations, showing a possible shift for the $G^+$ peak in zig-zag tubes. In case of the metallic zig-zag tubes they show an influence on both modes, because both LO and TO mode may couple with electron-hole pairs. Therefore the modes show a dependence of the Fermi energy (see Fig. 5.7) It is most likely that this influence is also the reason for the observed effects in the nanotube derivatives. The G mode data in Fig. 5.6 was taken at 514 nm excitation wavelength, where predominantly metallic tubes are in resonance. The DFT calculations in Fig. 5.7 show a symmetric behavior around zero eV. Assuming that the pristine sample was not completely undoped, because of impurities, remains from catalysts etc., would cause the observed shifts with opposite sign for the different moieties. This means the starting material is in a state of the rising or trailing edge of

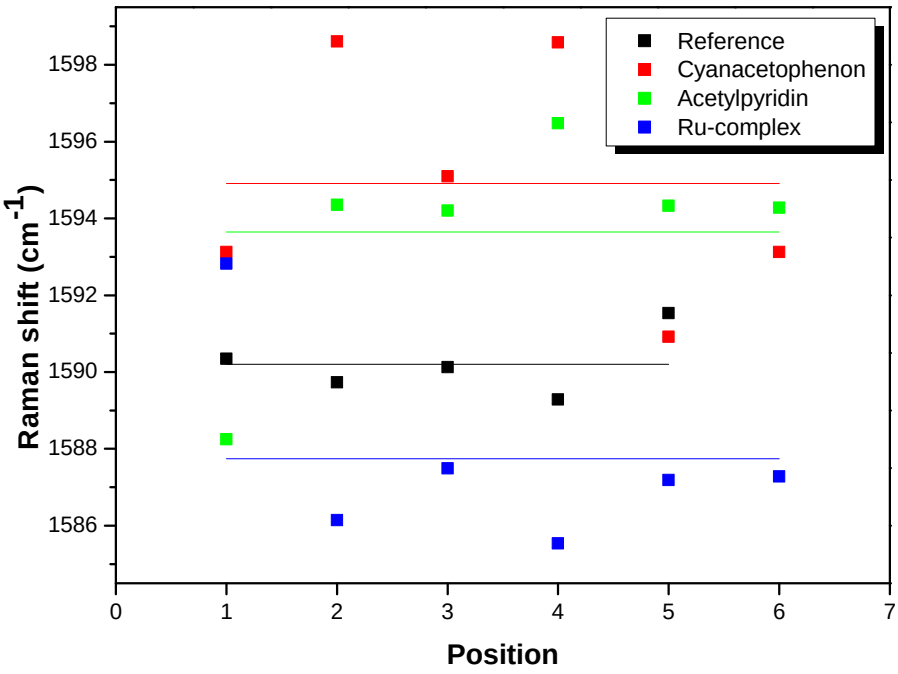


Figure 5.6: G mode position of functionalized samples (colored) compared to reference sample(black). In contrast to the tubes with only the different quinoline chains the material with the Ruthenium complex shows a significant downshift of the G mode frequency.

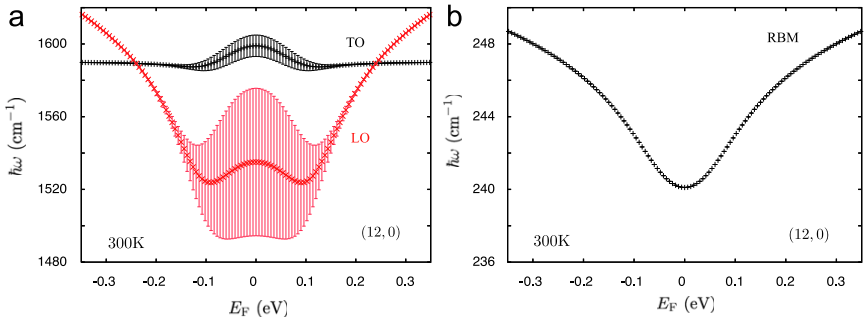


Figure 5.7: Raman peak positions as function of Fermi energy. (a) The $E_F$ dependence of the LO (red curve)and TO(black curve) phonon energy in the case of the a metallic zig-zag SWNT. Not only the frequency of the LO mode but also that of the TO mode is shifted due to the curvature effect. (b)The $E_F$ dependence of the RBM energy. From Ref. [91].

the curve in Fig. 5.7 (a). For the charging of the tubes due to the ruthenium ion two concepts are competing: the first is a charging via the whole polymer chain, as it were “by wire”. The second, and more likely concept takes into account the small distances between each ion and the tube surface because of the typical polymer wrapping. This means that lots of ions come very close to each nanotube surface, the architecture of the metal complex may even allow a direct contact between them.

In this chapter various polymer-decorated nanotubes have been characterized. It has been shown that chemical functionalization may lead to Kohn anomalies in the slightly doped metallic nanotubes.

*Data without generalization is just gossip.*

Robert M. Pirsig

# 6 Individual carbon nanotubes

The correlation between high resolution transmission electron microscopy (HRTEM) and resonant Raman spectroscopy on the same individual (here: multi-walled) carbon nanotube is a first step towards possible future analysis of functionalized individual tubes. Isolated tubes, in contrast to the bucky paper discussed so far, offer the chance to investigate a particular nanotube without the environmental effects. The separation from bundling/debundling effects for studying the optical transitions and charge transfer between the tubes and a functionality might become a versatile tool for a deeper understanding of nanotube chemistry. So far, the reactions applied to nanotubes are usually established in solution. Therefore one might consider two alternatives for the preparation of future samples for combined HRTEM/Raman analysis: Either the functionalization is prepared first and then the tubes are placed on an appropriate substrate (e.g., by spin coating), or the growth process takes part on the substrate first. This would require a chemical reaction out of the gas phase, because a solvent would wash the tubes overboard while functionalizing.

This chapter shows the great potential of the combination of the two experimental methods. It demonstrates the detailed characterization that is possible and may also give an idea of the experimental limits of future work. Individual - non-functionalized - multi-walled nanotubes and small bundles have been investigated, the initial aim of the work was to study the coupling between the shells of a single multi-walled tube [95]. Section 6.1 closely follows this work, focusing on the experimental part of it. In section 6.2 additional data on small bundles is discussed concerning the possibility to record resonance profiles of the radial breathing mode which will be of great benefit for the work on functionalized carbon nanotubes.

## 6.1 Breathing-like modes in multi-walled carbon nanotubes

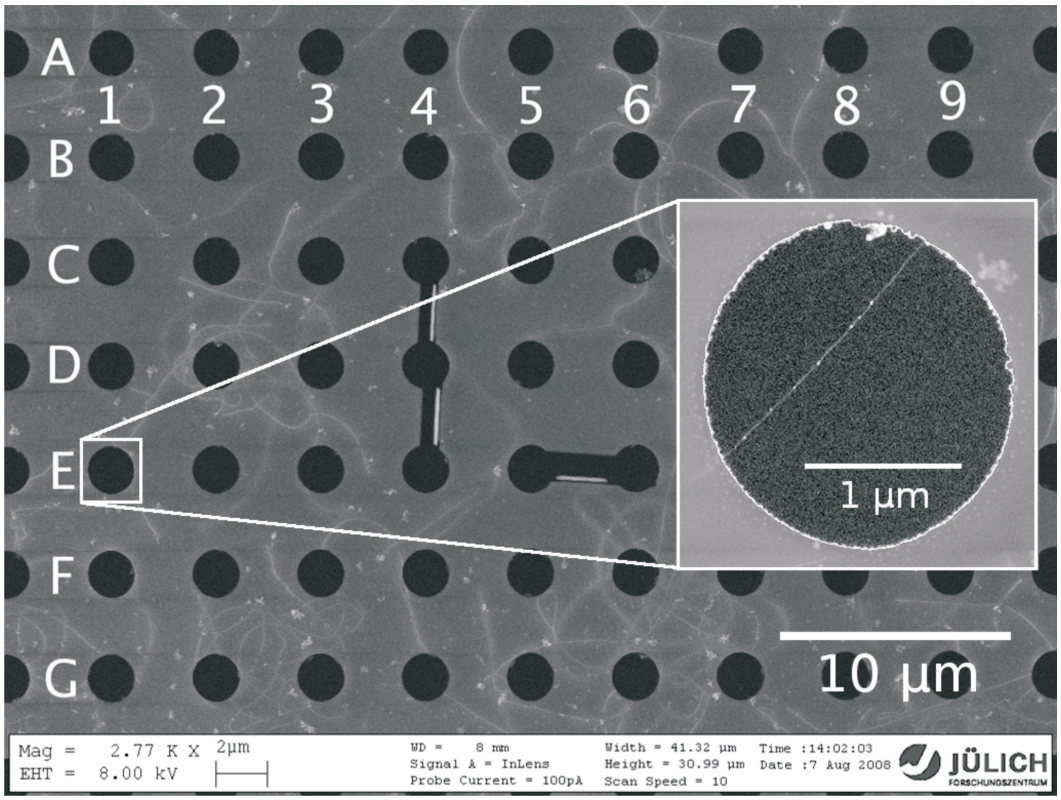


Figure 6.1: SEM picture of the $Si_3N_4$ TEM grid after CVD growth of the carbon nanotubes. The marker shown in the center of the picture was created using a focused ion beam. The single tube intersecting the hole in position E1 shown in the inset was chosen for TEM and Raman characterization. The SEM images were taken in UHV conditions to prevent deposition of amorphous carbon. From Ref. [95].

For multi-walled nanotubes, the coupling of the radial oscillation of the tubes to breathing-like modes was predicted by Popov and Henrard [96]. The strength of this coupling has a direct impact on the oscillatory properties and the Raman signal of the breathing-like modes reveals the oscillation of the layers and shells against each other. The Raman shift of these BLMs can be derived from the 1/d dependence of RBMs for single-walled tubes. The effect from the interaction between the walls becomes very strong especially for the inner tubes of a MWCNT. In this case the deviation in mode energy is found to be up to 23%. To compare the coupling between the nanotube

shells to the coupling expected for few layer graphene a model has been introduced by Meyer and Spudat [95, 97].

In order to correlate Raman spectroscopy with TEM measurements on the same nanotube, a TEM grid with a marker structure is used as substrate (see Fig. 6.1). The investigated MWCNTs are synthesized by chemical vapor deposition (CVD) directly on a TEM grid as described in Ref [98]. To study the BLMs, a position was investigated, where only one single MWCNT is crossing the hole (inset Fig. 6.1).

The high-resolution TEM image (Fig. 6.2a)) reveals that this MWCNT is composed of six walls. Fig. 6.2 c) compares line profiles of the experimental tube image and the simulated tube image based on the model resulting from the iterative refinement of shell diameters [95]. The resulting image after refining the model is shown in Fig. 6.2 b). The shell diameters of the tubes are given as those of the refined model and range from d = 0.78 nm for the innermost tube to d = 4.34 nm for the outermost tube. Note that the maxima of the image intensity cannot be used to determine the diameters directly.

The Raman measurements of the same MWCNT are shown in Fig. 6.3 a). They were performed before the TEM imaging in order to avoid any influence of defects that might be induced by electron irradiation. Three modes can be observed, showing a good signal to noise ratio due to a strong resonance effect. They have a line width of 3 - 4 $cm^{-1}$, which is a typical value for RBMs [99]. Therefore, we assume that these peaks arise from the breathing modes of the tubes, which built the multi-walled tube.

In Fig. 6.3 b) the resonance energies of the three breathing modes from the Raman measurements and the diameters obtained from the TEM measurements are compared to the optical transition energies $E_{ii}$ calculated within the framework of a non-orthogonal tight-binding model [100]. This model underestimates the transition energies, which have to be up-shifted by 0.3 eV if compared to experimental data [100]. The interaction of the walls within the MWCNT might influence this shift, but without more data about MWCNTs it is not possible to determine the shift in the transition energy exactly. Assuming an error of $\pm$ 50 meV for the blue-shifted transition energies, the observed resonances can still be attributed to the $S_{22}$ transition for the first and to the $S_{33}$ transition for the second innermost tubes, respectively. The third signal may be attributed either to the $S_{44}$ or the $M_{22}$ transition. The measured signal obviously belongs to the three innermost tubes.

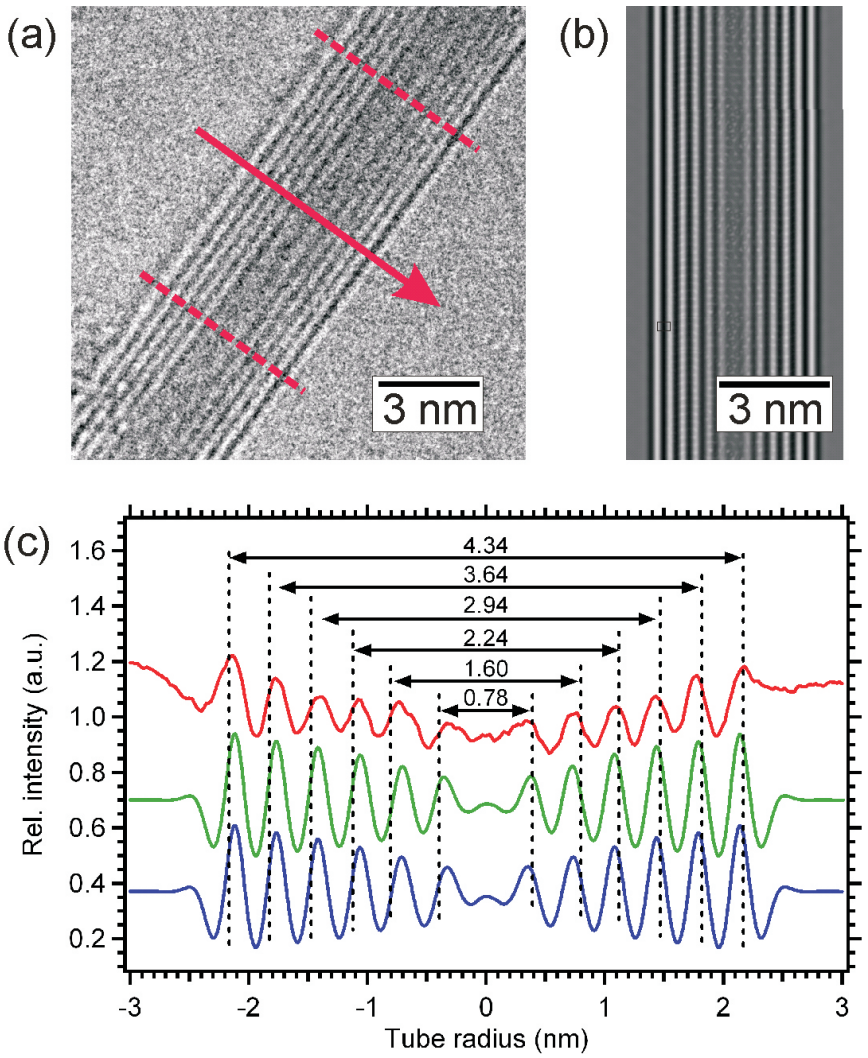


Figure 6.2: a) HRTEM micrograph of MWCNT. The nanotube shells appear bright above mean value under the chosen imaging conditions. b) Simulation of the image in (a). (c) Line profile of the image intensity (red) along the arrow in (a) compared to the line profile of the simulation based upon the refined (blue) model and the regularized (green) model. The line profiles are off-set for clarity. The diameters were obtained from the refined model. All values are given in nm. From Ref. [95].

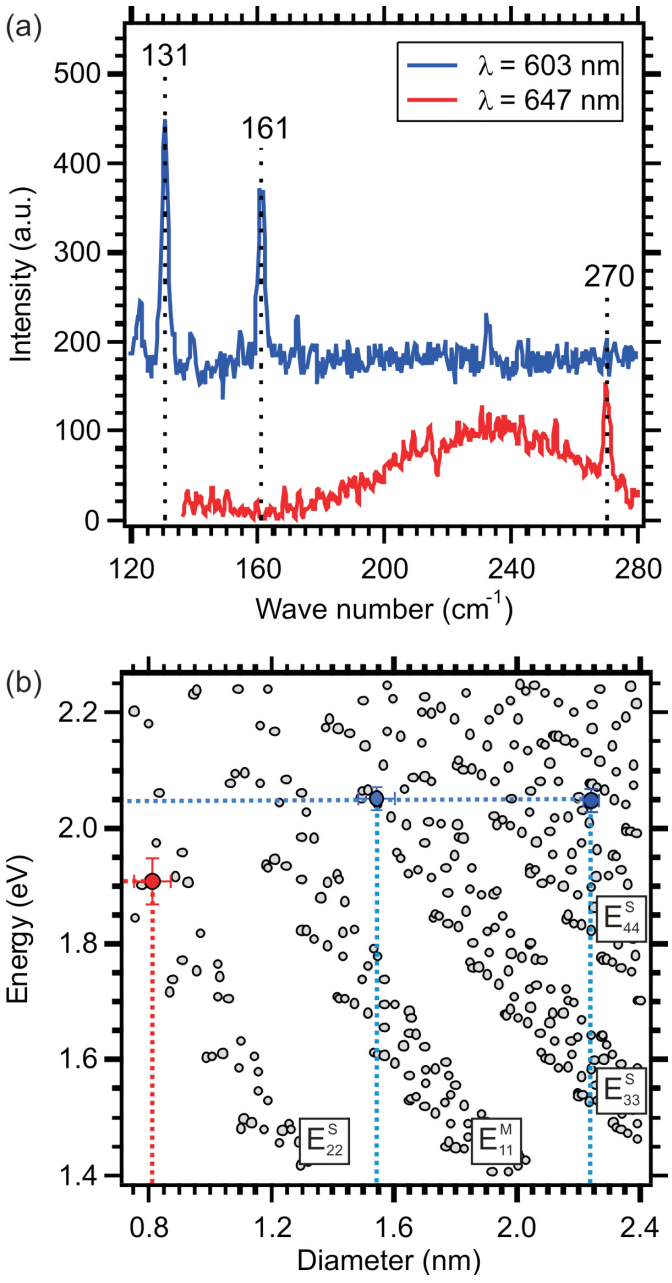


Figure 6.3: a) Resonant Raman spectrum of the single MWCNT. b) Assignment of the transitions for the observed Raman resonances in the Kataura plot (by Popov [100]) for the laser energies E = 2.06 eV (blue line) and E = 1.92 eV (red line) used in (a).From Ref. [95]

To briefly sum up the further analysis: the Raman shifts of the modes observed have been compared with the diameters obtained in the TEM measurements. Strong shifts toward higher wave numbers are found in the experiment, up to 23% with respect to the RBM position expected from the TEM measurement.The stiffening of the Raman modes can be explained by a coupling of phonon modes due to van der Waals interactions between the walls of the MWCNT. Therefore, coupled breathing-like modes as predicted by Popov *et al*. are observed instead of individual RBMs. To investigate the influence of the mode coupling in MWCNTs on the Raman shift, a model has been constructed based upon previous calculations for double-walled tubes [57] assuming the shells of a MWCNT to be a one-dimensional chain of coupled harmonic oscillators.

## 6.2 Small bundles, special configurations

The preparation on a TEM grid enables one to find one particular tube quite easily in a micro-Raman setup. The diameter of the holes of the grid is comparable to the diameter of a typical laser spot. The holes and the marker structure simplifies the recovery of an individual tube comparable to the growth of tubes over a trench [101]. This allows measurements at well-defined positions and the pre-characterization by SEM as shown here provides studying small nanotube bundles with interesting structures, that accidentally built up in the growth process. In case of one position (see Fig. 6.4) a T-shaped structure formed. This is a prime example for the use of Raman spectroscopy, because it reveals features observable by polarization dependent measurements. As the laser used for excitation provides linear polarized light, the signal from an individual tube shows the so-called antenna effect. This has been reported first by Wang *et al.*, showing the polarization dependent absorption of small nanotubes grown in zeolithe crystals [14]. The antenna effect arises from the one-dimensionality of the structure. Light is only observed in case of a parallel electric field vector to the tube axis. This phenomena also reveals in the Raman spectra (see Fig. 6.5).

The G mode has been recorded for excitation a) parallel to the long tube bundle crossing the hole of the TEM grid and b) rotated 90° , so the small thin part of the bundle is parallel to the incoming light. The spectra clearly show the difference of the number of nanotubes, that contribute to the Raman signal. As the G mode offers a very wide resonance window, it is most likely to find it even for unknown tube diameters and chiralities. The experi-

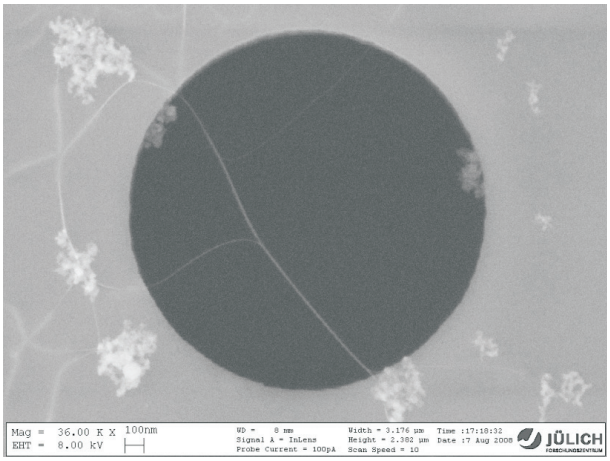


Figure 6.4: SEM picture of a particular position on the TEM grid. It shows a small nanotube bundle, which has split up during the growth process. The T-like structure allows to observe polarization dependent Raman features like the antenna effect.

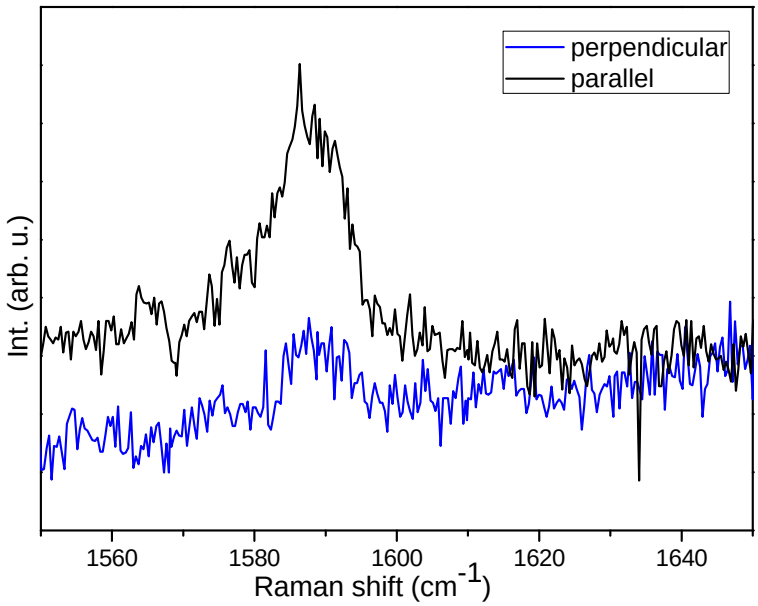


Figure 6.5: The G mode recorded with light parallel and perpendicular to the long, thicker part of the T-shaped bundle shown in Fig. 6.4. The decrease of the intensity showing up for the small, thin part of the bundle reveals the contribution of less nanotubes to the signal.

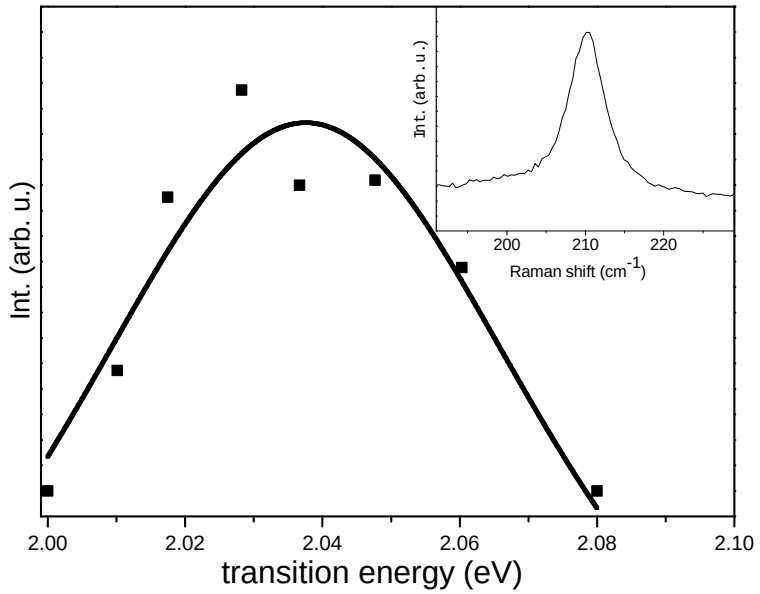


Figure 6.6: Resonance profile recorded from one of the inner shells of the MWCNT bundle. The inset shows the RBM itself close to resonance. The spectrum reveals the very good signal-to-noise ratio.

mental challenge working on such small bundles is to find a radial breathing mode in resonance for a detailed characterization. The resonance condition is limited to a small energy range due to the very small phonon energy compared to the G mode. However, it has been possible to detect a pronounced RBM signal for one of the nanotubes in the bundle. The resonance profile is shown in Fig. 6.6. It has been recorded using light polarized parallel to the longer, thicker part of the tube bundle. The inset shows the very sharp RBM signal close to the resonance. In comparison with the TEM data and the typical diameter distribution of the used growth process, it can be concluded that the signal arises from one of the inner tube shells [97].

In this chapter a characterization of individual nanotubes is presented. The experimental benefit of combined Raman/TEM measurements is shown in order to analyze a particular nanotube. It reveals that it will surely be promising to analyze functionalized materials in the same way, overcoming the overlaps of other environmental effects.

*Why do I waste my time with carbon? - Carbon is crazy, that's why we love it!*

Ado Jorio, Kirchberg winterschool 2010

# 7

# Summary and Outlook

In recent years carbon nanotubes have already taken the step from a pure research object to more and more applied research and expanded into various fields of industrial production. However, most of the desired technological application is still a challenge due to the processability of the pristine carbon nanotubes. It has been shown that chemical functionalization is a prerequisite for many applications.

In this work Raman spectroscopy was utilized to determine the impact of chemical functionalization especially on the electronic properties of carbon nanotubes. This is probed via resonant Raman spectroscopy of the radial breathing modes of the tubes, which reflects changes in the optical transitions.

The first part of the work reveals the general influence of chemical bonds on the Raman features of the nanotube derivatives. It demonstrates how powerful Raman spectroscopy is investigating especially covalent bonding to the tube framework. It proves a successful addition reaction due to the increase of the defect induced $D$ mode in combination with attenuated radial breathing modes. Following the resonance of a particular tube chirality, the different reactivity of nanotubes, depending on diameter and tube species, is studied. The diameter dependence arises from the different curvature of the tubes. It is shown that this effect is always interfering with the different reactivity due to the tubes species. Metallic or semiconducting tubes may be affected differently by addition reactions, depending on the reaction conditions. A preferred reaction of semiconducting tubes has been proved, however an exclusive reaction can be ruled out. The reactivity reflects the different density of states near the Fermi level. It is shown that in selective reactions also localization of charge during the reaction sequence may come into play.

The second part focuses on the optical transitions and the changes of the electronic structure of a nanotube due to functionalization. The charge transfer between the tube and the addend causes more or less changes in the electronic structure of the tubes, depending on the moiety. The changes are reflected in the optical transitions, which can be observed via Raman spectroscopy by recording resonance profiles of the radial breathing modes. It is shown that any charge transfer between the tubes and the addends causes redshifts in the optical transitions, acompanied by a braodening of the resonance condition. A polar bonding appears as a doping effect, introducing donor or acceptor levels within the gap of the transition. This leads to a redshift, because the effective gap is decreased. The resonance window is broadened, because more real states are offered to be possibly matched in an incoming or outgoing resonance of the Raman process. This is consistent with the findings that a non-polar bonding like an addition of alkanes does not cause significant shifts or broadening. The studies of the electronic structure are elaborated investigating composite materials containing carbon nanotubes. In various approaches nanotubes have been decorated with polymers. By means of Raman spectroscopy the influence of the functional groups has been investigated. It is shown that the electronic effects due to charge transfer can be separated from the structural effects, which also influence the electronic structure of the tubes.

In the final part isolated nanotubes prepared on a grid are investigated. The combination of Raman measurements and high resolution transmission electron microscopy (HRTEM) is shown to be of great us for the characterization of carbon nanotubes. The low frequency Raman signal of multiwalled tubes has been assigned to breathing-like modes by correlating the Raman data with diameter analysis via HRTEM. It has been shown that the expansion of chemical functionalization to isolated tubes could offer new opportunities to observe the effects of functionalization without the overlap of effects driven by bundling or other environmental effects. Isolated tubes also offer the possibility of polarization dependent measurements which may be of great benefit for fundamental research also on functionalized carbon nanotubes.

The recent awarding of the Nobel prize to Andre Geim and Konstantin Novoselov for their work on graphene reveals the importance of carbon nanostructures. Time will tell, if carbon is replacing, or at least complementing silicon in all day electronics, but as far as chemistry is concerned, carbon nanostructures have already shown their readiness for marketing. Global players in the field have started nanotube projects in recent years, improv-

ing the cost effective industrial production of nanotubes and are expecting growing markets for innovative products based on carbon. The impact of nanotubes on fundamental research is reflected in the enormous number of publications. No matter what future products will come, nanostructures will always pique a scientist's curiosity, because of strangeness and beauty.

# A

# Sample preparation

## A.1 Propylamin-tubes

The samples were prepared by Zois Syrgiannis according to Ref. [8, 50] The solution of lithium amide was prepared as follows: In a nitrogen-purged and heat dried four-necked round bottom flask (250 mL), equipped with two gas inlets and pressure compensation, $n$-propyl amine ( f1 = 0.5 mmol, f4 = 10.0 mmol) was dissolved in dry THF. The solution was cooled to $0\,^{\circ}\mathrm{C}$ for 15 min. To this solution the respective amount of $n$-butyllithium (90 % of the $n$-propyl amine amount) was added dropwise over a period of 10 min. Then the solution was stirred at room temperature for 1 h. In another 250 mL nitrogen-purged and heat dried three-necked round bottom flask, equipped with two gas inlets, 5 mg of purified HiPCo SWCNTs were dispersed in 100 mL anhydrous solvent (THF) by sonication (15 min). This dispersion of SWCNTs was added to the first flask through a heat dried dropping funnel. After the completion of the addition, the resulting suspension was stirred for 30 min at room temperature and sonicated for 30 min, resulting in a stable, black, homogeneous dispersion. The reaction mixture was stirred at room temperature overnight and subsequently quenched by bubbling oxygen for 1 h through the solution. The resulting dispersion was diluted with 100 mL cyclohexane, transferred to a separation funnel and purged with water. The organic layer with the nanotubes was filtered through a 0.2 $\mu$m PP membrane filter and washed with cyclohexane, methanol, ethanol and water. The resulting black solid was dried in a vacuum oven at $50\,^{\circ}\mathrm{C}$ overnight.

## A.2 Decyne-tubes

The samples were prepared by Benjamin Gebhardt according to Ref. [51]: The functionalization of the tubes was performed as follows: The corresponding lithium acetylide of decyne was prepared in situ by deprotonation with 0.9 eq. of n-butyllithium in THF. Single walled carbon nanotubes (HiPCO) were dispersed in o-DCB by ultrasonication for 15 min under air exclusion. This SWCNT dispersion was then added to the solution of lithium decynylide. The nucleophilic addition step is accompanied by the introduction of a negative charge to the SWCNT framework, yielding a charged intermediate species. The resulting Coulomb repulsion of the negatively charged SWCNTs leads to a debundling of the aggregated tube material as revealed by the formation of a homogeneous black dispersion. The subsequent reoxidation of the charged intermediates by oxygen yields neutral derivatives, which exhibit a pronounced dispersability in organic solvents such as THF.

## A.3 Pentyl-tubes

The samples were prepared by David Wunderlich: HiPCO-grown and HCl-purified nanotubes were used to prepare pentyl-SWCNTs functionalized by reductive alkylation with sodium and 1-bromopentane in liquid ammonia. The bulk-like samples contain 1.7% alkylated C atoms, as determined by thermogravimetric analysis.

## A.4 tpy-Ru(II)-tpy tubes

Starting from SWCNTs functionalized with ATRP initiator sites a vinyl terpyridine monomer is polymerized. The free side-terpyridine groups of SWCNT-Poly(tpy) were then complexated with the didodecyloxy- tpy-Ru(III)$Cl_3$ monocomplex (II) affording the final hybrid nanotubemetallopolymeric complex SWCNT-Poly(tpyRu(II)tpy-2x$C_{12}H_{25}$). The final SWCNT-Poly(tpyRu(II)tpy-2x$C_{12}H_{25}$) presented a 20.9 % weight loss compared to the SWCNT-initiator. Its total weight loss compared to the pristine SWCNT at 800 °C, was found to be 47.4 %. Comparing the polymeric functionalized SWCNT-Poly(tpyRu(II)tpy-2x$C_{12}H_{25}$) with the monomeric one, SWCNT-tpyRu(II)tpy-2x$C_{12}H_{25}$, the same

decomposition stages are observed, with the main weight loss obtained between 300 ℃ and 550 ℃.

## A.5 Quinoline-tubes

The samples were prepared in the group of Joannis K. Kallitsis in collaboration with Kostas Papagelis, university of Patras, Greece

Synthesis of quinoline monomers (M1, M2, M3)

M1: A 50 ml round bottom flask equipped with 2-amino-5-bromophenyl phenyl methanone (1) (3 g, 10.86 mmol) and p-Cyanacetophenon (3.15 g, 21.72 mmol) was degassed and filled with argon. As a solvent was used acetic acid 35 mL with the addition of 3 drops of sulfuric acid 95%. The reaction mixture was heated in reflux temperature for 3 days producing an orange solution. After cooling the solution, a light yellow solid appeared. Purification was achieved after filtration in a Por.3 filter and washed with pure methanol. The yellow solid was vacuum dried over night resulting 3.37g (80%) (1). Then, a 100 mL round bottom flask with 1 (3.3 g, 8.57 mmol), 4-vinylphenylboronic (1.9 g, 12.8 mmol), $K_2CO_3$ (5 g, 36.2 mmol) in 2M aqua solution, $Pd(PPh_3)_4$ (0.2 g, 0.166 mmol) and Toluene 50 mL was degassed and filled with argon 3x times. The reaction mixture was then heated for reflux for 4 days. Then the mixture was filtered from paper filter followed by the extraction of the organic layer with EtOAc (3x 40 mL) and distilled water (3x 40 mL). The organic part was then dried with $MgSO_4$ and after filtration the solution was evaporated at reduced pressure in rotary evaporator resulting yellow solid. This was dried and then dispersed in MeOH for further purification. The solid was then filtered from Por.3 and the light yellow solid was vacuum dried over night resulting 2.7g (80%) (M1).

M2: A 50 ml round bottom flask equipped with 2-amino-5-bromophenyl phenyl methanone (1) (3 g, 10.86 mmol) and acetyl pyridine (2.631 g, 21.72 mmol) was degassed and filled with argon. As a solvent was used acetic acid 35 mL with the addition of 3 drops of sulfuric acid 95%. The reaction mixture was heated in reflux temperature for 3 days producing an orange solution. After cooling the solution, a light brown cotton like solid appeared. Purification was achieved after filtration in a Por.3 filter and washed with pure methanol. The white solid was vacuum dried over night resulting 3.37 g (86%) (2). Then, a 100 mL round bottom flask with 2 (2 g, 5.54 mmol), 4-

vinylphenylboronic (1 g, 6.65 mmol), $K_2CO_3$ (2.3 g, 16.62 mmol) in 2M aqua solution, $Pd(PPh_3)_4$ (0.2 g, 0.166 mmol) and Toluene 50 mL was degassed and filled with argon 3x times. The reaction mixture was then heated for reflux for 4 days. Then the mixture was filtered from paper filter followed by the extraction of the organic layer with EtOAc (3x 40 mL) and distilled water (3x 40 mL). The organic part was then dried with $MgSO_4$ and after filtration the solution was evaporated at reduced pressure in rotary evaporator resulting yellow solid. This was dried and then dispersed in MeOH for further purification. The solid was then filtered from Por.3 and the light yellow solid was vacuum dried over night resulting 1.61 g (76%) (M2).

M3: In a 50 mL round bottom flask with M2 (0.15 g, 0.3916 mmol) and cis-$(tpy)_2-RuCl_2$ was degassed and filled with argon. As solvent was used ethanol absolute 40 mL. The reaction mixture was heated for 3 days at reflux temperature. Next, the solvent was evaporated in reduced pressure resulted a dark red solid. This was washed with 40 mL $H_2O$ for an hour and filtered for removing the insoluble part. In the soluble part the addition of 30 mL aqua solution of 15 g $NH_4PF_6$ resulting the formation of red crystals. Then the mixture was placed in the refrigerator for 2 hours and then by slow filtration the red solid was collected. Finally, we washed the solid with 200 mL distilled cold water and 50 mL DEE. The solid was vacuum dried over night resulting 0.28 g (76%) (M3).

Synthesis of hydroxy functionalized SWNT:

A 20 mL round bottom flask with SWNTs (100 mg, 8.33 meq C), p-amino phenol (1 g, 9.17 mmol) and isopentyl-nitrite 3 mL, was degassed and filled with argon. The reaction mixture was stirred at 65℃ for 36 hours. Then 15 mL of pure acetone was added and left for stirring for 12 hours. Filtration of the black solid, from Nylon 200 nm membrane and continuous wash with acetone was made until colorless precipitate. Then the solid was dispersed in DMF 100 mL and stirred at 50℃ for additional purification. Again, filtration from same type membrane resulted black solid which was vacuum dried over night at 7℃ (C1).

Synthesis of ATRP initiator groups onto SWNT:

A 100 mL round bottom flask with C1 (50 mg), CPC (3 mL, 30 mmol), $Et_3N$ (4 mL, 31.2 mmol) and distilled DMF 60 mL, was degassed, filled with argon and placed in the ultrasonic bath for 20 min. The reaction mixture was stirred at 100℃ for 48 hours. Filtration of the black solid from Nylon 200 nm membrane and continuous wash with acetone and dichloromethane until

colorless precipitate was made. Then the solid was dispersed in DMF 100 mL and stirred at 50℃ for additional purification. Again, filtration from same type membrane resulted black solid which was vacuum dried over night at 75℃ (C2).

Polymerization of quinoline monomers onto SWNT:

A 5 mL round bottom flask with C2 (20 mg), CuBr (10 mg, 0.07 mmol) and PMDETA (15$\mu$L, 0.07 mmol) was degassed, and filled with argon. The distilled DMF and the monomers M1, M2, M3 and M4 (1 mmol) were added with a syringe and then placed in the ultrasonic bath for 20 min. The reaction mixture was stirred at 90℃ for 24 hours. Then the mixture was dissolved in chloroform. The suspension was filtered from Nylon 200 nm membrane for purification from any unreacted monomers. Then the solid was dispersed in DMF 100mL and stirred at 50℃ for additional purification. Again, filtration from same type membrane resulted black solid which was vacuum dried over night at 75℃ (CM1, CM2, CM3).

# Bibliography


[1] S. Iijima, *Nature*, 1991, **354**, 56.

[2] D. S. Bethune, C. H. Kiang, M. S. deVries, G. Gorman, R. S. J. Vazques and R. Beyers, *Nature*, 1993, **363**, 605.

[3] P. Avouris and J. Chen, *Materials Today*, 2006, **9**, 46.

[4] R. Krupke, F. Hennrich, H. von Lohneysen and M. M. Kappes, *Science*, 2003, **301**, 344 – 347.

[5] G. S. Duesberg, M. Burghard, J. Muster and G. Philipp, *Chem. Commun.*, 1998, **1998**, 435 – 436.

[6] M. Zheng, A. Jagota, M. S. Strano, A. P. Santos, P. Barone, S. G. Chou, B. A. Diner, M. S. Dresselhaus, R. S. Mclean, G. B. Onoa, G. G. Samsonidze, E. D. Semke, M. Usrey and D. J. Walls, *Science*, 2003, **302**, 1545 – 1548.

[7] M. S. Strano, C. A. Dyke, M. L. Usrey, P. W. Barone, M. J. Allen, H. Shan, C. Kittrell, R. H. Hauge, J. M. Tour and R. E. Smalley, *Science*, 2003, **301**, 1519.

[8] Z. Syrgiannis, B. Gebhardt, C. Dotzer, F. Hauke, R. Graupner and A. Hirsch, *Angew. Chem. Int. Edition*, 2010, **49**, 3322.

[9] S. Kazaoui, N. Minami, R. Jacquemin, H. Kataura and Y. Achiba, *Phys. Rev. B*, 1999, **60**, 13339.

[10] L. Grigorian, K. A. Williams, S. Fang, G. U. Sumanasekera, A. L. Loper, E. C. Dickey, S. J. Pennycook and P. C. Eklund, *Phys. Rev. Lett.*, 1998, **80**, 5560.

[11] P. M. Rafailov, J. Maultzsch and C. Thomsen, *Phys. Rev. B*, 2005, **72**, 045411.

[12] S. Reich, C. Thomsen and J. Maultzsch, *Carbon Nanotubes*, Wiley-VCH, 2004.

[13] C. Thomsen and S. Reich, in *Light Scattering in Solids IX*, ed. M. Cardona and R. Merlin, Springer, Berlin, 2007.

[14] N. Wang, Z. K. Tang, G. D. Li and J. S. Chen, *Nature*, 2000, **408**, 50 – 51.

[15] X. Wang, Q. Li, J. Xie, Z. Jin, J. Wang, Y. Li, K. Jiang and S. Fan, *Nano Lett.*, 2009, **9**, 6 – 10.

[16] E. W. Wong, P. E. Sheehan and C. M. Lieber, *Science*, 1997, **277**, 1971.

[17] S. Berber, Y.-K. Kwon and D. Tománek, *Phys. Rev. Lett.*, 2000, **84**, 4613–4616.

[18] E. Pop, D. Mann, Q. Wang, K. Goodson and H. Dai, *Nano Lett.*, 2006, **6**, 96 – 100.

[19] V. Popov, *New Journal of Physics*, 2004, **6**, 17.

[20] L. V. Hove, *Phys. Rev.*, 1953, **89**, 1189 – 1193.

[21] P. Kim, T. Odom, J. Huang and C. Lieber, *Phys. Rev. Lett.*, 1999, **82**, 1225–1228.

[22] T. Ando, *NPG Asia Materials*, 2009, **1**, 17 – 21.

[23] J. Maultzsch, H. Telg, S. Reich and C. Thomsen, *Phys. Rev. B*, 2005, **72**, 205438.

[24] H. Telg, J. Maultzsch, S. Reich, F. Hennrich and C. Thomsen, *Phys. Rev. Lett.*, 2004, **93**, 177401.

[25] C. Raman, *Nature*, 1928, **121**, 619.

[26] P. Y. Yu and M. Cardona, *Fundamentals of semiconductors*, Springer Verlag, Berlin, 1996.

[27] M. Müller, R. Meinke, J. Maultzsch, B. Gebhardt, F. Hauke, A. Hirsch and C. Thomsen, *phys. stat. sol. (b)*, 2010.

[28] M. J. O'Connell, S. Sivaram and S. K. Doorn, *Phys. Rev. B*, 2004, **69**, 235415.

[29] J. Maultzsch, S. Reich and C. Thomsen, *Phys. Rev. B*, 2001, **64**, 121407.

[30] C. Thomsen and S. Reich, *Phys. Rev. Lett.*, 2000, **85**, 5214.

[31] M. Müller, J. Maultzsch, D. Wunderlich, A. Hirsch and C. Thomsen, *phys. stat. sol. (rrl)*, 2007, **1**, 144.

[32] R. Graupner, J. Abraham, D. Wunderlich, A. Vecelová, P. Lauffer, J. Rörl, M. Hundhausen, L. Ley and A. Hirsch, *J. Am. Chem. Soc.*, 2006, **128**, 6683.

[33] H. Telg, *Raman studies on individual nanotubes and nanotube ensembles vibrational properties and scattering efficiencies*, Dissertation TU Berlin, 2009.

[34] I. O. Maciel, N. Anderson, M. A. Pimenta, A. Hartschuh, H. Qian, M. Terrones, H. Terrones, J. Campos-Delgado, A. M. Rao, L. Novotny and A. Jorio, *Nature Materials*, 2008, **7**, 878 – 883.

[35] M. Cardona, in *Light Scattering in Solids II*, ed. M. Cardona and G. Güntherodt, Springer, Berlin, 1982, vol. 50.

[36] R. Meinke, *priv. comm.*

[37] H. Lange, M. Mohr, M. Artemyev, U. Woggon and C. Thomsen, *Nano Lett.*, 2008, **8**, 4614 – 4617.

[38] K. Kamaras, A. Pekker, M. Bruckner, F. Borondics, A. G. Rinzler, D. B. Tanner, M. E. Itkis, R. C. Haddon, Y. Tan and D. E. Resasco, *phys. stat. sol. (b)*, 2008, **245**, 2229.

[39] E. Ruska, *Z. Physik*, 1934, **87**, 580.

[40] B. W. Smith and D. E. Luzzi, *J. Appl. Phys.*, 2001, **90**, 3509.

[41] J. L. Bahr, E. T. Mickelson, M. J. Bronikowski, R. E. Smalley and J. M. Tour, *Chem. Commun.*, 2001, 193.

[42] A. D. McNaught and A. Wilkinson, *IUPAC. Compendium of Chemical Terminology, 2nd ed. (The "Gold Book")*, Blackwell Scientific Publications, 1997.

[43] Z. Chen, W. Thiel and A. Hirsch, *ChemPhysChem*, 2003, **4**, 93.

[44] F. Simon, C. Kramberger, R. Pfeiffer, H. Kuzmany, P. M. Singer and H. Alloul, *Phys. Rev. Lett.*, 2005, **95**, 017401.

[45] A. Hirsch and O. Vostrowsky, *Top Curr Chem*, 2005, **245**, 193.

[46] P. Singh, S. Campidelli, D. Bonifazi, A. Bianco and M. Prato, *Chemical Society Reviews*, 2009, **38**, 2214.

[47] A. Hirsch and O. Vostrowsky, *Functionalization of carbon nanotubes*, Wiley-VCH, 2007.

[48] M. Holzinger, O. Vostrowski, A. Hirsch, F. Hennrich, M. Kappes, R. Weiss and F. Jellen, *Angew. Chem. Int. Ed.*, 2001, **40**, 4002.

[49] D. Wunderlich, F. Hauke and A. Hirsch, *Chem. Eur. J.*, 2008, **14**, 1607.

[50] Z. Syrgiannis, F. Hauke, J. Röhrl, M. Hundhausen, R. Graupner, Y. Elemes and A. Hirsch, *Eur. J. Org. Chem.*, 2008, 2544.

[51] B. Gebhardt, R. Graupner, F. Hauke and A. Hirsch, *Europ. J. Org. Chem.*, 2010, 1494.

[52] M. S. Strano, *J. Am. Chem. Soc.*, 2003, **125**, 16148.

[53] P. R. Marcoux, J. Schreiber, P. Batail, S. Lefrant, J. Renouard, G. Jacob, D. Albertini and J.-Y. Mevellec, *Phys. Chem. Chem. Phys.*, 2002, **4**, 2278.

[54] *Raman/IR Atlas*, Verlag Chemie, 1975.

[55] C. Thomsen and S. Reich, *Phys. Rev. Lett.*, 2000, **85**, 5214.

[56] C. Fantini, A. Jorio, M. Souza, R. Saito, G. Samsonidze, M. S. Dresselhaus and M. A. Pimenta, *Phys. Rev. B*, 2005, **72**, 085446.

[57] E. Dobardžić, J. Maultzsch, I. Milošević, C. Thomsen and M. Damnjanović, *phys. stat. sol. (b)*, 2003, **237**, R7.

[58] C. Fantini, M. L. Usrey and M. S. Strano, *J. Phys.Chem. C*, 2007, **111**, 17941.

[59] C. A. Dyke and J. M. Tour, *Chem. Eur. J.*, 2004, **10**, 812.

[60] J. Kim, Y. Jung, Y.-J. Kwark and Y. Jeong, *J. Appl. Polym. Sci.*, 2010, **118**, 1335 – 1340.

[61] H. Hu, B. Zhao, M. A. Hamon, K. Kamaras, M. E. Itkis and R. C. Haddon, *J. Am. Chem. Soc.*, 2003, **125**, 14893.

[62] E. Joselevich, *ChemPhysChem*, 2004, **5**, 619.

[63] D. Wunderlich, F. Hauke and A. Hirsch, *J. Mater. Chem.*, 2008, **18**, 1493.

[64] R. B. Woodward and R. Hoffmann, *J. Am. Chem. Soc.*, 1965, **87**, 395.

[65] K. Fukui, *Angew. Chem. Int. Ed.*, 1982, **21**, 801 – 809.

[66] T. W. Odom, J.-L. Huang, P. Kim and C. M. Lieber, *J. Phys. Chem. B*, 2000, **104**, 2794.

[67] M. S. Strano, C. A. Dyke, M. L. Usrey, P. W. Barone, M. J. Allen, H. Shan, C. Kittrell, R. H. Hauge, J. M. Tour and R. E. Smalley, *Science*, 2003, **301**, 1519.

[68] Y. Miyata, Y. Maniwa and H. Kataura, *J. Phys. Chem. B*, 2006, **110**, 26.

[69] C. Fantini, A. Jorio, M. Souza, M. S. Strano, M. S. Dresselhaus and M. A. Pimenta, *Phys. Rev. Lett.*, 2004, **93**, 147406.

[70] S. Niyogi, M. A. Hamon, H. Hu, B. Zhao, P. Bhowmik, R. Sen, M. E. Itkis and R. C. Haddon, *Accounts of Chemical Research*, 2002, **35**, 1105.

[71] R. Haddon, *Science*, 1993, **261**, 1545 – 1550.

[72] O. Kiowski, S. Lebedkin, F. Hennrich, S. Malik, H. Rösner, K. Arnold, C. Sürgers and M. M. Kappes, *Phys. Rev. B*, 2007, **75**, 075421.

[73] V. Skákalová, J. Maultzsch, Z. Osváth, L. P. Biró and S. Roth, *phys. stat. sol. (RRL)*, 2007, **1**, 138.

[74] M. Müller, J. Maultzsch, D. Wunderlich, A. Hirsch and C. Thomsen, *phys. stat. sol. (b)*, 2008, **245**, 1957.

[75] M. Müller, J. Maultzsch, K. Papagelis, A. A. Stefopoulos, E. K. Pefkianakis, A. K. Andreopoulou, J. K. Kallitsis and C. Thomsen, *phys. stat. sol. (b)*, 2009, **246**, 2721.

[76] M. Müller, R. Meinke, J. Maultzsch, Z. Syrgiannis, A. Hirsch and C. Thomsen, *ChemPhysChem*, 2010, **11**, 2444.

[77] M. Burghard, *Surf. Sci. Rep*, 2005, **58**, 1–109.

[78] A. E. Aliev, *Science*, 2009, **5921**, 1575 – 1578.

[79] J. Siqueira, M. Abouzar, M. Bäcker, V. Zucolotto, A. Poghossian, O. N. Oliveira and M. J. Schöning, *Phys. Status Solidi A*, 2009, **206**, 462.

[80] S. V. Ahir, *Nature Materials*, 2005, **4**, 491 – 495.

[81] A. Nduwimana and X.-Q. Wang, *ASCNano*, 1995, **3**, 1995 – 1999.

[82] V. G. Hadjiev, M. N. Iliev, S. Arepalli, P. Nikolaev and B. S.Files, *Appl. Phys. Lett.*, 2001, **78**, 3193.

[83] B. Kilbride, J. Coleman, J. Fraysse, P. Fournet, M. Cadek and A. Drury, *Journal of applied physics*, 2002, **92**, 4024–4030.

[84] J. Hone, M. C. Llaguno, N. M. Nemes, A. T. Johnson, J. E. Fischer, D. A. Walters, M. J. Casavant, J. Schmidt and R. E. Smalley, *Appl. Phys. Lett.*, 2000, **77**, 666–668.

[85] P. M. Ajayan, L. S. Schadler, C. Giannaris and A. Rubio, *Polym. Compos.*, 2000, **12**, 750.

[86] D. Tasis, *Macromol. Rapid Commun.*, 2007, **28**, 1553 – 1558.

[87] U. S. Schubert and C. Eschbaumer, *Angew. Chem. Int. Ed.*, 2002, **41**, 2892.

[88] K. A. Aamer, W. H. de Jeu and G. N. Tew, *Macromolecules*, 2008, **41**, 2022 – 2029.

[89] A. A. Stefopoulos, E. K. Pefkianakis, K. Papagelis, A. K. Andreopoulou and J. K. Kallitsis, *J. Polym. Sc. Part A: Polym. Chem.*, 2009, **47**, 2551.

[90] Y. K. Kang, O.-S. Lee, P. Deria, S. H. Kim, T.-H. Park, D. A. Bonnell, J. G. Saven and M. J. Therien, *Nano Lett.*, 2009, **9**, 1414 – 1418.

[91] K. Sasaki, H. Farhat, R. Saito and M. Dresselhaus, *Physica E*, 2010, **42**, 2005 – 2015.

[92] N. Caudal, A. M. Saitta, M. Lazzeri and F. Mauri, *Phys. Rev.*, 2007, **75**, 115423.

[93] A. Jorio, A. G. Souza Filho, G. Dresselhaus, M. S. Dresselhaus, A. K. Swan, M. S. Ünlü, B. B. Goldberg, M. A. Pimenta, J. H. Hafner, C. M. Lieber and R. Saito, *Phys. Rev. B*, 2002, **65**, 155412.

[94] S. Piscanec, M. Lazzeri, J. Robertson, A. C. Ferrari and F. Mauri, *Phys. Rev. B*, 2007, **75**, 035427.

[95] C. Spudat, M. Müller, L. Houben, J. Maultzsch, K. Goss, C. Thomsen, C. M. Schneider and C. Meyer, *Nano Lett.*, **10**, 4470.

[96] V. N. Popov and L. Henrard, *Phys. Rev. B*, 2002, **65**, 235415.

[97] C. Spudat, *Correlation between Raman spectroscopy and electron microscopy on individual carbon nanotubes and peapods*, Dissertation Universität Duisburg-Essen, Jülich, 2010.

[98] C. Meyer, C. Spudat, L. Houben and C. M. Schneider, *Nanotechnology*, 2009, **20**, 065603.

[99] X. L. Zhao, Y. Ando, L. C. Qin, H. Kataura, Y. Maniwa and R. Saito, *Chem. Phys. Lett.*, 2002, **361**, 169 – 174.

[100] V. N. Popov and L. Henrard, *Phys. Rev. B*, 2004, **70**, 115407.

[101] H. Telg, M. Fouquet, J. Maultzsch, W. Y. Wu, B. Chandra, H. J. Hone, T. F. Heinz and C. Thomsen, *phys. stat. sol. (b)*, 2008, **245**, 2189 – 2192.

## Acknowledgments

This work would not have been possible without the assistance, close collaboration and supervision of others. It is my pleasure to thank those who made this thesis possible. Thank you very much!